

A Procedure for Estimating Total Evapotranspiration using Satellite-Based
Vegetation Indices with Separate Estimates from Bare Soil

A Thesis

Presented in Partial Fulfillment of the Requirements for the

Degree of Master of Science

With a Major in

Civil Engineering

In the

College of Graduate Studies

University of Idaho

Moscow, Idaho

By

Boyd Burnett

2007

Major Professor Dr. Richard Allen

“The waters flow eastwards from their sources, resting neither by day nor by night. Down they come inexhaustibly, yet the deeps are never full. The small stream become large and the heavy waters in the sea become light and mount to the clouds.”

Lu Shihh Chhun Chhiu
Third century B.C.

AUTHORIZATION TO SUBMIT THESIS

This thesis of Boyd Burnett, submitted for the degree of Master of Science with a major in Civil Engineering and titled “A Procedure for Estimating Total Evapotranspiration using Satellite-Based Vegetation Indices with Separate Estimates from Bare Soil,” has been reviewed in final form. Permission, as indicated by the signatures and dates given below, is now granted to submit final copies to the College of Graduate Studies for approval.

Major Professor _____ Date _____

Dr. Richard G. Allen

Committee
Members _____ Date _____

Dr. Fritz Fiedler

Committee
Members _____ Date _____

Dr. Russell Qualls

Department
Administrator _____ Date _____

Dr. Sunil Sharma

College Dean _____ Date _____

Final Approval and Acceptance by the College of Graduate Studies

_____ Date _____

Dr. Margrit von Braun

ABSTRACT

Remote sensing of evapotranspiration (ET) that is based on surface energy balance has been considered a reliable method for estimating ET over large spatially varying areas and at high resolution. Energy balance techniques require both short wave and thermal satellite information to produce estimates of surface fluxes including ET, and the accuracy of those estimates is directly dependent upon proper model calibration. A method to obtain estimates of ET using only satellite based vegetation indices, requiring only short wave satellite data, coupled with separate estimates of evaporation from bare soil has been examined. The use of Kcb-NDVI relationships coupled with procedures for estimating evaporation using water balance model techniques can assist water managers in the estimation of seasonal ET fluxes over agricultural areas of southern Idaho, when thermal satellite information is not available to supply more accurate energy balance based techniques. Seasonal ET estimates using the satellite based Kcb-NDVI relationship coupled water balance models were within $\pm 5\%$ of ET observations from the energy balance based model Mapping Evapotranspiration at High Resolution with Internalized Calibration (METRIC), for most crops within the Magic Valley of southern Idaho. Statistical methods were also examined for the statistical selection of 'anchor' pixels used in the calibration of the energy balance based METRIC ET estimation model. Statistically calibrated METRIC application produced differences in seasonal ET from user calibrated METRIC estimates that were less than 3% of the total seasonal reference ET. The statistical calibration procedure can reduce the uncertainty in ET estimates associated with the subjective user defined calibration for inexperienced users or for users without good background in ET fluxes and radiation physics.

TABLE OF CONTENTS

AUTHORIZATION TO SUBMIT THESIS.....	iii
ABSTRACT.....	iv
TABLE OF CONTENTS.....	v
LIST O FIGURES.....	viii
LIST OF TABLES.....	xiv
1.0 INTRODUCTION	1
1.1. Problem Statement.....	2
1.2. Objectives	3
1.3. Study Area	3
2.0 LITERATURE REVIEW	5
2.1. Evapotranspiration Theory.....	5
Reference Evapotranspiration.....	6
2.2. Crop Coefficient ET Estimation Methods	9
2.3. FAO 56 dual Crop Coefficient Method	10
2.4. Point Based ET measurements.....	11
3.0 THEORY OF THE REMOTE SENSING OF ET	13
3.1. Satellite Based Surface Energy Balance Methods.....	13
3.2. METRIC Calibration Strategy Using ETr	20
3.3. Testing of METRIC	21
3.4. Crop Coefficients from short wave satellite data.....	22
3.5. Basal Kc from vegetation index.....	26
4.0 METHODOLGY	28
4.1. Basal crop coefficients from NDVI	28
General crop K_{cb} from at-surface NDVI.....	29
Crop specific Kcb from NDVI.....	32
4.2. FAO 56 dual crop coefficient method to add estimate of evaporation from soil	34
Water Balance of the Surface Evaporation Layer.....	34

	Water Balance of the Root Zone.....	39
	Irrigation simulations	42
	Sample fields locations	43
	Water Balance Model Inputs	47
4.3.	Parameter Development.....	49
	Soil Properties.....	49
	Crop Characteristics.....	50
5.0	$K_{cb} + K_e$ WATER BALANCE MODEL WITH CROP CLASSIFICATION	53
5.1.	Statistical Analysis.....	53
5.2.	Ten Field Simulations for each Crop under Consideration	56
5.3.	Accuracy of Individual Field Simulations	76
5.4.	Average Field Condition Simulation using 3,754 Sampled Fields.....	78
5.5.	K_e Simulation Sensitivity	79
6.0	CROP CLASSIFICATION FREE $K_{cb} + K_e$ WBM	83
6.1.	Ten Field Simulations for Each Crop under Consideration.....	83
6.2.	Individual Field Simulation using General Crop Characteristics	96
6.3.	$K_{cb} + K_e$ WBM for Average Field Condition in the Magic Valley	97
6.4.	Evaporation Fraction of total ET	99
6.5.	Loss or Gain of Accuracy with Classification Free Approach	100
7.0	COMPARISON OF ET ESTIMATES FROM $K_{cb} + K_e$ WBM AND K_{c_mean} METHODS	102
7.1.	Analysis of Variance.....	105
8.0	TESTING SPATIAL AND TEMPORAL APPLICABILITY	108
8.1.	Path 40 year 2000.....	108
9.0	AUTOMATIC ANCHOR PIXEL SELECTION.....	115
9.1.	T_s and NDVI statistics	116
9.2.	Statistical Selection of the Cold pixel.....	117
9.3.	Statistical Selection of the Hot pixel.....	121
9.4.	Path 40 year 2000.....	125
9.5.	Application of Statistically Derived Anchor Pixels for METRIC Processing	132

10.0	CONCLUTIONS AND RECOMENDATIONS.....	140
10.1.	Conclusions.....	140
10.2.	Recommendations.....	141
	REFERENCES	143
	APPENDIX.....	148
A.	Comparison of Kcb Curves with Literature.....	148
B.	STATISTICS FOR “COLD” PIXEL SELECTION	150
C.	SENSITIVITY TO AOI DELINEATION.....	156
D.	METRIC ANCHOR PIXEL DATA PATH 40, ROW 30, YEAR 2000	159

LIST O FIGURES

Figure 1.3-1 Magic Valley agricultural area in Southern Idaho (Taken from Tasumi et al, 2007).....	4
Figure 2.1-1 Partitioning of evaporation and transpiration over an entire growing season (following FAO 56 Allen et al 1998).....	6
Figure 2.1-2 Performance of the ACSE Standardized Penman Monteith equation for calculating hourly alfalfa reference ET (taken from Allen 2006, Lysimeter data from Dr. J.L. Wright, USDA-ARS).....	9
Figure 2.3-1 Generalized crop coefficient curve showing the evolution of the crop coefficient throughout the growing season, the basal K_c , and the effects of evaporation due to wetting events. (Taken from Wright, 1982, 1990).....	11
Figure 3.1-1 Sensible heat flux diagram showing the near surface temperature difference dT (Taken from Allen).....	16
Figure 3.1-2 Linear relationship between dT and T_s used in the METRIC calibration process for the sensible heat H	18
Figure 3.4-1 Comparison of remotely sensed average E_{TrF} and average NDVI (computed at the surface) from ten randomly sampled Sugar Beet fields for 12 image dates throughout the growing season (K_c data from METRIC processing Tasumi, 2003, reprocessed for this study).	23
Figure 3.4-2 Comparison of NDVI and SAVI vegetation indices for determining crop coefficients (K_c data from METRIC processing Tasumi, 2003, reprocessed for this study).....	25
Figure 3.5-1 METRIC K_c (E_{TrF}) versus NDVI showing separation of total K_c into the basal and evaporation components K_{cb} and K_e	27
Figure 4.1-1 K_{cb} versus NDVI for all crop types showing both General relationship as well as crop specific relationships.	31
Figure 4.1-2 Comparison of K_{cb} curve derived from regional average NDVI for corn using the general crop relationship with K_{cb} developed by Allen Robison (2007) from standardized K_{cb} curves by Wright (1982) for the Hazelton area within the Magic Valley (custom crop specific K_{cb} curve for corn performed similarly (seen in Appendix A)) ...	34
Figure 4.2-1 Behavior of the soil evaporation reduction coefficient, K_r as water is evaporated from the evaporation layer (following Allen et al., 1998).....	37
Figure 4.2-2 Behavior of the water stress reduction coefficient, K_s , as water is extracted from the root zone (following Allen et al., 1998).	41
Figure 4.2-3 Sampled alfalfa fields used in water balance model calibration.	44
Figure 4.2-4 Crop classification created by Tasumi et al, 2003 for major agricultural crops of the Magic Valley.....	45
Figure 4.2-5 Cloud cover map of Magic Valley showing total number of image dates with cloud cover.....	46
Figure 4.2-6 Comparison of splined versus linear interpolated K_{cb} for average Bean crop in the Magic Valley for year 2000 ('custom' K_{cb} versus NDVI).....	47
Figure 4.2-7 Simulated irrigation for average Sugar Beet field using average NDVI from ten fields.....	48

Figure 4.2-8 Seasonal $K_{cb} + K_e$ curve for average Sugar Beet field constructed using FAO 56 dual crop coefficient approach with simulated Irrigation events.....	49
Figure 5.2-1 Average NDVI and METRIC K_c from ten randomly sampled alfalfa fields	58
Figure 5.2-2 Comparison of K_{cb} curves developed from satellite NDVI to the K_{cb} curve generated by Allen and Robison (2007) using the Wright (1982) K_{cb} procedure for the Hazelton area within the Magic Valley	59
Figure 5.2-3 Soil water balance of the root zone and corresponding simulated irrigations using rooting characteristics specific to alfalfa.....	60
Figure 5.2-4 $K_{cb} + K_e$ curve generated using water balance model for alfalfa with crop specific characteristics ($K_{cb} +$ smoothed K_e curve: K_e smoothed using 10 day running average for visual curve comparison).....	60
Figure 5.2-5 Average NDVI from ten bean fields along with the average METRIC K_c sampled from the same ten fields.....	62
Figure 5.2-6 Soil water balance of the root zone for Beans using average field conditions.....	63
Figure 5.2-7 $K_{cb} + K_e$ curve for Beans constructed using custom (bean specific) K_{cb} -NDVI relationship from average NDVI of ten fields and simulated irrigations ($K_{cb} +$ smoothed K_e curve: K_e smoothed using 10 day running average for visual curve comparison).....	63
Figure 5.2-8 Average NDVI and observed METRIC K_c for ten randomly sampled Corn fields within the Magic Valley.....	64
Figure 5.2-9 Soil water balance and simulated irrigation events for average Corn field constructed using average NDVI from ten randomly sampled corn fields.....	65
Figure 5.2-10 $K_{cb} + K_e$ curve for Corn constructed using custom (corn specific) K_{cb} -NDVI relationship from the average NDVI of ten fields and simulated irrigations ($K_{cb} +$ smoothed K_e curve: K_e smoothed using 10 day running average for visual curve comparison).....	66
Figure 5.2-11 Average NDVI and METRIC K_c from ten randomly sampled Potato fields.....	67
Figure 5.2-12 Soil water balance of the root zone and corresponding simulated irrigations for Potatoes using crop specific crop characteristics.....	68
Figure 5.2-13 $K_{cb} + K_e$ curve for Potatoes generated using custom (potato specific) K_{cb} -NDVI relationship from average NDVI of ten fields and simulated irrigations ($K_{cb} +$ smoothed K_e curve: K_e smoothed using 10 day running average for visual curve comparison).....	68
Figure 5.2-14 Average NDVI and METRIC K_c from ten randomly sampled Sugar Beet fields.....	69
Figure 5.2-15 Soil water balance of the root zone with corresponding simulated irrigations.....	70
Figure 5.2-16 $K_{cb} + K_e$ curve generated using water balance model for Sugar Beets with crop specific rooting characteristics and the general K_{cb} -NDVI relationship ($K_{cb} +$ smoothed K_e curve: K_e smoothed using 10 day running average for visual curve comparison).....	71
Figure 5.2-17 Average NDVI and METRIC K_c from ten randomly sampled Spring Grain fields.....	72

Figure 5.2-18 Soil water balance of the root zone with corresponding simulated irrigations.	73
Figure 5.2-19 $K_{cb} + K_e$ curve for Spring Grain generated using water balance model with crop specific rooting characteristics and the general K_{cb} -NDVI relationship ($K_{cb} +$ smoothed K_e curve: K_e smoothed using 10 day running average for visual curve comparison).....	73
Figure 5.2-20 Average NDVI and METRIC K_c from ten randomly sampled Winter Grain fields.....	74
Figure 5.2-21 Soil water balance of the root zone and corresponding simulated irrigations.	75
Figure 5.2-22 $K_{cb} + K_e$ curve for Winter Grain generated using water balance model with crop specific rooting characteristics and the general K_{cb} -NDVI relationship ($K_{cb} +$ smoothed K_e curve: K_e smoothed using 10 day running average for visual curve comparison).....	76
Figure 5.3-1 Comparison of predicted average daily ET to METRIC observed average daily ET for 10 individual Corn fields (n=120).	78
Figure 5.5-1 $K_{cb} + K_e$ curve for an average Magic Valley Potato field using K_e derived from one individual irrigation simulation and specific crop characteristics.	80
Figure 5.5-2 $K_{cb} + K_e$ curve for the average Potato field condition within the Magic Valley using K_e averaged from individual field irrigation simulations from ten fields, using specific crop characteristics.	81
Figure 6.1-1 Soil water balance of the root zone for the average alfalfa field using general crop characteristics.	85
Figure 6.1-2 $K_{cb} + K_e$ for average alfalfa field constructed using water balance model. METRIC K_c is overlaid for comparison ($K_{cb} +$ smoothed K_e curve: K_e smoothed using 10 day running average for visual curve comparison).....	86
Figure 6.1-3 Soil water balance of the root zone and corresponding simulated irrigations using general crop characteristics.	87
Figure 6.1-4 $K_{cb} + K_e$ curve for Beans generated using water balance model with general crop characteristics ($K_{cb} +$ smoothed K_e curve: K_e smoothed using 10 day running average for visual curve comparison).	87
Figure 6.1-5 Soil water balance of the root zone for Corn using general crop characteristics.	88
Figure 6.1-6 $K_{cb} + K_e$ curve for Corn generated using water balance model with general crop characteristics ($K_{cb} +$ smoothed K_e curve: K_e smoothed using 10 day running average for visual curve comparison).	89
Figure 6.1-7 Soil water balance of the root zone for Potatoes using general crop characteristics.	90
Figure 6.1-8 $K_{cb} + K_e$ curve for Potatoes generated using water balance model with general crop characteristics ($K_{cb} +$ smoothed K_e curve: K_e smoothed using 10 day running average for visual curve comparison).	91
Figure 6.1-9 Soil water balance of the root zone for Sugar Beets using general crop characteristics.	92
Figure 6.1-10 $K_{cb} + K_e$ curve for Sugar Beets generated using general crop characteristics ($K_{cb} +$ smoothed K_e curve: K_e smoothed using 10 day running average for visual curve comparison).....	92

Figure 6.1-11 Soil water balance of the root zone for Spring Grain using general crop characteristics.....	94
Figure 6.1-12 $K_{cb} + K_e$ curve for Spring Grain generated using general crop characteristics ($K_{cb} +$ smoothed K_e curve: K_e smoothed using 10 day running average for visual curve comparison).....	94
Figure 6.1-13 Soil water balance of the root zone for Winter Grain using general crop characteristics.....	95
Figure 6.1-14 $K_{cb} + K_e$ curve for Winter Grain generated using water balance model with general crop characteristics ($K_{cb} +$ smoothed K_e curve: K_e smoothed using 10 day running average for visual curve comparison).....	96
Figure 6.5-1 Seasonal ET estimates from METRIC compared with seasonal ET estimates using general K_{cb} -NDVI relationships and general crop characteristics.	101
Figure 6.5-1 Comparison of daily crop coefficients for potato crops (average NDVI from ten randomly sampled potato fields) using various K_c estimation techniques within the Magic Valley for the year 2000.	104
Figure 8.1-1 Seasonal ET map generated using K_{cb} -NDVI + K_e approach for the year 2000 (1-Mar to 31-Oct) within the Magic Valley near the communities of Murtagh and Hansen Idaho.	109
Figure 8.1-2 Seasonal ET map generated using METRIC processing for the year 2000 (1-Mar to 31-Oct) within the Magic Valley near the communities of Murtagh and Hansen Idaho.	109
Figure 8.1-3 Cloud free sampled pixels within the agricultural area of the Magic Valley for the year 2000.	110
Figure 8.1-4 Comparison of seasonal ET estimates from the crop specific $K_{cb} + K_e$ water balance model and observed METRIC estimates no filtration of possible thermal contamination.....	112
Figure 8.1-5 Seasonal ET comparison between METRIC and the custom K_{cb} -NDVI water balance model results using crop specific crop characteristics.....	113
Figure 9.1-1 NDVI versus K_c analysis for fields sampled with in Path 39 exhibiting K_c (ie. ET_rF) near that of the "cold anchor" pixel and the "hot anchor" pixel.....	117
Figure 9.2-1 Path 39 study area near Aberdeen Idaho, water body shown is American Falls Reservoir, and area of interest (AOI) is outlined in blue.	118
Figure 9.2-2 Coefficient of Variation in NDVI used to filter out edges of fields where contamination of Landsat data can occur due to the thermal pixel.....	119
Figure 9.2-3 Comparison of user defined cold pixel temperature with statistically determined temperature for path 39, row 30 for year 2000.	120
Figure 9.3-1 Temperature histogram for June 4, 2000 Landsat image (Created in ERDAS IMAGINE).....	122
Figure 9.3-2 Relative difference between hot desert pixels and the hottest agricultural soils throughout the growing season for Path 39 year 2000.	123
Figure 9.3-3 Comparison of statistically determined T_s for hot pixel and user defined T_s for path 39, row 30, year 2000.	125
Figure 9.4-1 Area of interest (outlined in blue) established within the Magic Valley for the testing of the Automatic anchor pixel selection process.....	126
Figure 9.4-2 Grid density for AOI delineation for Path 40 year 2000.....	127

Figure 9.4-3 Comparison of user defined cold pixel and statistically defined for Path 40 year 2000 (User defined T_S from UI METRIC processing, Tasumi 2003).	128
Figure 9.4-4 Hot pixel temperature comparison between experienced user defined and statistically derived T_s	129
Figure 9.4-5 Difference between monthly minimum temperatures and dew point temperatures plotted against the ratio of monthly precipitation and monthly reference ET (Taken from FAO 56 Annex 6, Allen et al., 1998).	130
Figure 9.4-6 Comparison of the Precipitation/ ET_r ratio for the 60 days immediately preceding Image dates to the difference between statistically derived T_S and the user defined T_S of the hot pixel (Weather data measured near Kimberly Idaho).	131
Figure 9.4-7 Hot pixel selection comparison with statistical method coupled with use of P/ ET_r ratio for correction due to desert heating.	132
Figure 9.5-1 Surface temperature image colorization for the selection of individual pixels used as the cold and hot anchor pixels for METRIC processing of Path 40 year 2000. ..	133
Figure 9.5-2 Seasonal ET comparison for 70 agricultural fields within the Magic Valley between standard METRIC processing and the statistically calibrated METRIC processing for the year 2000 with the albedo for the cold pixel used in the statistical calibration method ranging from 0.2 to 0.25.	134
Figure 9.5-3 Difference in ET_{rF} images using standard METRIC processing and METRIC calibrated by statistical selection of cold and hot anchor pixels for late July image.	135
Figure 9.5-4 Difference in ET_{rF} images using standard METRIC processing and METRIC calibrated by statistical selection of cold and hot anchor pixels when albedo at the cold pixel condition and the hot pixel condition were the same.	136
Figure 9.5-5 Difference in ET_{rF} images using standard METRIC processing and METRIC calibrated by statistical selection of cold and hot anchor pixels when albedo at the cold pixel condition was higher for the statistical calibration method.	137
Figure 9.5-6 Difference in METRIC methods when albedo at the cold pixel is selected so that it is lower than the albedo of user defined METRIC processing when albedo at the cold pixel condition was slightly smaller for the statistical calibration method (same pixels sampled as in Figure 9.5-5).	137
Figure 9.5-7 Seasonal ET comparison between standard METRIC processing and METRIC processing using statistical calibration for 70 agricultural fields within the Magic Valley for the year 2000.	138
Figure 10.21 Comparison of General K_{cb} curves from NDVI with Allen and Robison (2007).	148
Figure A.2 Comparison of crop specific K_{cb} curves developed from NDVI to Allen and Robison (2007).	149
Figure 10.2B.1 Rectangular AOI's (outlined in dashed black and white) for the statistical selection of cold and hot anchor pixels for path 39, row 30, year 2000.	150
Figure 10.2B.2 Comparison of varying statistics for cold pixel selection looking at the highest 5 % of NDVI.	153
Figure B.3 Comparison of results from several statistical methods for the selection of cold anchor pixels looking at the highest 5 to 10% NDVI.	154
Figure C.1 Carefully delineated agricultural AOI's for the statistical selection of cold and hot anchor pixels for path 40, row 30, year 2000.	156

Figure C.2 Rectangular agricultural AOI's for the statistical selection of the cold and hot anchor pixels for path 40, row 30, year 2000. 157

Figure C.3 Comparison of the statistically selected hot pixel for path 40 with the user defined hot anchor pixel using multiple AOI's throughout the Magic Valley..... 158

Figure C.4 Comparison of the statistically selected hot pixel for path 40 with the user defined hot anchor pixel using single AOI (central AOI Figure 10.2-2) throughout the Magic Valley..... 158

LIST OF TABLES

Table 4.1-1 Total number of fields sampled for each crop type within the Magic Valley during the year 2000.	28
Table 4.1-2 K_{cb} versus NDVI calibration constants for the Magic Valley Path 40 year 2000.....	33
Table 4.3-1 Soil properties used in $K_{cb} + K_e$ water balance model, calibrated for the Magic Valley during previous ET studies (Allen Personal communication).	50
Table 4.3-2 Crop characteristics used for both the crop specific and general crop simulations.	51
Table 5.1-1 Time periods corresponding to Landsat satellite overpass for March 1, to October 31, 2000.....	54
Table 5.2-1 Summary of simulations of each crop type using specific crop rooting characteristics, custom K_{cb} versus NDVI relationship and the average NDVI over ten sampled fields to define the average field condition	57
Table 5.3-1 Summary of the accuracy of individual field simulations using specific crop characteristics and custom crop K_{cb} -NDVI curves ($n = 120$, 12 image sub-period estimates for 10 fields for each crop).....	77
Table 5.4-1 Average field condition (average crop defined by average NDVI over all sampled fields of that crop type) simulation using K_e from single irrigation simulation for average condition and crop specific characteristics.....	79
Table 5.5-1 Average field condition simulation using specific crop characteristics for each crop and K_e averaged from individual simulations for ten fields for each crop type (average field condition is defined by averaging NDVI over all fields of each given crop).	82
Table 6.1-1 Summary of average field condition simulation using the universal (crop coefficient free) K_{cb} -NDVI relationship for ten sampled fields for each of the crop types considered.	84
Table 6.2-1 Summary of individual field simulations for all crop types using general crop characteristics and general K_{cb} -NDVI relationship (10 field simulations for each crop with 12 image sub-period observations gives a total $n = 120$ for each crop type).	97
Table 6.3-1 Summary of average field condition simulations for all crops using general crop characteristics and K_e from one individual irrigation simulation per crop type using general K_{cb} -NDVI relationship (average field condition defined using NDVI averaged over all fields sampled for each crop type).....	98
Table 6.3-2 Results for average field condition simulations using general crop characteristics and the K_e averaged from ten individual field simulations for each crop type using general K_{cb} -NDVI relationship.....	99
Table 6.4-1 Fraction of seasonal Evaporation to seasonal ET (March 1 to October 31) for simulations using the average field condition for the Magic Valley (Average field created using average NDVI from all sampled fields of a specific crop type).....	100
Table 6.5-1 Sampled pixels used for the construction of K_c _mean-NDVI relationships by Allen et al, (in preparation) for crops within the Magic Valley for the year 2000.	102

Table 6.5-2 Results of K_c _mean-NDVI relationship ET estimates from the average NDVI of ten randomly sampled fields of each crop type for March 1 to October 31 (same ten fields as discussed for water balance results in chapter 5 and 6).	103
Table 6.5-3 Comparison of ET estimates from both general and crop specific water balance model simulations to ET estimates from K_c _mean-NDVI for average field conditions within the Magic Valley (n = 84, 12 image sub-period estimates for 7 crop types) Average field condition is using the average NDVI from all fields listed in Table 4.1-1 for each crop type.	105
Table 7.1-1 Analysis of Variance output table generated in SYSTAT 11 testing average daily ET estimates of four model types.	106
Table 7.1-2 Games-Howell Test for pair-wise comparison of average daily ET estimates for each model considered (generated using SYSTAT 11).	107
Table 8.1-1 Sampled "cloud free" fields for seasonal ET comparison for crops within the Magic Valley for the year 2000.	110
Table 8.1-2 Percentage deviation in seasonal ET estimates of $K_{cb} + K_e$ water balance model from observed METRIC seasonal ET from 8,521 sampled pixels. Negative values represent under estimation of the water balance model compared to METRIC observations.	111
Table 8.1-3 Sampled fields based on crop type within the Magic Valley for the year 2000. All sampled fields are taken well within field edges to avoid contamination by thermal pixels (thermal contamination can cause within-field bias in METRIC ET estimation), as well as filtered so that no cloud cover was observed for any of the Landsat image dates.	112
Table 8.1-4 Average deviation for METRIC seasonal ET estimates using the $K_{cb} + K_e$ water balance model with crop specific characteristics and custom K_{cb} -NDVI relationships for each crop. Negative values represent under estimation by the water balance model compared to METRIC observations.	114
Table 9.2-1 Comparison of user defined T_{s_dem} and statistically derived T_s for the cold anchor pixel throughout the growing season for path 39, row 30.	121
Table 10.2B.1 Difference in cold anchor pixel temperature statistically determined and user defined for six different combinations of statistical selection processes.	153
Table D.1 Anchor pixel characteristics for pixels selected by experienced METRIC user for path 40, row 30, year 2000.	159
Table D.2 Anchor pixel characteristics for pixels selected using statistical procedures for path 40, row 30, year 2000 METRIC processing.	159
Table D.3 Anchor pixel characteristics for statistical selection using tighter range fo albedo values at the cold pixel for path 40, row 30, year 2000.	160

1.0 INTRODUCTION

Increasingly higher demands are being placed on water resources each year. With the increasing stress, water resource managers must continually expand methods to assist them in the quantification and allocation of water consumptive use. In 2000, irrigation was the single largest use of fresh water with an estimated 153 million acre-feet of water used in the United States for irrigating over 60 million acres of agricultural fields, golf courses, parks and nurseries (Hutson et al, 2004). In the arid region of the western United States, where irrigated agricultural practices, species conservation and drought often collide, quantifying water use becomes increasingly vital.

The quantification of water consumption requires knowledge of the evaporation of water from the earth and plant surfaces as well as how water is consumed by plants by way of transpiration. The combination of these two phenomena, namely surface evaporation and transpiration, are collectively referred to as evapotranspiration. Evapotranspiration (ET) is the largest consumer of irrigated water and quantifying the amount of ET occurring in an area provides water managers a valuable tool for quantifying water consumption.

ET is difficult and expensive to measure on an operational basis. The weather conditions of a given area determine, to a large extent, the amount of energy available for evaporation while soil moisture and crop cover determine how that available energy will be used (Wright 1990). Traditionally water managers have used reference ET and reference ET based crop coefficients (K_c) to assess how much of the available energy is utilized in ET.

The reference ET based crop coefficient method was developed for optimal growing conditions, which can overlook actual stressed crop conditions. The crop coefficient method is also limited in its ability to describe spatial variability; therefore, it can only give highly accurate estimates over medium-scale areas (multiple fields).

In order to increase the utility of ET estimates, water planners must acquire data over large areas and over long periods of time, such as entire water seasons. It is also

important to have capability to estimate ET from individual fields or water holdings. ET can be estimated in various ways and at varying spatial and temporal time scales. Direct measurement techniques, while well documented, cannot provide sufficiently large spatial data and are not well suited for watershed level management; however, direct measurement techniques do provide vital information for model calibration and crop coefficient development. Considering the large spatial and temporal variation in the parameters controlling ET processes, it is not surprising that Remote Sensing (satellite) and GIS-based applications have become powerful tools in large scale ET calculation in the arid western United States.

1.1. Problem Statement

The energy balance method based on remote sensing techniques requires radiation information in the visible and near infrared wavelengths, as well as in the thermal infrared wavelengths. Data collected from satellites within the thermal infrared wavelength is critical for surface temperature determination and accurate estimation of the soil and sensible heat fluxes used in energy balance. Thermal data have been available from satellites since 1982 with the launch of Landsat 4. Since that time, thermal data have been available from several different satellites. In 2003, the Landsat 7 satellite was severely damaged leaving Landsat 5 as the remaining Landsat satellite available for obtaining high-resolution spatial thermal data. The Landsat 5 satellite is well past its planned operational life of ten years and to date no concrete plans have been made for replacement with Landsat-resolution satellites equipped with high spatial resolution thermal imagers. At the earliest, any future Landsat satellite equipped with a thermal sensor would be launched in 2011 (Irons, J. NASA 2006 Press conference).

Several satellites exist which are equipped with thermal imagers but none can compare with the utility and spatial and temporal resolution of Landsat. The Advanced Spaceborne Thermal Emission and Reflection Radiometer (ASTER), for example, is equipped with a reasonable high-resolution thermal sensor (90 by 90m), but images from ASTER have limited and intermittent coverage. NASA's Moderate Resolution Imaging Spectrometer (MODIS) has thermal capabilities but lacks vital spatial resolution with

thermal images at the 1 by 1km resolution. This makes it impossible to analyze ET fluxes within individual fields.

With the oncoming gap in thermal information, an alternative method for obtaining accurate ET estimates using only the high resolution visible and near infrared wavelengths of alternative satellites would be a valuable tool for water resource managers. Spectral combinations of the visible and near infrared bands can be used to calculate vegetation indices that in turn can be coupled with methods for determining evaporative losses from the soil surface using soil water balance to produce estimates of total ET. This combination could provide a useful remote sensing based tool for obtaining accurate estimates of ET between image dates and for entire growing seasons.

1.2. Objectives

- The first objective of this study was to develop and test a method for combining basal crop coefficients (K_{cb}) derived from the normalized vegetation index (NDVI), or other index derived from the short wave bands, for crops located in southern Idaho with K_e derived via the FAO 56 dual crop coefficient procedure for estimating the evaporation component, K_e . K_e is added to the K_{cb} obtained from NDVI to produce the total crop coefficient K_c . Account will be given for precipitation and irrigation events in determination of K_e using soil water balance procedures.
- The second objective of this project is to examine possible methods for the automatic selection of the cold and hot pixel selection process used in the calibration of METRIC. This will provide users having little background in energy balance physics with an accurate method for anchor pixel selection and model usage. This method will improve estimates in the soil and latent heat fluxes used to complete the energy balance.

1.3. Study Area

The study area is the Magic Valley located in south central Idaho. The area is a major agricultural area having a wide range of crops. For this study the major crops of

alfalfa, potatoes, beans, corn, sugar beets, spring grain, and winter grain were analyzed based on a satellite based crop classification conducted in years 2000 (Tasumi et al 2003). The major methods of irrigation within the Magic Valley are center pivot, furrow irrigation, wheel line, and hand line irrigation systems. Water is collected from a combination of surface water from the Snake River and groundwater from the underlying Snake River Aquifer. The area has a semiarid climate and receives a mean average precipitation of 280 mm.

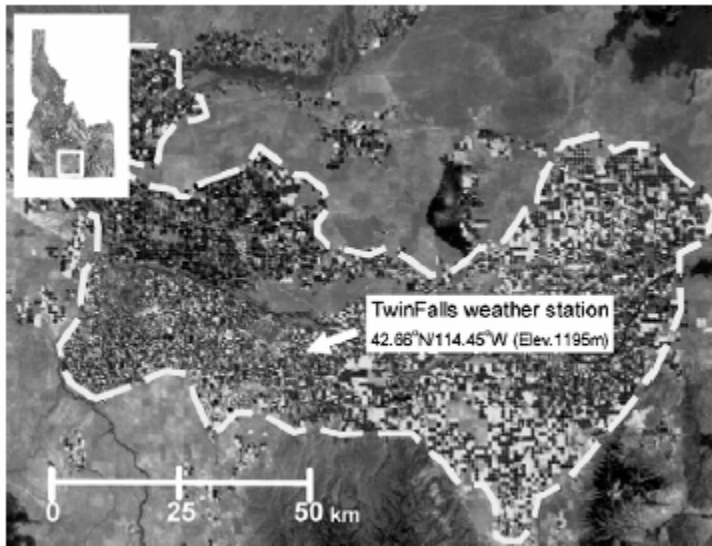


Figure 1.3-1 Magic Valley agricultural area in Southern Idaho (Taken from Tasumi et al, 2007)

Extensive research in crop ET within the Magic Valley has been carried out for many years, and significant lysimeter and weather data collected for many years make the area well suited for continued ET studies (Wright et al 1972, Wright 1982, Allen et al 1989). The study was conducted using year 2000 Landsat 5 and Landsat 7 images obtained over the Magic Valley (Path 40 Row 30). A total of 12 images were available for the analysis.

2.0 LITERATURE REVIEW

2.1. Evapotranspiration Theory

ET is the combination of evaporation from the surface and transpiration from plants. The term ET can be used synonymously with consumptive use, and is a vital component of the hydrologic cycle. Its role and quantification within the hydrologic cycle can be particularly important in arid climates as well as other parts of the world where water resource reallocation is necessary to accommodate expanding populations, and changing land uses. An understanding of the processes involved with ET is becoming increasingly vital for the proper planning and operation of water resource projects (ASCE, 2007).

Evaporation from soil surfaces makes up a significant portion of the total ET occurring from a given land surface. The process of evaporation requires energy and is the process of changing the state of liquid water to a gaseous state. The amount of evaporation occurring from a land surface or water body is governed mainly by the amount of energy available at the surface to facilitate the change of state coupled with ability of the surrounding air to transfer the wet air to the atmosphere.

Plants take up nutrients and water through their root systems and the water molecules taken up are lost as vapor, through the plants leaves in the process of transpiration. Nearly all of this vaporization of water occurs within the plants leaves and the vapor exists into the atmosphere through the plants stomata. The stomata can open and close releasing lesser amounts of vapor in times of water shortage or plant stress. The amount of transpiration occurring is strongly related to crop characteristics and environmental conditions. Through the transpiration process some water is retained within the plant tissue, but the amount is sufficiently small to permit its neglecting in total ET estimation. Jensen (1968) observed that the total amount of water retained within the plant tissue is less than 1% of the total growing season ET.

Because it is very difficult to distinguish between the processes of evaporation and transpiration, measurement techniques look at the combined process of total ET. At

varying times of the year one process may play a larger role than the other in the process of transferring water vapor to the atmosphere. As seen in Figure 2.1-1 early in the year when a crop has yet to develop, the majority of the total ET occurring is due to evaporation from the ground surface. As a given crop develops a larger percentage of the total ET is represented by crop transpiration.

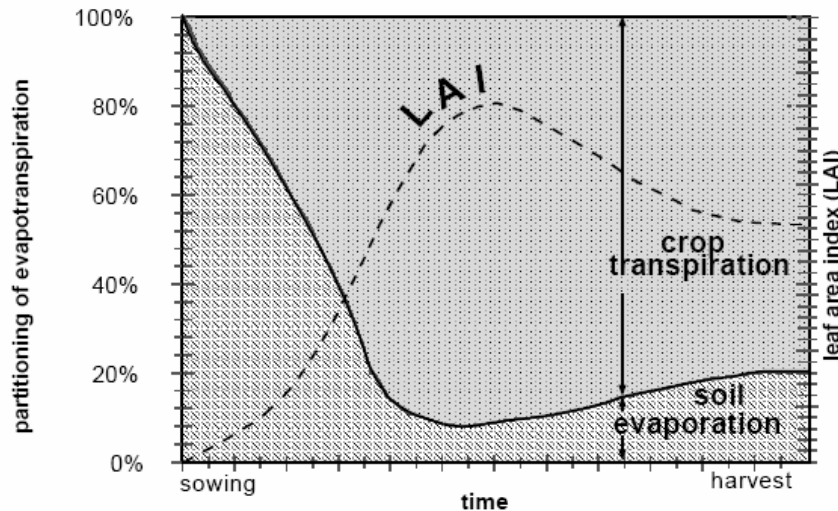


Figure 2.1-1 Partitioning of evaporation and transpiration over an entire growing season (following FAO 56 Allen et al 1998)

The ET process is controlled by the combination of water supply for evaporation, energy available to vaporize the water, air humidity, and the ability of the surrounding air to transport the vapor away from the surface. A useful concept in the analysis of ET is the potential ET. The potential ET is defined as the amount of ET which can occur under a given climatic and atmospheric condition, where water supply is not limited. The potential ET can be thought of as the maximum amount of ET possible given an area's soil, plant, and atmospheric conditions. The units of ET are generally expressed as a unit depth over a given time (ex. mm/day, mm/year).

Reference Evapotranspiration

Because crop surfaces rarely remain wet for long periods of time, the potential ET has limited usefulness. In 1968 Jensen introduced the use of reference crop ET which refers to the rate of ET occurring from a reference surface which again is not limited by

water supply. Typically the reference ET is determined for a hypothetical clipped grass or alfalfa crop. The determination of reference crop ET identifies the evaporative power of the atmosphere at a given location, on a typical reference crop surface (Allen et al, 1998). The reference ET (ET_r) is calculated using weather data collected at or near the area of interest and is then used as a reference to estimate specific crop evapotranspiration using crop coefficients.

The evolution of methods for ET_r calculation has been a constant process over the last half a century. Major estimation methods have been utilized which are based on radiation physics, aerodynamic transport, open water pan evaporation, and various forms of the Penman formulation (Penman, 1948). Some of the most trusted estimation techniques use a combination method using both energy balance concepts as well as aerodynamic equations.

In an effort to develop a standardized method for calculating ET_r , the Irrigation Association (IA) called on the American Society of Civil Engineers (ASCE) in 1999, to determine a benchmark reference evapotranspiration equation that could be used by federal and private entities throughout the United States. As a result of this request the Evaporation in Irrigation and Hydrology Committee – Environmental and Water Resources Institute (ASCE-ET) set out to test current reference ET equations used throughout the United States and the World.

The ASCE-ET evaluated the results of ET estimates from a total of 13 equations representing data from 36 sites and a total of 61 test years (Allen et al, 2002). With a combination of over a hundred years of experience using the various reference ET equations, the ASCE-ET members quickly established the ASCE Standardized Penman Monteith equation. While many equations exist the ASCE Standardized Penman Monteith equation (Allen et al, 2005) has produced strong results and is given by:

$$ET_r = \frac{0.408\Delta(R_n - G) + \gamma \frac{C_n}{T + 273} u_2 (e_s - e_a)}{\Delta + \gamma(1 + C_d u_2)} \quad (1)$$

Where Δ is the slope of the saturation vapor pressure curve (kPa/°C), R_n is net radiation (MJ/m²/day), G is the soil heat flux (MJ/m²/day), γ is the psychrometric constant (kPa/°C), T is the mean air temperature (°C), u_2 is the mean wind speed measured at 2 meters above the ground surface (m/s), e_s is the saturation vapor pressure (kPa), e_a is the actual vapor pressure of the air (kPa), and C_n and C_d are coefficients which vary depending on the time scale used for the calculation as well as the type of reference crop (ASCE-EWRI, 2002).

The ASCE-ET defined two standardized reference surfaces, one representing a short crop with a vegetation height of approximately 0.12 m, and the other surface representing a tall crop with a height of approximately 0.5 m (ASCE-EWRI, 2002). The two reference surfaces were selected due to their similarity to the commonly used grass and alfalfa references used throughout the world as well as their widespread applicability to both agricultural and landscape irrigation projects, as stipulated in the original IA request (Allen et al, 2002).

As seen in Figure 2.1-2, when coupled with accurate weather data, the ASCE standardized Penman-Monteith equation produces highly accurate estimates of actual crop ET. The comparisons made in Figure 2.1-2 were compiled using hourly weather data from the Twin Falls Idaho weather station near Kimberly Idaho (Allen et al, 2006). Measurements of alfalfa ET were collected by Dr. James Wright using a precision weighing lysimeter. The first plot on the left is constructed using data from a cloud free, September 4, 1990. The plot on the right shows data collected from the same lysimeter several days later with cloud cover occurring later in the day. The ability of the equation to respond to rapid changes in weather parameters and reproduce precise lysimeter ET measurements provides confidence when accurate weather data are available.

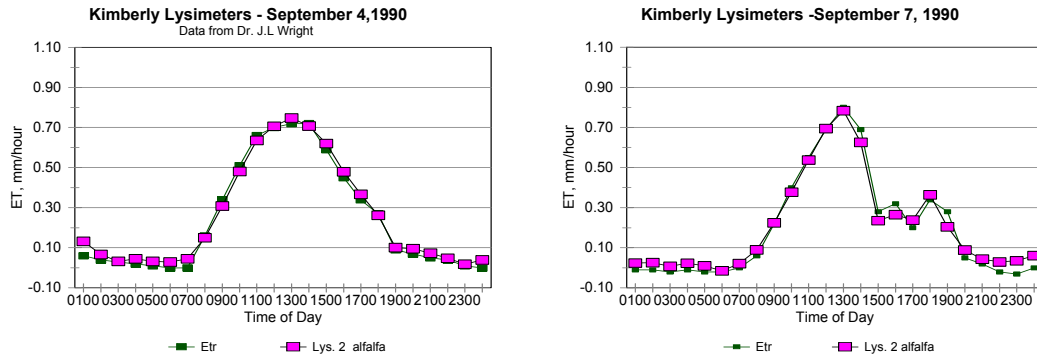


Figure 2.1-2 Performance of the ACSE Standardized Penman Monteith equation for calculating hourly alfalfa reference ET (taken from Allen 2006, Lysimeter data from Dr. J.L. Wright, USDA-ARS)

2.2. Crop Coefficient ET Estimation Methods

Crop coefficients were first defined by Jensen (1968) for agricultural practice and are simply experimentally derived ratios of actual measured ET from a specific crop to the ET of a reference crop. Reference ET (ET_r) is calculated from weather data for a defined reference crop such as alfalfa or grass, as described in chapter 2.1, and then the crop coefficient (K_c) relates the ET for the specific crop to the ET_r reference. This type of ET estimation has been widely applied by water managers for its simplicity coupled with its respected accuracy and is given by:

$$ET_c = K_c ET_r \quad (2)$$

where ET_c is the crop ET, K_c (ET_c/ET_r) is obtained from predetermined crop specific table values based on extensive research, which are sometimes adjusted for local climatic conditions and ET_r is the reference crop ET generally calculated using the ASCE Standardized Penman Monteith equation, or FAO Penman-Monteith equation, and local hourly and daily weather data (Allen et al 1998, ASCE EWRI 2005).

The method requires meteorological weather data and specific crop type information and is often referred to as the single crop coefficient method (Allen et al,

1998). This crop coefficient procedure does not explicitly consider the effects of evaporation from the soil surface after wetting events.

2.3. FAO 56 dual Crop Coefficient Method

The FAO 56 dual crop coefficient method provides a procedure for estimating the evaporative effects of precipitation and irrigation events on the overall crop coefficient. In the dual method, the crop coefficient is divided into two coefficients representing crop transpiration (K_{cb}), and evaporation from bare soil (K_e) (Allen et al. 1998).

$$ET_c = (K_s K_{cb} + K_e) ET_r \quad (3)$$

Here K_{cb} represents the basal crop coefficient and is defined as the ratio of the crop ET to the reference ET, when the soil surface is dry but there is sufficient water within the root zone for transpiration to occur at the potential rate (Allen et al, 1998). The factor K_s is a water stress coefficient applied to the basal crop coefficient which describes any effect of water stress on the crop transpiration. The evaporation component K_e is obtained by conducting a water balance in the upper most layer of the soil profile. It is from this upper layer, usually taken as the top 0.1 to 0.15m of the soil (Allen et al, 1998), that most of the soil evaporation included within ET occurs.

Figure 2.3-1 shows a representation of a generalized crop curve developed by Dr. James Wright with the USDA-ARS near Kimberly Idaho (Wright, 1982, 1990). The dark solid line in the figure shows the basal coefficient, K_{cb} and the sharp spikes drawn as dashed lines represent K_e . The two curves combine to form the total K_c . It becomes apparent that the magnitude of K_e can be significant during periods of low crop cover. The average value of the K_c curve can be seen drawn in as a dotted line and labeled K_{cm} . As expected the average K_c curve lies slightly above the K_{cb} curve.

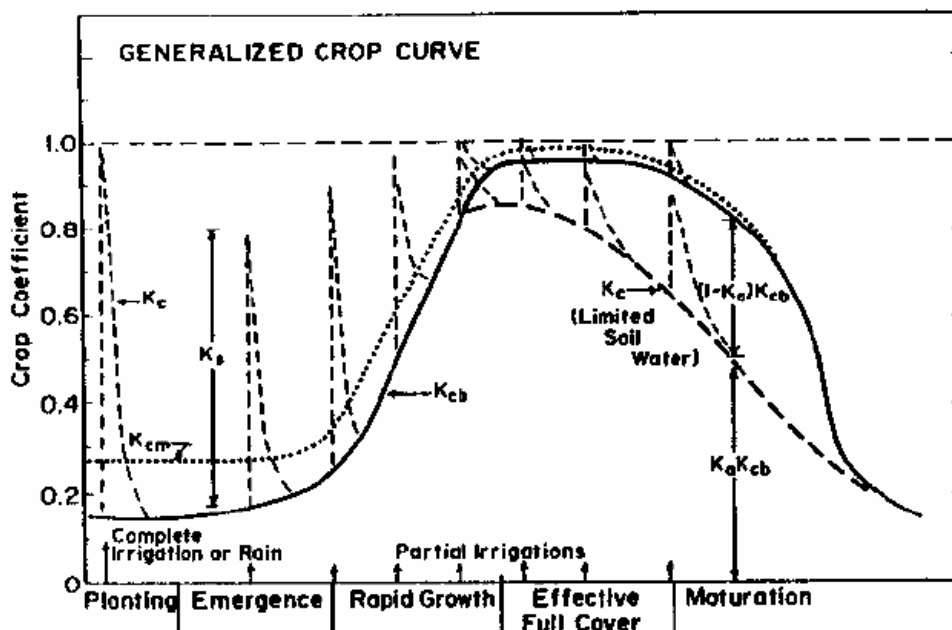


Figure 2.3-1 Generalized crop coefficient curve showing the evolution of the crop coefficient throughout the growing season, the basal K_c , and the effects of evaporation due to wetting events. (Taken from Wright, 1982, 1990)

The dual crop coefficient method is used when daily ET values are needed and when the effects of wetting events are under consideration. The dual crop coefficient method has been shown to give precise estimates of ET by incorporating evaporation from bare soil due to irrigation and precipitation events (Allen et al, 2005). Splitting the total K_c into the plant and evaporation components better captures the impacts on total ET of soil water holding capacity, irrigation and precipitation frequency.

2.4. Point Based ET measurements

Evapotranspiration is very difficult to accurately measure. While several methods do exist, they are typically very expensive and require significant amount of experience and training. Routine measurements are not practical, and usually limited to measurements made by trained researchers for the validation of the more indirect measurement techniques discussed above (Allen et al, 1998).

The most trusted method for the direct measurement of ET fluxes is the use of weighing lysimeters. Weighing lysimeters are isolated tanks of similar soil and crop type,

where water input and output are well controlled. The amount of ET is determined by the changes in weight as water evaporates. While highly accurate for time steps as short as an hour, the accuracy of the lysimeter is directly dependent upon expert set up and maintenance (Allen et al, 1991).

Other techniques include the Bowen ratio and eddy covariance. Both require a high level of expertise and technical instrumentation. The Bowen ratio technique is considered the most practical and accurate micro-meteorological method (ASCE-EWRI, 2005), but can overestimate ET when the readily available water in the root zone is low and when daily ET rates are greater than 6 mm per day.

All point based ET measurement methods provide valuable information to water resource managers in quantifying consumptive use. They are limited however to experienced technicians, and their ability to accurately assess the complex spatial variation in ET processes.

3.0 THEORY OF THE REMOTE SENSING OF ET

3.1. Satellite Based Surface Energy Balance Methods

Satellites can collect data over a given surface relatively frequently and as in the case of the Landsat 7 satellite, at a 30 by 30m resolution in the short wave spectrum and 60 by 60m resolution in the thermal spectrum. This, coupled with meteorological data from a given area, can combine for accurate estimates of ET over large watersheds and for individual fields. This method of water consumption quantification has been extremely valuable in the intermountain west by assisting water managers in hydrologic modeling, quantifying water rights, estimating aquifer depletions from groundwater extraction, and quantifying the use of water by natural systems (Allen et al, 2007b).

Many of the remotely sensed data techniques are based on the surface energy balance and have been considered the most accurate methods for estimating ET over large spatially varying areas and at high resolution (individual fields). Of the energy balance methods the Surface Energy Balance Algorithms for Land (SEBAL) (Bastiaanssen et al, 1998), and Mapping ET at High Resolution using Internalized Calibration (METRIC) (Allen et al, 2002) have been extensively used and tested for operational accuracy in the western United States (Bastiaanssen et al, 2005, Allen et al 2007a,b). Other models developed for remote sensing techniques and energy balance methods are the Two Source Energy Balance (TSEB) (Norman et al, 1995) and the Surface Energy Balance System (SEBS) (Su et al, 2002). Both TSEB and SEBS have not been tested for operational accuracy.

All energy balance models are based on determining the energy available to change the state of water from liquid to vapor from the energy balance equation given by:

$$LE = R_n - G - H \quad (4)$$

where LE is the latent heat of vaporization available for ET (W/m^2), R_n is the net radiation (W/m^2), G is the soil heat flux (W/m^2), and H is the sensible heat flux (W/m^2).

Remotely sensed data from satellites are well suited for energy balance based determination of ET. Satellite data include valuable information for both short wave and long wave radiation reflected and emitted from the earth's surface, where the net fluxes of these radiation types and the surface are the primary sources of the energy required to change water molecules from liquid to vapor. Each term in the energy balance equation is calculated in both SEBAL and METRIC on a pixel-by-pixel basis. The net radiation at the surface providing the energy available for ET is calculated by:

$$R_n = (1 - \alpha)R_{s\downarrow} + R_{L\downarrow} - R_{L\uparrow} - (1 - \varepsilon_0)R_{L\downarrow} \quad (5)$$

where $R_{s\downarrow}$ is the incoming short wave radiation (W/m^2), $R_{L\downarrow}$ is the incoming long wave radiation (W/m^2), $R_{L\uparrow}$ is the outgoing long wave radiation (W/m^2), α is the surface albedo (dimensionless), and ε_0 is the surface thermal emissivity (dimensionless).

The soil heat flux, G is defined as the heat storage into the soil and is calculated in METRIC and SEBAL by first calculating the ratio of G to R_n . In METRIC this is normally done utilizing the relationship developed Tasumi et al., (2003) given as:

$$\frac{G}{R_n} = 0.05 + 0.18e^{-0.521LAI} \quad (6)$$

when LAI (leaf area index) is greater than or equal to 0.5 and

$$\frac{G}{R_n} = 1.80 \frac{(T_s - 273.16)}{R_n} + 0.084 \quad (7)$$

when LAI is less than 0.5 m^2/m^2 . The relationships for the G (W/m^2) and R_n (W/m^2) were developed specifically for the western United States, using soil heat flux data collected by Dr. J.L. Wright (USDA-ARS, ret.) near Kimberly Idaho. The ratio in equations 6 and 7 is a function of the surface temperature T_s (K) and LAI (m^2/m^2) (the leaf area index). The LAI is equal to the total one-sided leaf area per unit area of ground surface and was calculated within METRIC by:

$$LAI = -\frac{\ln\left(\frac{0.69 - SAVI_{ID}}{0.59}\right)}{0.91} \quad (8)$$

Here $SAVI_{ID}$ is the soil adjusted vegetation index which is another commonly used dimensionless vegetation index and is discussed later in section 3.4. The subscript ID on SAVI refers to the use of SAVI calculation parameters which have been calibrated for Southern Idaho soils (section 3.4). Once this ratio from equation 6 or 7 is determined, G is simply calculated by multiplying the ratio by the previously determined value of R_n for each pixel within the image.

The most difficult term in the energy balance equation to calculate using remote sensing is the sensible heat flux, H (W/m^2). The sensible heat flux is given by:

$$H = \frac{\rho c_p dT}{r_{ah}} \quad (9)$$

where ρ is the density of air (kg/m^3), c_p is the specific heat ($1004 J/kg/K$), dT is the vertical temperature difference between two heights (K), and r_{ah} is the aerodynamic resistance to heat transport (s/m). In this formulation, dT is the near surface air temperature difference between two elevations (Figure 3.1-1).

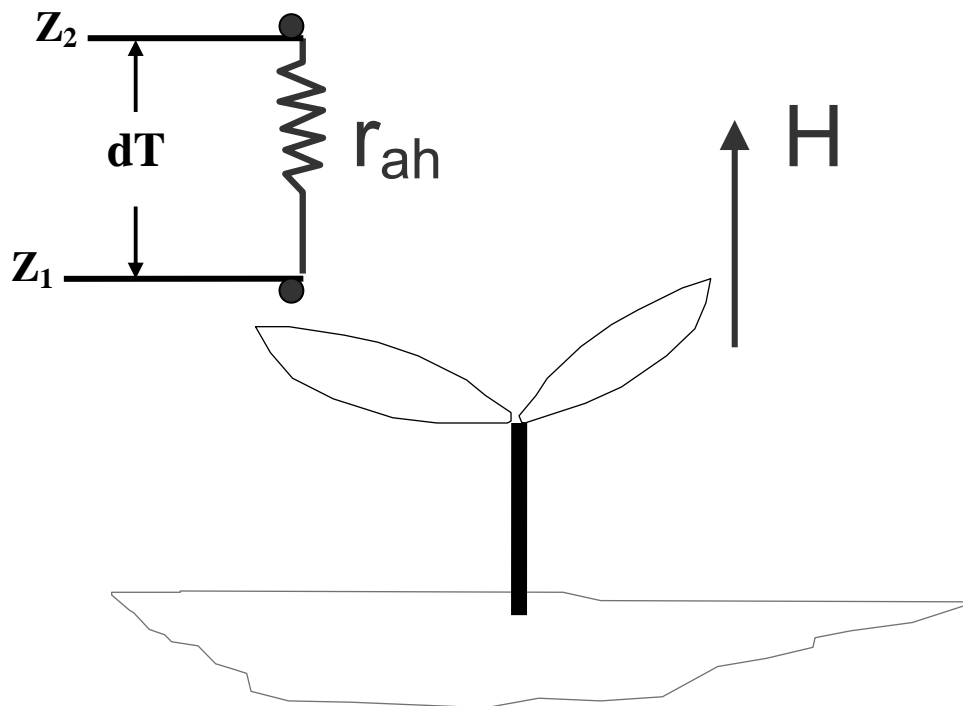


Figure 3.1-1 Sensible heat flux diagram showing the near surface temperature difference dT (Taken from Allen)

This temperature difference floats above the surface and is used because of the difficulty in estimating precise surface temperatures using remote sensing due to radiometric scattering by atmospheric constituents and biases in the satellite sensors. Furthermore, the surface temperature measured by the satellite is not the same as the aerodynamic temperature needed for the heat transport process and work by Kustas et al. (1994), Norman et al. (1995), and Qualls and Brutsaert (1996) has shown that the temperature measured by radiometric means can deviate significantly from the aerodynamic temperature. In addition, ground based air temperature measurements are sparse and can not be used to explain the regional distribution of temperatures over varying land covers. Therefore, rather than parameterize both aerodynamic temperature and air temperature over an area, the simple temperature gradient dT is used, where dT 'floats' above the surface between two heights Z_1 and Z_2 (Allen et al, 2007a).

The use of dT allows for a method that is indexed from T_s but does not depend upon the absolute value of T_s . Bastiaanssen (1995) suggests that a strong linear relationship exists between dT and the radiometric surface temperature (Figure 3.1-2)

(Basstiaannssen et al (1998, 2005), Allen et al (2007a), Jacob et al (2002). The relationship can be expressed as:

$$dT = b + aT_s \quad (10)$$

where the units of dT are in degrees K, T_s is the radiometric surface temperature (K), and the coefficients a (K/K) and b (K) are empirical constants. While the linearity of the relationship between the radiometric surface temperature and the near surface temperature difference, dT , has been the topic of some debate (Norman et al, 2005), it is not the purpose of this thesis to prove its linearity. Future PhD work at the University of Idaho may more precisely analyze the linearity of the relationship and accompanying accuracy of ET estimates from METRIC based upon this assumption.

To determine the values of the coefficients a and b used in equation 10, METRIC and SEBAL use two “anchor pixels” where accurate values of H can be estimated and utilize an iterative process for determining dT and r_{ah} . METRIC does this by selecting a “cold” anchor pixel at a location where the maximum ET and therefore minimum H is expected to occur. In METRIC this pixel is selected from an actively growing agricultural field and allows for the determination of the dT at the cold pixel (K) of:

$$dT_{cold} = \frac{H_{cold} r_{ah_cold}}{\rho_{cold} c_p} \quad (11)$$

where r_{ah_cold} is the aerodynamic surface resistance to heat transport (s/m), ρ_{cold} is the density of air at the cold pixel (kg/m³), c_p is the air specific heat (1004 J/kg/K), and H_{cold} is determined from the previous calculations of R_n (equation 5), G (equations 6 and 7), and ET_r (equation 1) as: $H_{cold} = R_n - G - 1.05 * \lambda * ET_r$, where λ is the latent heat of vaporization defined in equation 16 (J/kg) and where R_n and G represent specific values for the cold pixel.

In a large image (Landsat images are 185 by 185km) it is possible that some fields will have a wet soil surface underneath the crop canopy, which can increase the total ET up to 5% above the computed reference ET (Allen et al 2006a). For this reason METRIC applies the factor of 1.05 to the ET_r for the H_{cold} . Also, it is noted that the use of ET_r at

the cold pixel in the calibration process, helps to minimize the impact of regional advection and wind speed on ET estimates at the moment of the satellite image (Allen et al, 2007). The utility of ET_r in reducing error in other energy balance parameters such as R_n , is discussed later in section 3.2. The aerodynamic resistance used in the dT_{cold} equation is then computed iteratively for stability correction, with the first iteration assuming neutral stability using the friction velocity determined using a logarithmic wind law. With the dT calculated at the cold pixel and the associated temperature at that pixel, the lower point on the dT versus surface temperature is defined (Figure 3.1-2).

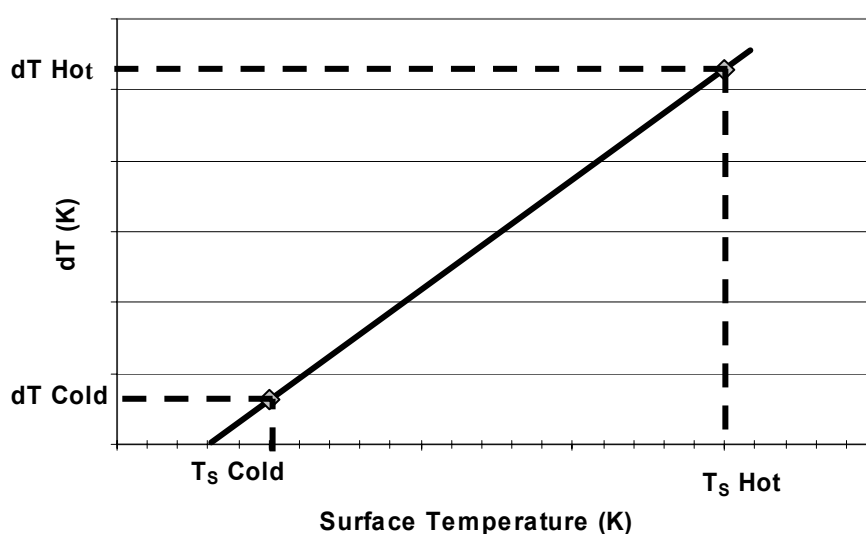


Figure 3.1-2 Linear relationship between dT and T_s used in the METRIC calibration process for the sensible heat H .

The METRIC calibration process also requires the selection of a “hot” anchor pixel (the second point on the dT versus T_s relationship seen in Figure 3.1-2), where it can be assumed that H is at a maximum value (i.e. $ET = 0$). This pixel is selected from a dry bare agricultural field within the image. If precipitation events have occurred within the last one to ten days, a soil water balance is conducted to determine if the ET can really be assumed to be equal to or 0 or near zero. In the presence of antecedent soil moisture conditions, some evaporation from the soil will exist and the value of ET for the hot pixel must be adjusted accordingly. Details for this adjustment are given in Allen et al, (2007a). The dT for the hot pixel is then given by:

$$dT_{hot} = \frac{H_{hot} r_{ah_hot}}{\rho_{hot} c_p} \quad (12)$$

where dT has units of degrees K, r_{ah_hot} is the aerodynamic resistance to heat transport at the hot pixel (s/m), ρ_{hot} is the air density at the hot pixel (kg/m^3), c_p is the specific heat (1004 J/kg/K), and with $H_{hot} = R_n - G - \lambda * ET_{hot}$. In most cases ET_{hot} is assumed to be zero and from a dry agricultural pixel with no vegetation cover and a dry soil surface layer. However, as mentioned previously, antecedent soil moisture conditions must be considered by running a soil water balance at the hot pixel. The FAO 56 (Allen et al, 1998) discussed latter, gives a procedure for conducting this water balance to determine the amount of residual evaporation likely to occur from any bare soil due to precipitation. Both the cold and hot anchor pixels used in METRIC are selected within about 20 km of the location of weather station from which precipitation and other weather parameters are measured, to reduce differences in wind speed and ET_r among the locations.

With the two equations for dT_{cold} and dT_{hot} the coefficients a and b are then calculated using:

$$a = \frac{dT_{hot} - dT_{cold}}{T_{S_hot} - T_{S_cold}} \quad (13)$$

and

$$b = dT_{hot} - aT_{S_hot} \quad (14)$$

Where T_{S_hot} is the radiometric surface temperature sampled at the hot pixel location (K), and T_{S_cold} is the surface temperature of the cold pixel (K). Again a has units of K/K and b has units of degrees K.

With both a and b , the resulting dT can be used to determine an improved estimate of r_{ah} and an iterative process on boundary layer stability correction (Allen et al., 2007a) follows until successive values for dT and r_{ah} have stabilized.

The latent heat loss from the surface caused by ET , LE (W/m^2) can now be determined using the energy balance equation described by equation 4 and the estimates

of R_n , G , and H . The instantaneous ET, ET_{inst} (mm/hr) at the time of satellite over pass is then calculated by:

$$ET_{inst} = 3600 \frac{LE}{\lambda} \quad (15)$$

Where λ (J/kg) is the latent heat of vaporization which is the heat absorbed when one kilogram of water evaporates. This can be calculated following Harrison (1963) as a function of surface temperature, T_s (K) as:

$$\lambda = (2.501 - 0.0023(T_s - 273)) * 10^6 \quad (16)$$

To effectively select reasonable cold and hot anchor pixels, the user must be skillful and understand the principles associated with the energy balance. Often, users of the METRIC program will not have sufficient background in radiation physics, and aerodynamic principles; and therefore, have difficulty in pixel selection and are often unsure of the accuracy of results. Methods to make the calibration process more automatic and built into METRIC would be advantageous and are discussed latter in chapter 9.

3.2. METRIC Calibration Strategy Using ETr

Uncertainties in ET estimates derived using the surface energy balance equations can and do exist from error and bias inherent in the calculation of the various components of the energy balance. These biases can include error due to atmospheric correction, albedo calculation, calculation of R_n , surface temperature, vertical air temperature gradient (dT), the soil heat flux, aerodynamic resistance and associated buoyancy impacts, wind speed field, and extrapolation from instantaneous ET to daily and longer periods (Allen et al, 2006 and 2007a). Many of the biases inherent in the estimation of the various components of the energy balance equation (R_n , G , and H etc.) are removed from the ET estimates, via the METRIC internal calibration using calculated hourly reference ET (ET_r) (Allen et al, 2006, 2007a).

Once the instantaneous ET at the time of the satellite over pass is determined using equation 15, METRIC calculates the reference ET fraction using ET_r and weather data by:

$$ET_{rF} = \frac{ET_{inst}}{ET_r} \quad (17)$$

Where ET_{rF} is the reference ET fraction, ET_{inst} is the instantaneous ET calculated using equation 15, and ET_r is the reference ET calculated using hourly weather data collected within the study area and the ASCE Standardized Penman Monteith equation (EWRI-ASCE, 2002). The ET_{rF} is calculated for each pixel within the image, and is the same as the traditional crop coefficient, K_c . The use of ET_r in the METRIC internal calibration process provides congruency with the traditional crop coefficient based ET_r methods (Allen et al., 2006). While each pixel within a given image has an individual value of ET_{inst} , the ET_r used in the calibration process has the same value for each pixel. With the use of hourly weather data and therefore ET_r , the construction of 24 hour, monthly, and seasonal ET maps are constructed.

3.3. Testing of METRIC

METRIC has been tested throughout much of the western United States, with operational applications in southern Idaho, southern California, and New Mexico. Currently METRIC processing is underway in both Nebraska and Colorado. METRIC has been applied by universities, state, federal, and private entities. Since 2000, the department of Idaho Water Resources has utilized METRIC derived ET maps to assess water rights compliance, transfers, and allocation (Morse et al., 2004). Recently the Idaho Department of Water Resources ET mapping program using METRIC, was recognized as one of the Top 50 innovations in American government for 2007 by the Ash Institute for Democratic Governance and Innovation (Rocchio, 2007). The institute is part of Harvard University's Kennedy School of Government.

Comparisons with METRIC ET estimates with ET measurements from precision weighing lysimeters has been carried out with data collected by Dr. James L. Wright of the USDA-ARS near Kimberly, Idaho as well as lysimeter data collected by Dr. R.W.

Hill of Utah State University, within the Bear River Basin at Montpelier, Idaho. Details of the lysimeter comparisons along with the discussion of Landsat image pixel selection and associated scaling considerations can be found in Allen et al., (2007b). Seasonal differences between METRIC and the precision weighing lysimeters was 4% for 1985 Bear River Basin data and less than 1% for a sugar beet crop for 1989 Kimberly data (Allen et al., 2007b). While good agreement with a handful of lysimeter observations does not guarantee exact spatial ET calculation, these comparisons coupled with the extensive operational applications that tend to produce ‘crop coefficient curves’ that correspond relatively closely with those made by independent, ground based processes (Allen et al., 2007b) such as with the USBR Agrimet program and a state wide independent study by Allen and Robison (2007) (see Appendix A), do provide strong confidence in ET estimates, provided proper model calibration for each image.

3.4. Crop Coefficients from short wave satellite data

Relationships between crop coefficients and remotely sensed vegetation indices within agricultural areas have been well documented beginning with Neale et al., (1989), and Choudhury et al., (1994). Vegetation indices are dimensionless quantities that indicate the relative abundance of non-stressed green vegetation. Vegetation indices have been used to analyze the percentage of green cover, leaf area index, and chlorophyll content (Jensen, 2005). When compared to remote sensing based ETrF measurements throughout the growing season, a relationship becomes apparent (Figure 3.4-1).

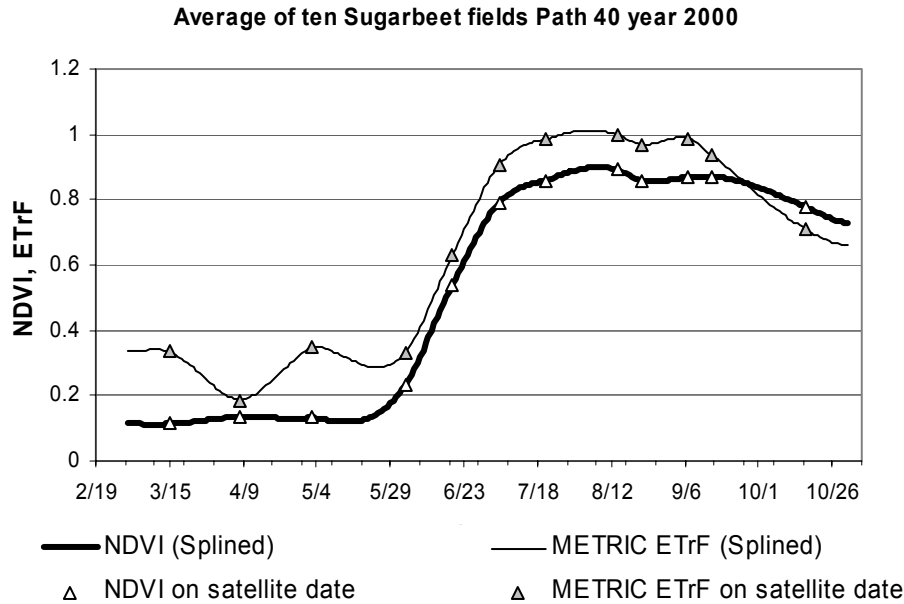


Figure 3.4-1 Comparison of remotely sensed average ETrF and average NDVI (computed at the surface) from ten randomly sampled Sugar Beet fields for 12 image dates throughout the growing season (Kc data from METRIC processing Tasumi, 2003, reprocessed for this study).

The Normalized Difference Vegetation Index (NDVI) is one of the most common vegetation indices used in ET analyses (Neale et al. (1989), Choudhury et al. (1994), Hunsaker et al. (2003), Allen et al., (2003), (2007)). NDVI is based on the relationship between the near-infrared and red reflectances, which provides a measure of green healthy vegetation (Jensen, 2005). NDVI is calculated using remotely sensed satellite data as:

$$NDVI = \frac{\rho_{nir} - \rho_{red}}{\rho_{nir} + \rho_{red}} \quad (18)$$

where ρ_{nir} and ρ_{red} are the reflectance values within the near-infrared and red wavelengths. As discussed previously, atmospheric scattering and absorption of radiation occurs due to atmospheric constituents such as dust particles and water vapor. Much of the impact of the atmosphere is reduced in the calculation of NDVI due to the division by ρ_{nir} and ρ_{red} . However, some differences in atmospheric attenuation between the two

bands can create a difference between the NDVI determined at the satellite ($NDVI_{\text{satellite}}$) and the NDVI that would be determined with full correction of atmospheric effects ($NDVI_{\text{surface}}$).

Another popular vegetation index used in ET analysis is the Soil Adjusted Vegetation Index (SAVI), which has displayed valuable characteristics for K_c determination in its ability to reduce impacts of soil wetness on the index when plant cover is low (Huete, 1988; Huete et al, 1992; Jayanthi et al, 2007). SAVI is calculated in a similar fashion as NDVI with the addition of a canopy background adjustment parameter following Huete (1988) as:

$$SAVI = \frac{(1 + L)(\rho_{nir} - \rho_{red})}{\rho_{nir} + \rho_{red} + L} \quad (19)$$

where L is the canopy background adjustment parameter and ρ_{nir} and ρ_{red} are again the reflectance values within the near-infrared and red wavelengths. The typical value for L is 0.5, which was found by the originator of SAVI to minimize soil brightness variation (Huete, 1988). However, Tasumi et al., (2003), and Allen et al., (2007b) found L equal to 0.1 to best reduce the impacts of soil wetness on variation in southern Idaho soils. It is important to note that this value is near zero at which point SAVI reverts to NDVI.

While many indices exist and various types have been used in comparisons with crop coefficients, the Normalized Difference Vegetation Index has exhibited the most desirable characteristics in K_c comparison due to its tendency to ‘saturate’ at about the same Leaf Area Index ($LAI \approx 3$) as the K_c tends to saturate (Allen et al., in review). The vegetation indices LAI, NDVI, and SAVI all give an indicator of the amount of green biomass present in a given pixel. Past studies have shown that as crops develop the maximum K_c typically occurs when the amount of plant biomass reaches a certain point described by an LAI of 2.5 to 3 (Wright 1982). At this point any increase in total LAI and thus vegetation amount does not correspond to an increase in K_c . The same scenario occurs for the NDVI where the maximum NDVI of 0.85 to 0.9 occurs at roughly $LAI \approx 3$ even though plant biomass and actual LAI continues to increase.

This ‘saturation’ in NDVI can be seen in Figure 3.4-2, where peak values of $NDVI \approx 0.8$ to 0.9 are reached for nearly all occurrences of $K_c \approx 0.9$ to 1.0 , while the SAVI tends to avoid saturation when K_c first reaches 0.9 to 1.0 , meaning that as a crop reaches its maximum K_c , SAVI continues to sense increases in vegetation biomass. This can be problematic when fitting linear relationships to determine the crop coefficients and therefore $NDVI_{\text{at surface}}$ was used in this study. Furthermore; work conducted by Allen et al (2007) showed that the use of the $NDVI_{\text{satellite}}$ and the $NDVI_{\text{surface}}$ in K_c functions, gave nearly the same results and accuracy when estimating average K_c values for seasonal ET determination.

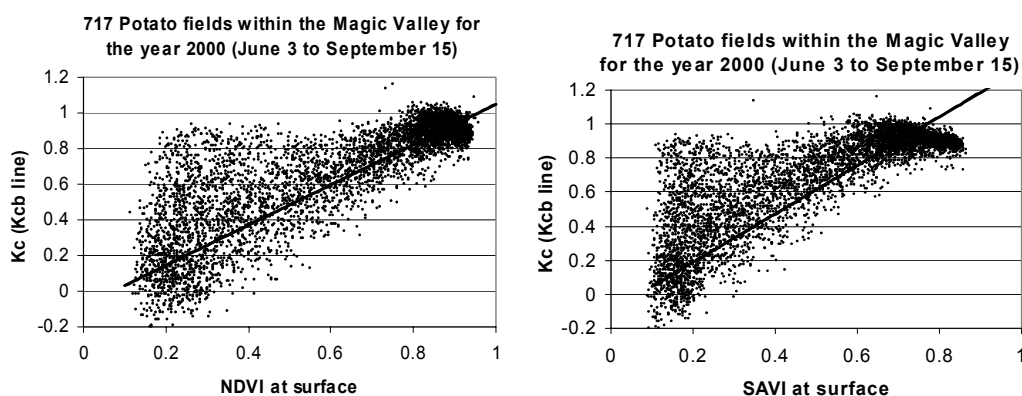


Figure 3.4-2 Comparison of NDVI and SAVI vegetation indices for determining crop coefficients (K_c data from METRIC processing Tasumi, 2003, reprocessed for this study).

In recent years several studies have suggested that a linear relationship exists between crop coefficients and vegetation indices (Allen et al 2003; Hunsaker, 2003; Calera et al, 2005; Duchemin et al, 2005; Jayanthi et al, 2007; Tasumi et al, 2007). Any crop coefficient estimated from NDVI can take the form:

$$K_c = a * NDVI + b \quad (20)$$

where a and b are calibrated constants. Two major factors exist for the strong linear relationship. The first is the high correlation between the NDVI and LAI or fraction of ground covered by vegetation, which in turn is directly related to the ET (Neale et al, 1989). As discussed above the NDVI also reaches its maximum value at roughly the

same time effective full cover is reached by a given crop. The point of effective full cover is often highly correlated with the peak value for relative ET represented by K_c (or ETrF).

3.5. Basal K_c from vegetation index

Tasumi et al, (2007) used a similar approach to estimate the ‘mean’ K_c , which includes the mean (average) effects of evaporation from bare soil. This method follows closely the single crop coefficient procedure discussed in the FAO 56. At any particular time however, the total crop coefficient can be greatly affected by the amount and frequency of evaporation occurring from wet exposed soil (Allen et al, 1998). Vegetation indices measure the amount of green biomass and can not be used to estimate variation in ET due to soil wetness (Tasumi, Allen, unpublished, 2007).

Because vegetation indices are highly correlated with plant biomass and LAI, we would expect K_{cb} versus NDVI relationships to be even more linear than ‘mean’ K_c vs NDVI, simply due to the fact that the transpiration component of ET is generally proportional to the amount of vegetation present. In a plot such as that shown in Figure 3.5-1, the triangular relationship between K_c (estimated from METRIC) and NDVI implies that a line representing K_{cb} (the basal K_c), should occur near the low side of the triangle. This line represents fields where the soil surface is dry but ET is occurring at the potential rate expected for the amount of vegetation present.

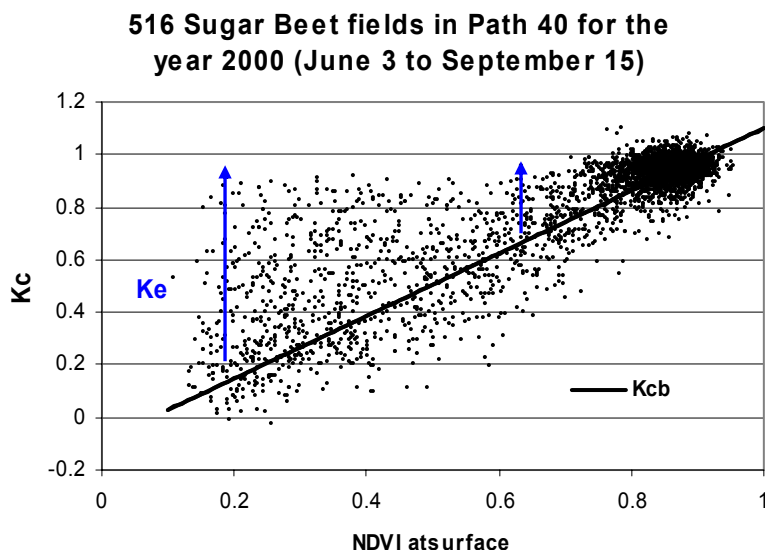


Figure 3.5-1 METRIC K_c (ETrF) versus NDVI showing separation of total K_c into the basal and evaporation components K_{cb} and K_e .

Figure 3.5-1 above, shows how the use of the FAO 56 dual crop coefficient method provides a framework to construct the total K_c by obtaining the basal component from NDVI, and then adding the evaporation component K_e . Points within the diagram lying above the K_{cb} relationship are experiencing an additional amount of evaporation due to surface wetting and points below the relationship correspond to locations where plant stress may be present due to under watering or other stress inducing process, or these may represent some normal random errors in the METRIC process for estimating K_c .

4.0 METHODOLOGY

4.1. Basal crop coefficients from NDVI

In order to examine the relationships between K_c and NDVI, image wide K_c values were sampled from K_c images generated using the energy balance based METRIC model (Tasumi, 2003 Lorite, 2005). Remote sensing energy balance models such as METRIC provide a unique opportunity to sample K_c from a large numbers of fields in the K_c vs NDVI analysis. In this study a total of 3,574 fields were sampled and utilized in the model development. METRIC has been tested throughout the arid regions of the Western United States (Tasumi et al, 2005, previously discussed in more detail in section 3.3), and produces high resolution K_c maps for which we have strong confidence provided the model is properly calibrated for each image. In lysimeter studies conducted using data collected from the USDA-ARS facility near Kimberly Idaho, Tasumi et al. (2005) found that the annual absolute difference between METRIC derived K_c and Lysimeter derived K_c averaged 0.05.

The METRIC model also has the NDVI function built into it and provided the NDVI images for comparison. METRIC produces NDVI and K_c images at a 30m by 30m pixel resolution. This allows sufficient resolution to sample information from specific fields, based on crop classifications, to develop crop specific K_c NDVI relationships. The specific crops analyzed for the study area were; potatoes, corn, beans, sugar beets, alfalfa, winter grains, and spring grains. Table 4.1-1 shows the total number of fields sampled within the study area for each specific crop type.

Table 4.1-1 Total number of fields sampled for each crop type within the Magic Valley during the year 2000.

Crop	# Fields	Crop	# Fields
Alfalfa	325	Spring Grain	546
Beans	432	Sugar Beets	516
Corn	474	Winter Grain	564
Potatoes	717		

While crop specific NDVI and ETrF data will be utilized in the development of the K_c vs NDVI relationships, a general relationship for all crop types will also be established and tested to determine if it can be applied to all major crops in southern Idaho without the need for specific classification of crop type. The general form of the relationship between K_{cb} and NDVI takes the form:

$$K_{cb} = a * NDVI + b \quad (21)$$

where a and b are again calibration constants. While a and b are locally calibrated, the use of the basal crop coefficient which are more representative of actual plant characteristics and not climate, should allow for regional and multi-year application. Also because the relationship represents primarily the crop transpiration component of the total ET, the relationships should be similar between crop types, thus increasing the utility of a generalized relationship useful for all crop types.

General crop K_{cb} from at-surface NDVI

The calibration process for a general K_{cb} curve was completed by first plotting METRIC K_c versus $NDVI_{atsurface}$ for each crop type, using data collected from all sampled fields of that type in the study area and from image dates corresponding to the growing season of each crop type. The plots shown for each crop type in figure 4.1-1 shows the corresponding days of the growing season considered for each crop. Two specific points were then defined representing the amount of transpiration occurring from bare agricultural soil with little evaporation due to wet soil, and the upper point where peak ET corresponds to full effective crop cover, again with little evaporation occurring from wet soil.

The first point in the K_{cb} NDVI relationship was for the bare soil condition of $NDVI_{atsurface} = 0.16$ and $K_{cb} = 0.1$. The value of $NDVI_{atsurface}$ of 0.16 appears to be the average value for bare soil within the Magic Valley. The corresponding K_{cb} of 0.1 was chosen following Wright (1982), and Allen et al., (1998) where K_{cb} of 0.1 represents the K_c from a dry bare agricultural soil which has been periodically tilled. Early in the

growing season some diffusive evaporation occurs from bare agricultural soils from beneath the dry surface (Allen et al., 1998).

The second point used in the development the linear relationship was selected in the vicinity of the NDVI representing achievement of full crop development. The selection of this point was conducted in such a way as to obtain a given percentage of total points lying below the K_{cb} line. This was done following past work carried out by Tasumi et al (unpublished) where 20% was selected for the percentage of fields that on average would be experiencing varying degrees of water shortage or normal, random error in METRIC estimated ET. The general (crop-type free) linear relationship (along with the crop specific 'custom' relationship discussed in the next section) plotted with each crop type can be seen for all crops considered in Figure 4.1-1.

It is noted that the assumption of a general linear relationship between NDVI and K_{cb} was not always observed for all crops under consideration (Figure 4.1-1). Row crops tended to exhibit a more linear relationship than did broadcast crops such as alfalfa, winter grains, and spring grains. In both winter and spring grain crops deviation from the linear relationship was observed late in the growing season. The points encircled in black above the K_{cb} line, seen in Figure 4.1-1, represent the NDVI and K_c sampled from the grain fields in late July corresponding to the development of grain heads.

Grain canopy reflectance is affected by the development grain heads. While grain continues to transpire (exhibiting fairly high ET) the development of heads and senescing leaves causes a decrease in near infrared reflectance (NIR) and an increase of red reflectance due to a decrease in chlorophyll absorption (Haboudane et al., 2004). This decrease in NIR and increase in red reflectance cause significant underestimation in vegetation indices such as LAI and NDVI. This can in part explain the fairly low NDVI seen with the corresponding high K_c for grain crops late in the year and associated deviation from the linear relationships presented.

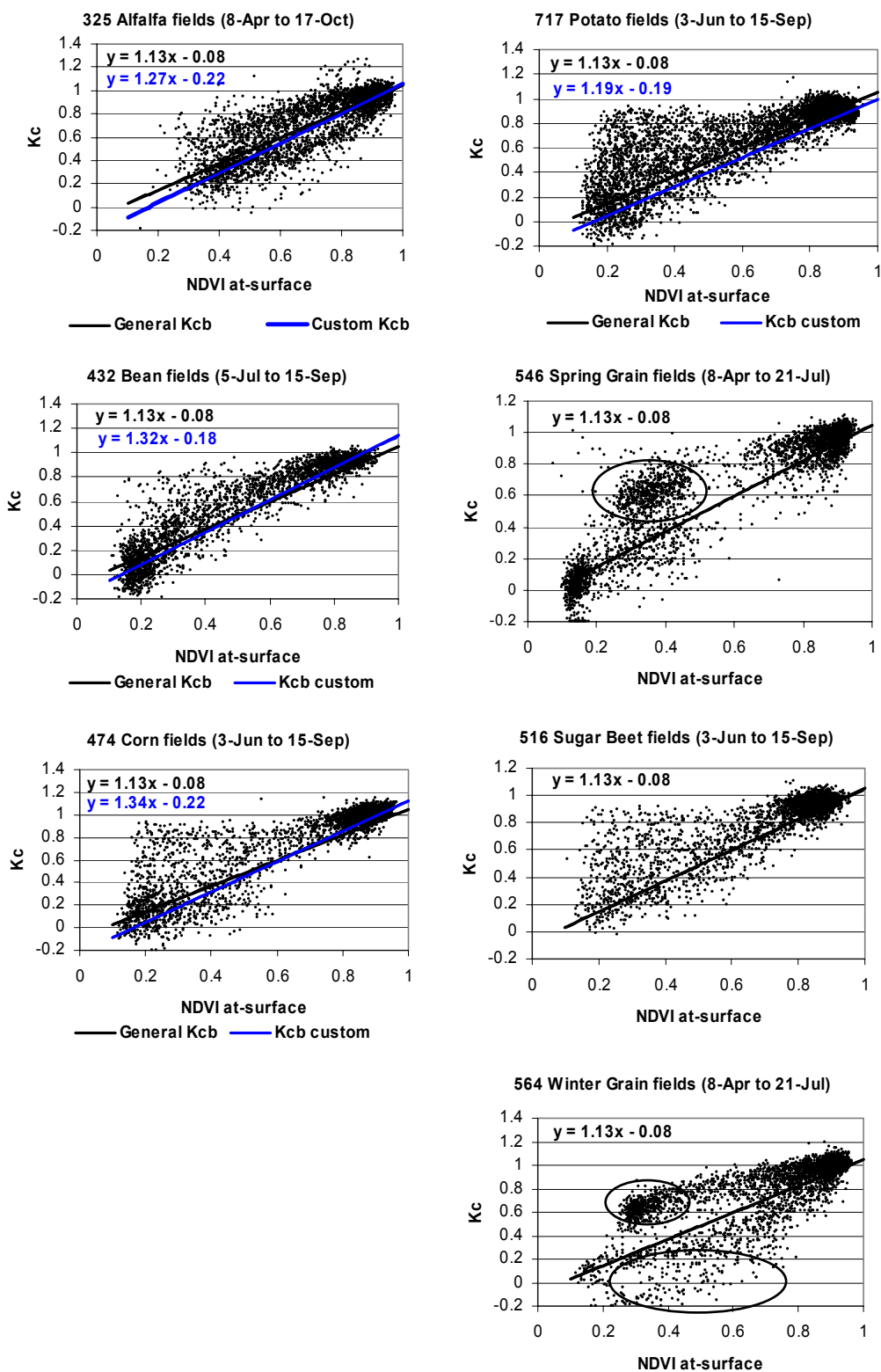


Figure 4.1-1 K_{cb} versus NDVI for all crop types showing both General relationship as well as crop specific relationships.

Also encircled in Figure 4.1-1 is the region below the K_{cb} relationship for winter grain crops. These data points correspond to observations made in early April before the beginning of the irrigation season within the Magic Valley. Winter grain is planted late in the fall, often immerses before winter and then lies dormant throughout the winter months. Much of the scatter of low K_c points seen for the sampled winter grain fields could be due to plant stress on the crops following a dormant winter and prior the start of the irrigation season.

The general linear K_{cb} -NDVI function also had poor agreement with sampled alfalfa field data. Some hystereses in the K_{cb} -NDVI is observed with alfalfa, where data collected early in the year tends to lie on and below the K_{cb} line and data collected late in the season tended to lie above the K_{cb} line (partial gap apparent in center of sampled data for alfalfa in Figure 4.1-1). Part of the deviation from the other crop relationships can be attributed to the frequent cuttings of alfalfa which occur throughout the growing season coupled with the effect of moist soil conditions following the first cutting. These cuttings occur essentially at random throughout an image and cause scatter in the K_c versus NDVI plots. Also alfalfa is a perennial crop with typically high percentages of ground cover. As seen in Figure 4.1-1 the sampled alfalfa fields had the highest NDVI from early in the growing season of all crops examined. All of these characteristics specific to alfalfa lead to the largest deviation from the general linear K_{cb} -NDVI relationship.

While some deviation from a linear K_{cb} -NDVI relationship was observed for some crops under consideration, the assumption was still used and tested, especially since the periods of deviation experienced for grain crops apply to a relatively short portion of the growing season (Tasumi et al., 2007). Most crops sampled in this analysis exhibit distinct linear relationships between K_{cb} and NDVI.

Crop specific K_{cb} from NDVI

In some cases where specific crop classification is known, the use of crop specific relationships would be advantageous. Relationships between K_{cb} and NDVI were also developed for crops that have characteristics significantly different from an average crop, such as the case of alfalfa where impacts of frequent cuttings can create significant

differences from an average agricultural crop. Crop specific relationships were constructed for Alfalfa, bean, corn, and potato crops. The calibration constants a and b used in equation 20 for each crop type as well as the constants obtained for the general crop are given in table 4.1-2. No error statistics were calculated for these linear relationships due to the influence of K_e embedded in the K_c samples.

Table 4.1-2 K_{cb} versus NDVI calibration constants for the Magic Valley Path 40 year 2000

Crop	a	b
General	1.13	-0.08
Alfalfa	1.27	-0.22
Beans	1.32	-0.18
Corn	1.34	-0.22
Potatoes	1.19	-0.19

Comparison of generated K_{cb} curves with curves in the literature show good agreement (Figure 4.1-2). In order to construct average K_{cb} curves for the Magic Valley NDVI was sampled for the year 2000 from a total of 3,754 fields and the average NDVI determined for each crop type throughout the growing season. The 3,754 fields sampled for NDVI were the same fields used in the development of the linear relationships. As described previously detailed crop classification was previously performed for the year 2000 making crop specific curve generation possible. All generated K_{cb} curves are compared to K_{cb} curves presented by Allen and Robison (2007) in Appendix A. All curves developed by Allen and Robison (2007) were strictly ground based (using growing degree days) and have as their primary source, the K_{cb} curves described by Wright (1982) based on lysimeter measurements near Kimberly, Idaho. Curves were generated by Allen and Robison (2007) for multiple locations and years based on local weather data and were adjusted for use with the ASCE Standardized Penman-Monteith reference ET equation (original K_{cb} curves by Wright (1982) were based on the 1982 Kimberly Penman Reference ET equation). The good agreement found between NDVI based K_{cb} and literature values shows promise to the use of K_{cb} derived from simple linear relationships to NDVI.

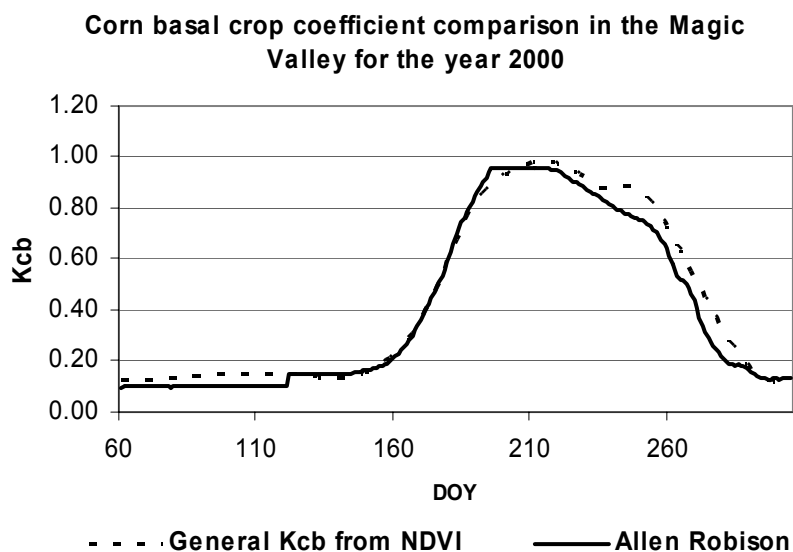


Figure 4.1-2 Comparison of K_{cb} curve derived from regional average NDVI for corn using the general crop relationship with K_{cb} developed by Allen Robison (2007) from standardized K_{cb} curves by Wright (1982) for the Hazelton area within the Magic Valley (custom crop specific K_{cb} curve for corn performed similarly (seen in Appendix A)) .

4.2. FAO 56 dual crop coefficient method to add estimate of evaporation from soil

Because NDVI and thus vegetation amount are most strongly correlated with transpiration, the major disadvantage in using NDVI to examine crop coefficients and therefore crop ET is the inability to quantify evaporation from the soil surface, and to detect plant stress due to water scarcity. To obtain improved estimates of total K_c from NDVI, the FAO 56 dual crop coefficient method was employed to estimate the evaporation component (K_e) to be added to K_{cb} determined from NDVI.

Water Balance of the Surface Evaporation Layer

The addition of evaporation from the soil surface will provide means to estimate total consumptive use of water by quantifying to some extent the effects of soil and plant conditions on K_e , which NDVI cannot sense. An FAO 56 evaporation model was used to

determine the amount of evaporation from bare soil due to wetting events and is given by:

$$K_e = K_r (K_{c_max} - K_{cb}) \leq f_{ew} K_{c_max} \quad (22)$$

where K_r is defined as the evaporation reduction coefficient, which varies depending on the amount of water in the surface soil layer still available for evaporation, K_{c_max} represents the maximum K_c possible following a wetting event, and f_{ew} is the fraction of bare soil that has been wetted and is exposed to sunlight (Allen et al. 1998, 2005 ASCE). The maximum value of K_c for individual fields within a large area following an irrigation event can range from 0.8 to as high as 1.1 for alfalfa reference ET_r depending on the time of year, soil temperature, crop type, and crop conditions (Tasumi et al., 2005). Wright (1981) recommends maximum values for 'mean' K_c ranging from 0.78 for potatoes to 1.0 for alfalfa when using alfalfa as the reference ET_r . Wright (1981) data was developed using the 1982 Kimberly Penman reference ET equation which when converted for use with the ASCE standardized Penman-Monteith equation gives K_{c_max} as high as 1.03 for spring grain (Allen and Wright, 2002). The value of K_{c_max} used in the evaporation model will vary slightly depending on the time of year, and best judgment following Allen et al (1998). A minimum value for K_{c_max} will be set as $K_{cb} + 0.05$, which suggests that wet soil will always increase the K_{cb} by roughly 5% even when the crop is at full cover (Allen et al 2005).

The fraction of bare soil that has been wetted (f_{ew}) can be estimated (Allen et al., 1998) as the minimum of the fraction of exposed soil ($1-f_c$) and the fraction of total wetted soil (f_w), where f_c is the fraction of vegetation cover estimated from K_{cb} and given by:

$$f_c = \left(\frac{K_{cb} - K_{c_min}}{K_{c_max} - K_{c_min}} \right)^{(1+0.5h)} \quad (23)$$

The height (h) of the vegetation can be estimated from a linear relationship between minimum and maximum plant heights and K_{cb} as:

$$h = h_{\max} \frac{K_{cb}}{K_{cb_{\max}}} \quad (24)$$

where K_{cb} is obtained from equation 20, and maximum plant height is obtained from FAO 56 tables when the crop specific simulation is conducted. Estimated h is set equal to 0.6 m for the ‘general crop’ simulation where specific crop type is unknown. $K_{c_{\min}}$ for bare soil conditions can be assumed to be approximately 0.15 for areas with occasional surface wetting and near 0 for areas where wetting events are infrequent, such as in desert areas (Allen et al. 2005).

As the soil surface dries we would expect the rate of evaporation to decrease. This decrease is accounted for in the evaporation reduction coefficient K_r , which can be estimated following Allen et al. (1998) by:

$$K_r = \frac{TEW - D_{e,j-1}}{TEW - REW} \quad (25)$$

for $D_{e,j-1} > REW$. $D_{e,j-1}$ represents the cumulative depth of evaporation within the surface soil layer modeled that dries to near air dry levels and the subscript $j-1$ refers to the previous day in the water balance. TEW is the total evaporable water equal to the maximum amount of water that can be evaporated from the soil surface after complete wetting and REW is the readily evaporable water. REW differs from TEW in that the REW can be evaporated with out any reduction in K_r . It is only after the REW has been evaporated that the K_r begins to decrease.

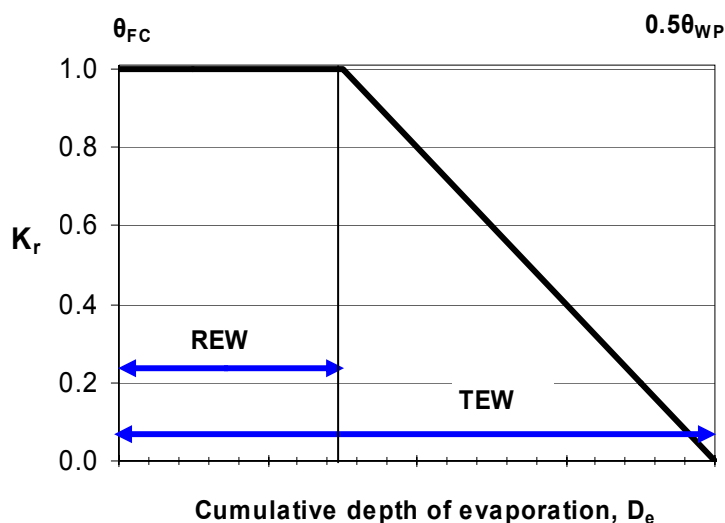


Figure 4.2-1 Behavior of the soil evaporation reduction coefficient, K_r as water is evaporated from the evaporation layer (following Allen et al., 1998)

The analysis of the evaporation reduction coefficient requires a soil water balance within the layer of soil where evaporation occurs. Because we are concerned here with the amount of evaporation occurring from the surface K_e , only the bare soil fraction will be modeled in this process, as the evaporation from soil surfaces covered by vegetation is assumed to be incorporated into the transpiration component K_{cb} . Allen et al (1998) suggest that the effective depth of a soil surface layer modeled be in the top 0.10 to 0.15m of the soil with 0.10m corresponding to coarse soils and 0.15m for fine textured soil types. With the effective depth of surface soil (Z_e) and soil properties the TEW can be determined by:

$$TEW = 1000(\theta_{FC} - 0.5\theta_{WP})Z_e \quad (26)$$

In estimating TEW, basic soil properties are needed for determining θ_{FC} , the soil moisture content at field capacity, and θ_{WP} , the soil moisture content at the wilting point of vegetation. Both θ_{FC} and θ_{WP} can be obtained from FAO 56 for a range of soil textures (Allen et al. 1998).

The soil water balance in the effective evaporation layer and for the exposed fraction of the soil surface is conducted on a daily basis and is given in Allen et al. (1998) by:

$$D_{e,i} = D_{e,i-1} - (P_i - RO_i) - \frac{I_i}{f_w} + \frac{E_i}{f_{ew}} + T_{e,i} + DP_{e,i} \quad (27)$$

where the subscript j is in days and $j-1$ corresponds to the previous day, P is the amount of precipitation occurring on that day, I is the amount of irrigation, E is the total evaporation from the surface ($E = K_e * ET_r$), T is the amount of transpiration and DP is the deep percolation through the soil layer. The surface runoff can be approximated using the USDA curve number procedure following Allen and Robinson (2006) but is typically so small in irrigated agricultural areas that it can be neglected. The fraction of the soil that is both exposed and wetted, f_{ew} is determined following Allen et al (1998) as the minimum between the fraction of the soil that is wetted, f_w , and the fraction of the soil that is exposed ($1-f_c$) and given by:

$$f_{ew} = \min(1 - f_c, f_w) \quad (28)$$

In many situations the amount of transpiration (T) occurring from the surface evaporation layer can be neglected (Allen et al, 1998). This is not the case for annual crops whose maximum rooting depth is less than approximately 0.5m (Allen et al, 2005). Under these conditions T can have a significant effect on the water balance conducted within the evaporation layer. In this study the magnitude of T is calculated at a daily time step following Allen et al, (2005) as follows:

$$T = K_T K_{cb} K_s ET_r \quad (29)$$

where K_T is the portion of the basal ET that is extracted by the plant from the fraction of the soil surface that is both wetted and exposed (f_{ew}). K_T is calculated by comparing the available water in the evaporation layer to the available water in the root zone as:

$$K_r = \left(\frac{1 - \frac{D_e}{TEW}}{1 - \frac{D_r}{TAW}} \right) \left(\frac{Z_e}{Z_r} \right)^{0.6} \quad (30)$$

Here TAW is the total available water within the plant root zone. TAW is calculated from soil properties and the crops rooting depth (Z_r) by:

$$TAW = 1000(\theta_{FC} - \theta_{WP})Z_r \quad (31)$$

D_r in equation 30 is the depletion of water within the plant root zone expressed as a depth of water. This depletion is discussed in further detail in the following section and presented in equation 35.

Water Balance of the Root Zone

Historical weather and precipitation data are widely available and were used to incorporate daily precipitation events over the study area. Irrigation wetting events are more complicated to quantify because they occur essentially randomly within the population of fields in an image. Due to the lack of knowledge regarding the timing and amount of irrigations for the large number of fields in an image a soil water balance is conducted and irrigations assumed to occur whenever the soil water content drops below the readily available water (RAW). The depth of water applied for each irrigation event will be based on soil properties as well as crop type throughout the study area. The RAW will be estimated based on crop type and soil properties by:

$$RAW = MAD(1000(\theta_{FC} - \theta_{WP})Z_r) \quad (32)$$

where MAD is the maximum allowable depletion within the root zone expressed as a decimal and Z_r is the root depth of the crop under consideration. Economics, soil, and water management are all considerations that determine irrigations and thus the percentage of the available water to the crop. For this reason the RAW is similar the term “management allowed deficit” following Keller and Bliesner (1990).

Within this context different crops within varying types of soil are managed to different irrigation schemes by adjustments made to the MAD. A typical value of 50%

was utilized for the general crop analysis, as this represents traditional irrigation schedules which apply irrigations to ensure the water level in the root zone is usually not sufficiently low as to induce plant stress. In the crop specific analysis the MAD was adjusted to best replicate actual irrigation practice of the region for soil water sensitive crops such as potatoes.

Furthermore, as a crop grows the readily available water increases due to the expansion of the crop root zone. It is then necessary to include, within the water balance, consideration of a “growing” root. Several functions for simulating root depth (Borg and Grimes, 1986; Allen et al., 1998) and in this study a simple linear growth relationship based on the relative K_{cb} value is used following Allen et al., (1998):

$$Z_r = Z_{r_min} + (Z_{r_max} - Z_{r_min}) \frac{K_{cb,i} - K_{cb_min}}{K_{cb_max} - K_{cb_min}} \quad (33)$$

This root depth is modeled such that it is always increasing and never exceeds the maximum value entered into the model.

As a crop transpires and the soil water content within the root zone drops to a certain level, the crop has difficulty extracting additional water by its roots and begins to experience stress. The effects of this water stress on crop ET is described in the FAO 56 dual crop coefficient method, by a reduction in the crop coefficient K_C (Allen et al., 1998). This reduction is achieved by determining a water stress coefficient, K_S , and then multiplying the K_C by K_S . The reduction coefficient is calculated as:

$$K_S = \frac{TAW - D_r}{TAW - RAW} \quad (34)$$

Where TAW and RAW, are as previously defined, and D_r is the soil water depletion within the root zone. The root zone depletion is determined by conducting a daily water balance of the soil column, to the depth of the crop roots. The depletion at the end of each day is described by the water balance as:

$$D_{r,i} = D_{r,i-1} - (P - RO)_i - I_i - CR_i + ET_{C,i} + DP_i \quad (35)$$

Here the subscript i represents the daily time step with $i-1$ representing the previous day of the water balance, P the amount of precipitation, RO the runoff from the soil surface, I the irrigation which infiltrates the soil, CR the capillary rise from the ground water table below, ET_C the ET from the given crop, and DP the amount of deep percolation through the root zone, all expressed in units of depth of water.

Graphically, K_S behaves in a similar fashion to the reduction coefficient for the surface water balance, K_r . As seen in figure 4.2-2, K_S has a value of 1 for all depletion depths up to the RAW. This corresponds to no reduction in the total K_c as the crop has no difficulty extracting water from the root zone. It is only after the depletion exceeds the RAW that K_S becomes less than one and therefore a reduction in K_c occurs.

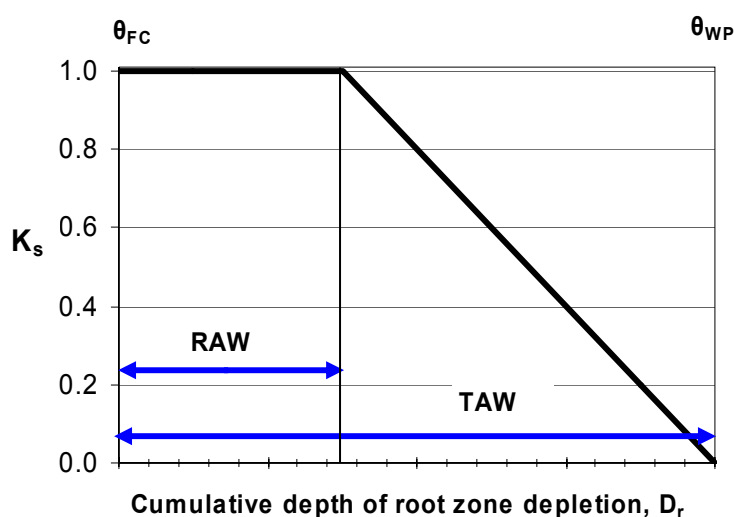


Figure 4.2-2 Behavior of the water stress reduction coefficient, K_s , as water is extracted from the root zone (following Allen et al., 1998).

In order to track the depletion of water within the root zone equation 32 requires knowledge of both inputs into the soil by way of rainfall and irrigation events, as well as outputs from the soil through ET, deep percolation, and runoff. The effects of capillary rise for common soils within the Magic Valley are insignificant due to generally large depths to ground water and were neglected. Allen and Robinson (2007) used a curve number method to calculate runoff and found that for irrigated agricultural areas in southern Idaho its magnitude is small and therefore runoff was neglected in this study.

Deep percolation through the root zone, DP was calculated following Allen et al. (1998) by:

$$DP_i = (P_i - RO_i) + I_i - ET_{C,i} - D_{r,i-1} \quad (36)$$

Here the amount of deep percolation is restricted to non negative values (greater than or equal to 0) and only occurs when the soil column is above field capacity.

In order to initiate the soil water balance initial soil water depletion conditions are needed ($D_{r,i-1}$). With the large spatial scale used in this study, measurements of soil moisture content were not feasible. Because we are conducting the analysis on an entire irrigation season starting in early March we can assume that the initial depletion in most soils is small. The Magic Valley receives the majority of its annual precipitation throughout the winter months and so assuming a root zone depletion of zero to initiate the soil water balance is considered an accurate approximation.

Irrigation simulations

Because the timing and magnitude of irrigation events occur throughout the area of a Landsat image essentially at random, an irrigation scheme was simulated based on the soil water balance of the root zone. Due to the large scale of the area of interest it is more important to replicate the frequency of irrigations than the precise timing of all irrigation events.

Irrigation events were simulated using information from the soil water balance of the root zone. In this scheme irrigations were assumed to occur when ever the root zone depletion reached the readily available water ($D_{r,i} = \text{RAW}$). The magnitude of each irrigation event was just large enough to refill the root zone ($I_i = D_{r,i-1}, \text{RAW}$). As a direct result, deep percolation through the root zone was infrequent. To reduce the need for irrigation season determination, a K_{cb} threshold was utilized to initiate irrigations. Irrigations were limited to times following development of K_{cb} above 0.25. This delayed the start of the irrigation period to when most farmers begin irrigating and seemed to provide for a reasonable irrigation season within the study area.

One difficulty in the implementation of simulated irrigations' into a spatially distributed water balance model that is applied on a pixel basis is its tendency to predict varying irrigation schedules from pixel to pixel within a given image and from neighboring pixels within the same fields. This can be problematic and depict scenarios that are unrealistic when compared to actual agricultural practices. Various techniques can be employed to combat this problem such as the development of an average regional irrigation schedule based on crop type to be applied to all fields within an image with the same crop type. This however would require crop classification which can be both costly and time demanding.

Other irrigation scheduling techniques may include developing average irrigation schedules for various soil classifications. The variation in seasonal NDVI may also be used as a method for grouping "likely" crop types into groups and average irrigation schedules developed. For the calibration of the water balance model developed in this study, average irrigation schedules were developed based on crop type and then used to examine the possibility of other methods where the crop classification would not be required.

Sample fields locations

In order to test the water balance model and irrigation simulations, ten random fields were sampled from each of the crop types under consideration and the effects of both 10-field average and individual field irrigation schedules examined. It was determined that ten fields selected throughout the entire study area would provide sufficient information and variation for the development of an average crop irrigation schedule representing the Magic Valley. Figure 4.2-3 shows the location of the ten randomly selected alfalfa fields used to develop irrigation schedules. Sampling was made possible with the use of a crop classification map by Tasumi et al, (2003) constructed for the Magic Valley for the year 2000 (Figure 4.2-4). The land classification map has the same 30 by 30 meter resolution of Landsat images.

Alfalfa Crop Sample Field Locations

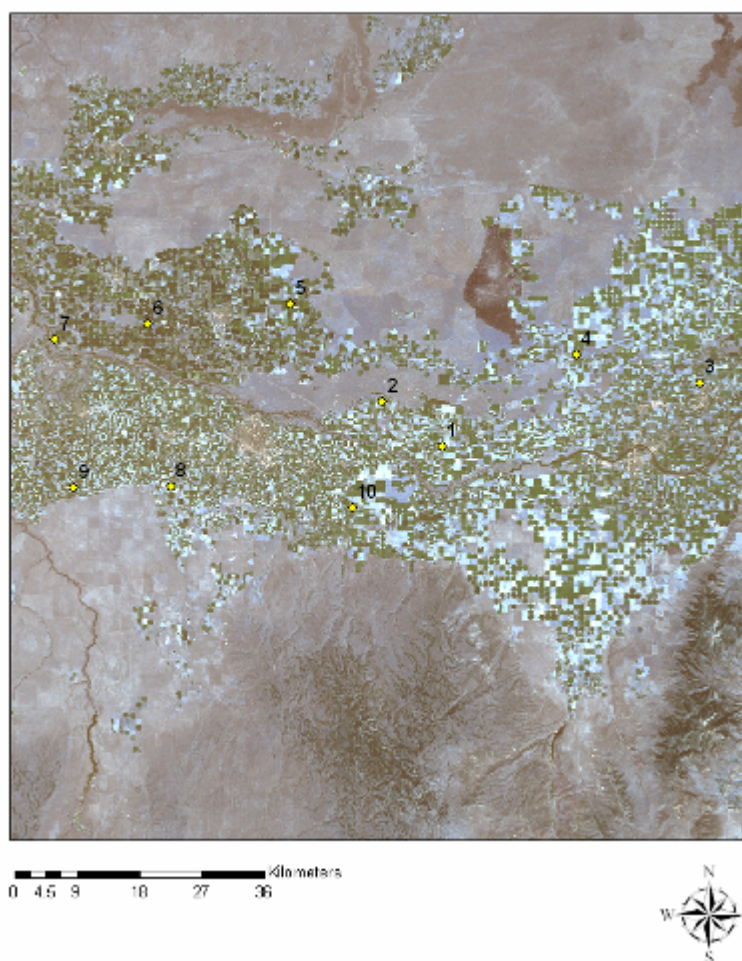


Figure 4.2-3 Sampled alfalfa fields used in water balance model calibration.

Fields were sampled randomly and care was taken to select pixels from fields with uniform crop classifications and well inside the field away from the field edges where thermal contamination can occur. As seen in Figure 4.2-4 some heterogeneity in classification exists within some fields due to difficulty distinguishing between similar crops. The crop classification was validated by Tasumi et al. (2003) using ground truth data acquired throughout the region during the 2000 growing season. In the year 2000 a significant amount of corn was grown in fields north of the Snake River. This corresponds to the high number of dairies in that area and the use of corn silage as feed in the dairy operations.

2000 Crop Classification for the Magic Valley

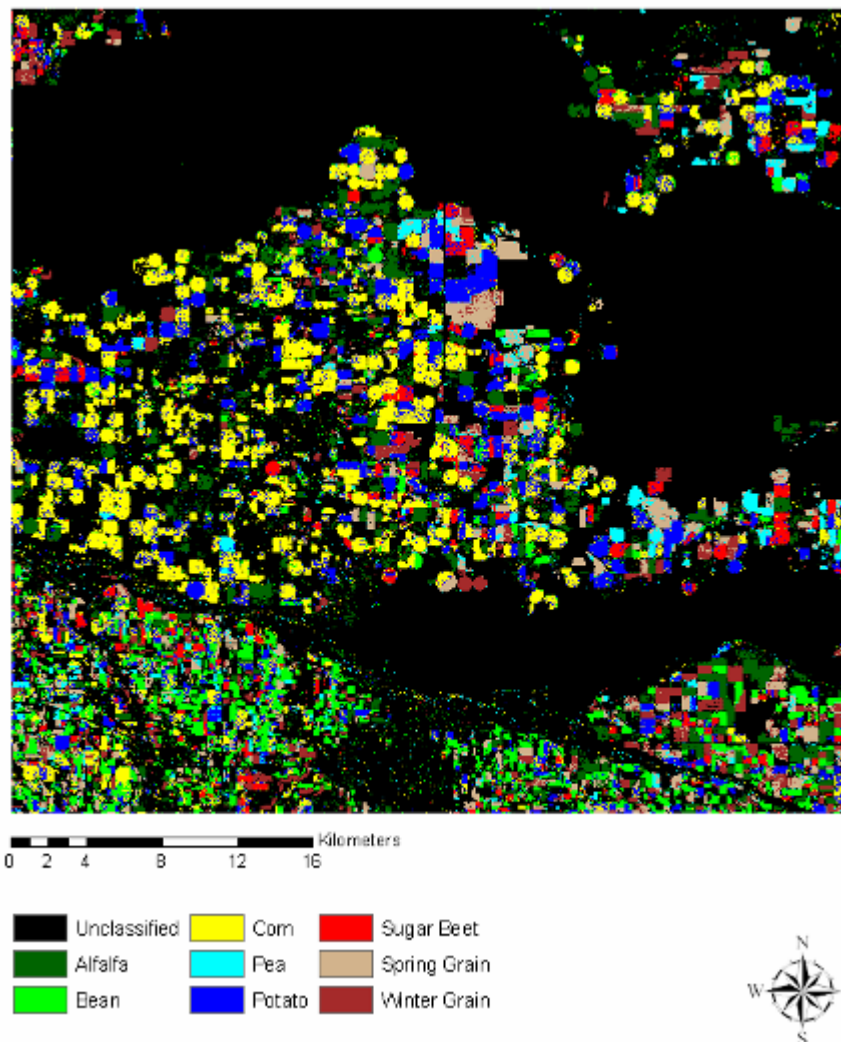


Figure 4.2-4 Crop classification created by Tasumi et al, 2003 for major agricultural crops of the Magic Valley.

Cloud cover was also considered in the selection of field samples. Cloud cover can significantly reduce the accuracy associated with all satellite based measurements. Cloud cover masks generated for the original processing of the year 2000 Path 40 by Tasumi et al. (2003) and used to sample from fields where no cloud cover was present for any of the twelve Landsat image dates. A significant portion of the study area was cloud free for all image dates (Figure 4.2-5).

Cloud Cover on 2000 Image Dates

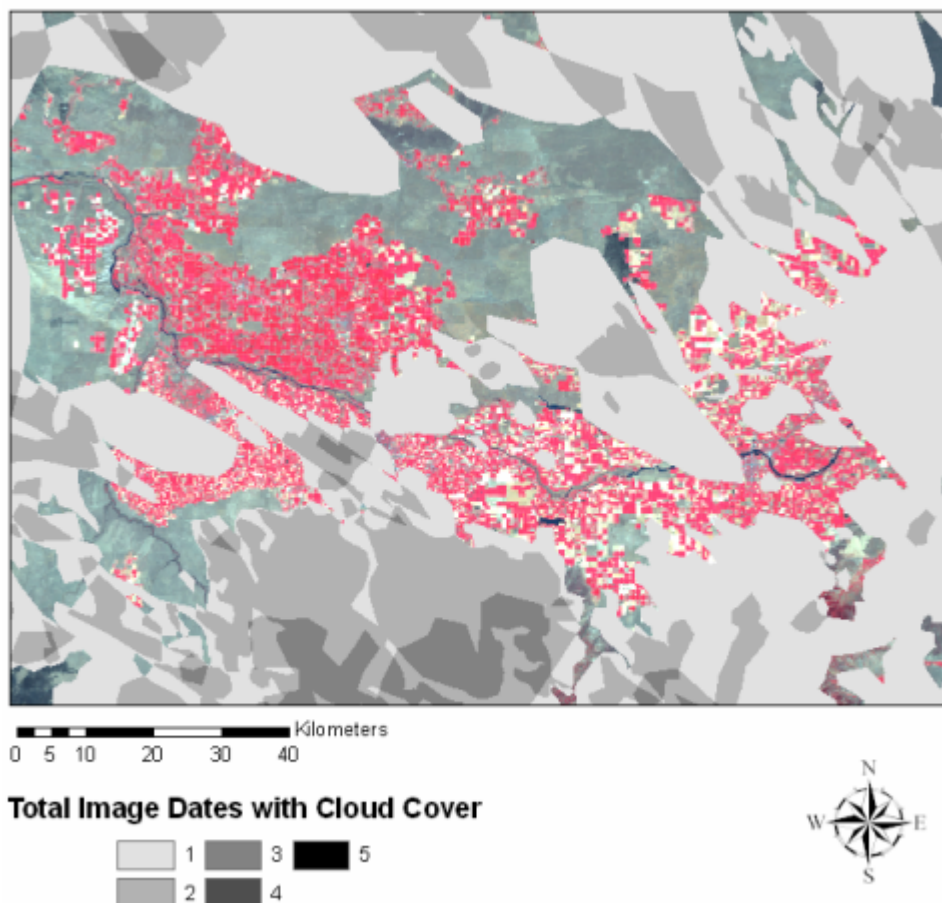


Figure 4.2-5 Cloud cover map of Magic Valley showing total number of image dates with cloud cover.

Each of the randomly selected fields was then sampled for METRIC K_c along with the NDVI for each image date throughout the growing season. In order to conduct the water balance model at a daily time step, daily NDVI and K_c values were interpolated using a cubic spline (ERH, K.T. 1972 Soil Science 144:333-338). This follows closely the manual fitting of K_{cb} curves by Wright (1982), which better captures the daily variation in K_{cb} values when only image date values are available. Linear interpolation tends to miss some of the variation in K_{cb} and can underestimate true ET around the time of peak ET (Figure 4.2-6).

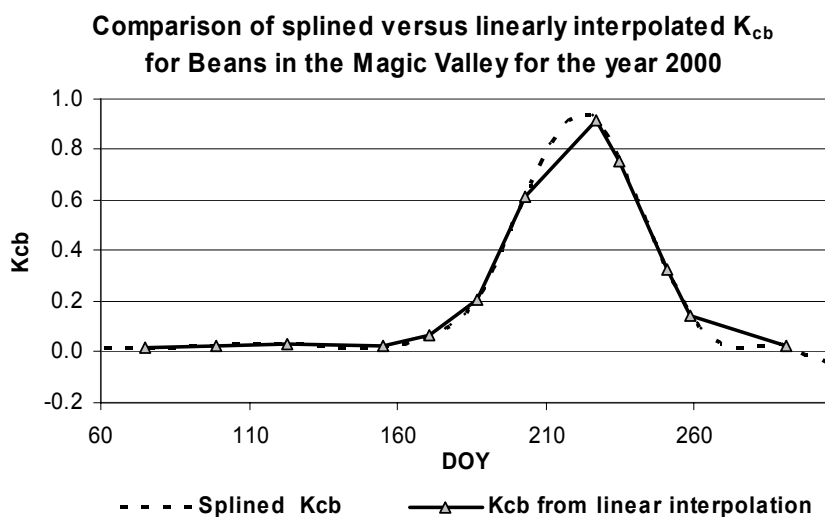


Figure 4.2-6 Comparison of splined versus linear interpolated K_{cb} for average Bean crop in the Magic Valley for year 2000 ('custom' K_{cb} versus NDVI).

Water Balance Model Inputs

Inputs needed for the water balance model were daily ET_r , interpolated daily NDVI, and daily precipitation. The model was coded in spreadsheet format for this preliminary application and simulations made from the first day of March until the last day of October. ET_r was calculated as previously described using the ASCE Standardized Penman Monteith equation and hourly weather data collected near Kimberly Idaho. Daily METRIC K_c values are also used as inputs into the model for comparative analysis of model performance.

With all data input into the water balance model, irrigations were simulated and seasonal crop coefficient curves generated. Figure 4.2-7 shows the output of the soil water balance and simulated irrigation events. This simulation was conducted using the general crop K_{cb} versus NDVI relationship as well as the averaged crop characteristics (eg. root depth, max height etc.) over all crop types. Here we note that 15 irrigations were simulated for the averaged Sugar Beet field condition which is typical of irrigations in the Magic Valley using center pivots.

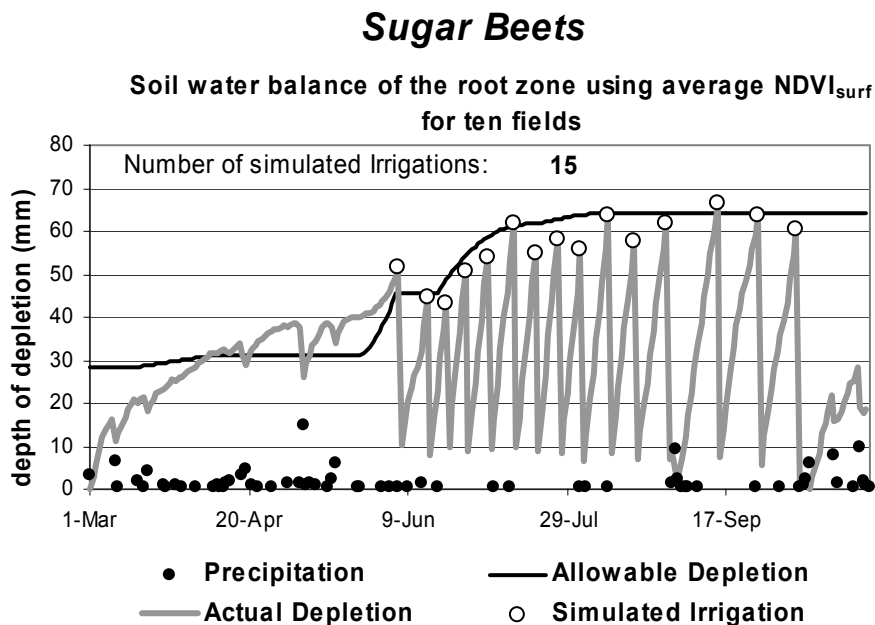


Figure 4.2-7 Simulated irrigation for average Sugar Beet field using average NDVI from ten fields

Combining K_e from simulated irrigations, precipitation, and K_{cb} from NDVI the water balance model provides the daily values of K_c throughout the irrigation season (Figure 4.2-8). Spikes in the $K_{cb} + K_e$ curve represent the addition of K_e due to the wetting of the soil surface as a result of simulated irrigations or measured precipitation events. Overlaying the $K_{cb} + K_e$ curve with instantaneous observations of K_c from METRIC on image dates provides for a good visual check of water balance model compliance.

The majority of the agricultural areas within the Magic Valley are underlain by Portneuf Silt Loam. Much of the lysimeter work carried out by Dr J. L. Wright (USDA) was conducted in fields of Portneuf Silt Loam. Table 4.3-1 gives all soil property values used for this study. The total evaporable water (TEW) was determined using a depth of the evaporation surface layer, Z_e of 0.1m. These soil properties have been calibrated for the study area during previous ET studies carried out by the University of Idaho (Allen personal communication).

Table 4.3-1 Soil properties used in Kcb + Ke water balance model, calibrated for the Magic Valley during previous ET studies (Allen Personal communication).

θ_{FC}	θ_{WP}	$\theta_{FC}-\theta_{WP}$	$\theta_{FC}-0.5\theta_{WP}$	TEW	REW
(mm/mm)	(mm/mm)	(mm/mm)	(mm/mm)	(mm)	(mm)
0.3	0.14	0.16	0.23	23	8

Crop Characteristics

The extent of a crops rooting depth plays a large role in the amount of water within the soil column available for plant use. As described above the root depth used in the water balance model depends on the development of the crop under consideration. A linear relationship between the crop seasonal variations and the maximum and minimum height and rooting depth were implemented. The values of maximum height as well as the minimum and maximum root depth were taken from a combination of Allen et al (1998), Keller and Bliesner (1990), and personal communication with local experts (Allen personal communication). Table 4.3-2 gives both the crop specific characteristics used in the crop classification based approach as well as the general crop characteristics used in the classification free approach.

Table 4.3-2 Crop characteristics used for both the crop specific and general crop simulations.

Crop Type	Max Height (m)	Max Rz (m)	Min Rz (m)
Alfalfa	0.7	2.0	0.25
Beans	0.4	0.9	0.10
Corn	2.0	1.7	0.25
Potatoes	0.6	0.6	0.10
Spring Grain	1.0	1.5	0.10
Sugar Beets	0.6	1.2	0.10
Winter Grain	1.0	1.8	0.25
General	0.6	1.0	0.25

****Note:** Values obtained from combination of FAO 56 and Keller Bliesner (1990)

The selection of the general crop characteristics which would best reflect the rooting characteristics of any given crop within the Magic valley was carried out by first reviewing the arithmetic average of the readily available table values for maximum height, minimum rooting depth and maximum rooting depth (calculated averages: h_{max} 0.9 m, minimum Rz 0.2 m, and maximum Rz 1.4 m). The general parameters were then adjusted so that the extreme cases (corn maximum height of 2 m and alfalfa with maximum rooting depth of 2 m) did not unrealistically influence the resulting irrigation simulations for the remaining crop types (Allen personal communication).

The duration of the irrigation season for any crop can have a large effect on the total estimated ET occurring for a given seasonal time period. In an attempt to create a model requiring the least amount of user definition, a K_{cb} threshold was used to initiate and end the watering season for each crop. This threshold was set at a K_{cb} of 0.25 and performed well for the simulation of most crops under consideration. Typically the irrigation season within the Magic Valley does not begin until mid April to early May. However, crop type plays a large role in irrigation season timing and therefore the threshold was established to replicate the beginning of irrigations for each crop under consideration. This provides an accurate assessment for spatial distribution of field planting and the different timing of crop development. A similar procedure was employed by Allen and Robison (2007).

When using the general crop characteristics (height, root depth, etc.) alfalfa field simulations continually yielded unrealistic numbers of predicted irrigations especially

early in the growing season. This was attributed to the high NDVI and thus K_{cb} for fields early in the analysis period of March 1 to October 31. With the high K_{cb} , irrigations were predicted as early as the first week of March. For the crop classification based water balance model approach, the maximum allowable depletion was adjusted to allow for more depletion of water within the root zone, and therefore reduce the number of predicted irrigations.

5.0 $K_{cb} + K_e$ WATER BALANCE MODEL WITH CROP CLASSIFICATION

5.1. Statistical Analysis

Validation of the $K_{cb} + K_e$ water balance model output was performed in comparison with ET estimates made from METRIC. METRIC has been applied throughout the western United States and extensively in southern Idaho (Allen et al., 2007b). While estimates from METRIC are well established their use in the validation of other ET estimation methods requires additional consideration in using common comparison statistics. This section defines the statistics used in the validation process and discusses additional steps taken to compare results to METRIC estimates as though METRIC is actual measured ET.

As an indicator of seasonal accuracy the simple ratio of seasonal ET determined via the water balance model to the seasonal ET from METRIC is computed as follows:

$$Seasonal_ratio = \frac{ET_{K_{cb}+K_e}}{ET_{METRIC}} \quad (37)$$

Where $ET_{K_{cb}+K_e}$ is the seasonal ET (mm) estimated using the $K_{cb} + K_e$ water balance approach, and ET_{METRIC} is the seasonal ET (mm) calculated using METRIC. It is noted here that seasonal estimates and measurements are for March 1 to October 31, 2000.

Remaining comparisons were made using the average daily ET (mm/day) estimated using the water balance model described and average daily ET (mm/day) observed by METRIC. The average daily ET was computed by summing the daily estimated ET over the Landsat image sub-period and then dividing the total ET by the number of days represented by each image sub-period (Table 5.1-1). This provided a total of twelve observations for each water balance model simulation.

Table 5.1-1 Time periods corresponding to Landsat satellite overpass for March 1, to October 31, 2000.

Image Date	Image sub-period	# days in period
3/15/00	3/1 to 3/28	27
4/8/00	3/29 to 4/21	24
5/2/00	4/22 to 5/19	28
6/3/00	5/20 to 6/12	24
6/19/00	6/13 to 6/28	16
7/5/00	6/29 to 7/14	16
7/21/00	7/15 to 8/3	20
8/14/00	8/4 to 8/19	16
8/22/00	8/20 to 8/31	12
9/7/00	9/1 to 9/12	12
9/15/00	9/13 to 10/2	20
10/17/00	10/3 to 10/31	29

The standard deviation for both the model predicted variable and observed (METRIC) variable were calculated as:

$$Stdev = \left[\sum_{i=1}^n \frac{(X_i - X_{ave})^2}{n-1} \right]^{\frac{1}{2}} \quad (38)$$

Where X_i is the predicted (model) or observed (METRIC) ET estimate and X_{ave} is the average predicted or observed ET estimate.

The efficiency of the model was analyzed by calculating the model efficiency (E) as:

$$E = 1 - \frac{\sum_{i=1}^n (P_i - O_i)^2}{\sum_{i=1}^n (O_i - O_{ave})^2} \quad (39)$$

Where P represents the ET predicted by the water balance model and O represents the ET observed by METRIC. The model efficiency is a dimensionless quantity and gives a measure of the performance of the model, with a value of 1 representing excellent model efficiency.

The root mean square difference (RMSD) was calculated by:

$$RMSD = \left[\frac{1}{n-1} \sum_{i=1}^n (P_i - O_i)^2 \right]^{\frac{1}{2}} \quad (40)$$

The RMSD is used here in place of the RMSE to consider the use of METRIC (O) values as a measure for water balance model accuracy but not as an absolute truth.

The mean absolute difference (MAD_{iff}) was also use in place of the mean absolute error and was calculated by:

$$MAD_{iff} = \frac{1}{n} \sum_{i=1}^n |P_i - O_i| \quad (41)$$

Typically the mean absolute difference is abbreviated as the MAD, however in this study the subscript is included to differentiate it from the maximum allowable depletion, MAD used in other portions of this study. The units for the MAD_{iff} are mm/day. The mean absolute percentage difference ($MAPD_{iff}$) was calculated by:

$$MAPD_{iff} = \frac{100}{O_{ave}} \left(\frac{1}{n} \sum_{i=1}^n |P_i - O_i| \right) \quad (42)$$

The mean bias error, which indicates the average difference between the predicted and the observed values (mm/day), was calculated as:

$$MBE = P_{ave} - O_{ave} \quad (43)$$

The final statistic analyzed was the coefficient of determination, r^2 , which gives a measure of correspondence between the predicted and observed values, and is calculated by:

$$r^2 = \left[\frac{1}{n-1} \left(\frac{\sum_{i=1}^n (O_i - O_{ave})(P_i - P_{ave})}{Stdev_o * Stdev_p} \right) \right]^2 \quad (44)$$

5.2. Ten Field Simulations for each Crop under Consideration

The performance of the water balance model was first tested by comparing ET estimates using averaged crop characteristics (over all crops) for each crop under consideration. The use of specific crop characteristics provided an indicator of how well the $K_{cb} + K_e$ approach can replicate observed METRIC ET. The overall results of simulations using the average NDVI over the ten fields for each crop is presented first to show the applicability of the method for each crop type. A separate analysis of all estimates made from the ten sampled fields will then be made to analyze the accuracy associated with an individual field sampled at random from a Landsat image.

Table 5.2-1 summarizes the results of simulations on the average field for each crop tested. All comparisons are, as stated in section 5.1, between the model predicted ET estimations with the observed METRIC ET. Simulations on corn and potatoes performed well seasonally with seasonal ratios near 1.00. Alfalfa simulations yielded the highest over estimation error (approximately 2%) relative to observed ET and the simulation conducted for beans gave the most under estimation (approximately 9%) for seasonal ET. Alfalfa also had the lowest model standard deviation of 1.7 mm/day as well as the lowest mean bias error of -0.01 mm/day. It is noted here that the negative MBE for alfalfa simulations would indicate an underestimation in ET estimates, however in this case the seasonal ratio was greater than one. The seasonal ratio is based upon the summation of daily ET estimates for each model for March 1, to October 31, while the MBE is calculated from average daily ET estimates over each of the image sub-periods (image sub periods span March 1 to October 31, but range in duration from 12 days up to 29 days). In this case the negative MBE is small but caused by using the average daily ET in place of actual daily ET estimates. Therefore, MBE gives equal weight to each sub-period (equal weight of daily average ET estimates for early in the year when ET is low as compared to later in the year when ET rates are high) while the ratio of seasonal ET gives larger weight to periods of high ET. Also it is noted that the ‘Stdev model’

represents the standard deviation of the model ET estimates and describes the variation in estimated K_c over time and among fields.

Table 5.2-1 Summary of simulations of each crop type using specific crop rooting characteristics, custom K_{cb} versus NDVI relationship and the average NDVI over ten sampled fields to define the average field condition .

n=12 Crop	Seasonal Ratio	Stdev model (mm/day)	Model Efficiency (E)	RMSD (mm/day)	MADiff (mm/day)	MAPDiff (%)	MBE (mm/day)	r^2
Alfalfa	1.02	1.70	0.88	0.62	0.44	9.7	-0.01	0.88
Beans	0.92	2.69	0.92	0.74	0.51	19.1	-0.22	0.93
Corn	1.00	2.95	0.99	0.30	0.25	6.3	-0.03	0.99
Potatoes	0.97	3.16	0.83	1.13	0.64	15.1	-0.03	0.88
Spring Grain	0.96	2.90	0.97	0.53	0.45	12.1	-0.23	0.98
Sugar Beets	0.96	2.79	0.96	0.55	0.41	8.9	-0.13	0.97
Winter Grain	0.95	2.94	0.91	1.01	0.77	19.7	-0.28	0.92

****Note:** Evaluation was conducted using the average daily ET (mm/day) over each satellite sub-period from the $K_{cb} + K_e$ water balance model (predicted) and METRIC (observed) for March 1, 2000 to October 31, 2000

Alfalfa

Alfalfa is a major crop grown throughout the western United States. Alfalfa is characterized by frequent cuttings, usually three to four, during the course of the growing season. Alfalfa provides a unique test of any ET estimation model in that the reference ET is calculated with Alfalfa as the reference crop.

The average NDVI from the ten sampled alfalfa fields can be seen in Figure 5.2-1. Of the ten fields sampled we see that the average number of cuttings of the sampled fields was four during the 2000 irrigation season. Individual water balance models were conducted for each of the ten crops as well as simulations for the average alfalfa crop. The average crop simulation was carried out using the average NDVI of the ten sampled crops (Figure 5.2-1).

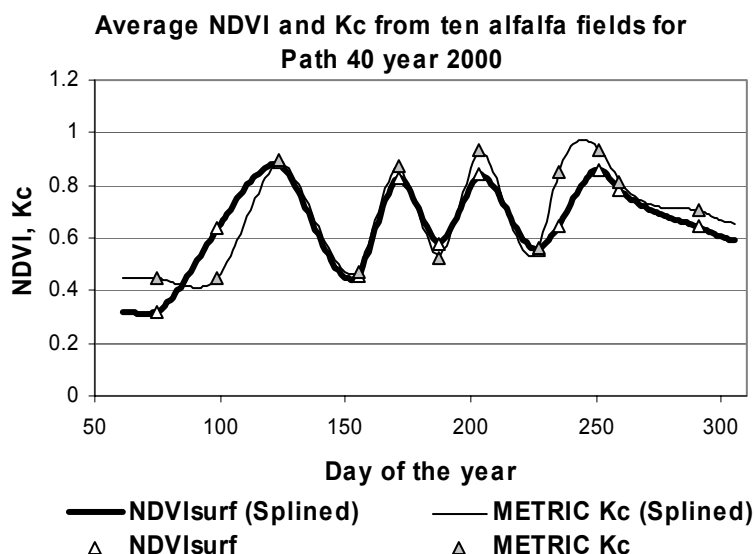


Figure 5.2-1 Average NDVI and METRIC K_c from ten randomly sampled alfalfa fields

The splined NDVI values of Figure 5.2-1 show the effect of frequent cuttings on NDVI, but the frequency of satellite images limits the ability to track the actual variation in NDVI throughout the growing season. For example from the satellite information we know that the alfalfa crops were cut at some time between the May 2 and June 6 image dates. However the precise date of the cutting remains unknown. This can create some error in calculated K_{cb} and thus the water balance models estimate of ET. A more precise daily K_{cb} curve developed for the study area by Allen and Robison (2000) can be seen in Figure 5.2-2 along with the K_{cb} computed from remotely sensed NDVI. As shown by the Allen Robison curve, the alfalfa K_{cb} curve increases to full cover at which time a distinct plateau is reached. At the time of cutting an immediate drop in vegetation and therefore K_{cb} occurs.

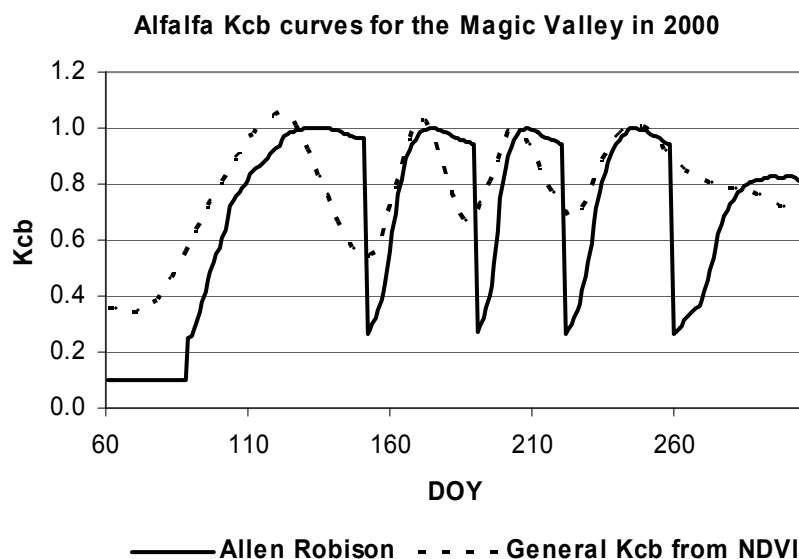


Figure 5.2-2 Comparison of K_{cb} curves developed from satellite NDVI to the K_{cb} curve generated by Allen and Robison (2007) using the Wright (1982) K_{cb} procedure for the Hazelton area within the Magic Valley

This difference between the actual daily behavior in K_{cb} and the K_{cb} estimated from remote sensing data could cause some of the error found in ET estimates from the water balance model. This can also be problematic when performing the water balance model to large areas due to the randomness in the timing of cuttings throughout satellite images relative to image dates.

The specific crop characteristics of alfalfa used in this set of simulations were a minimum and maximum root depth of 0.25 and 2.0 meters respectively. The maximum crop height of 0.7 meters was also used. With these crop specific characteristics and the K_{cb} -NDVI relationship custom fitted for alfalfa, the water balance model predicted 6 irrigation simulations for the average alfalfa field. Figure 5.2-3 shows the water balance of the root zone and accompanying simulated irrigation events. It is noted that the y-axis is the depth of depletion of water within the alfalfa crop root zone. The total number of irrigations simulated for alfalfa using the water balance model is consistent with agricultural practices in Southern Idaho.

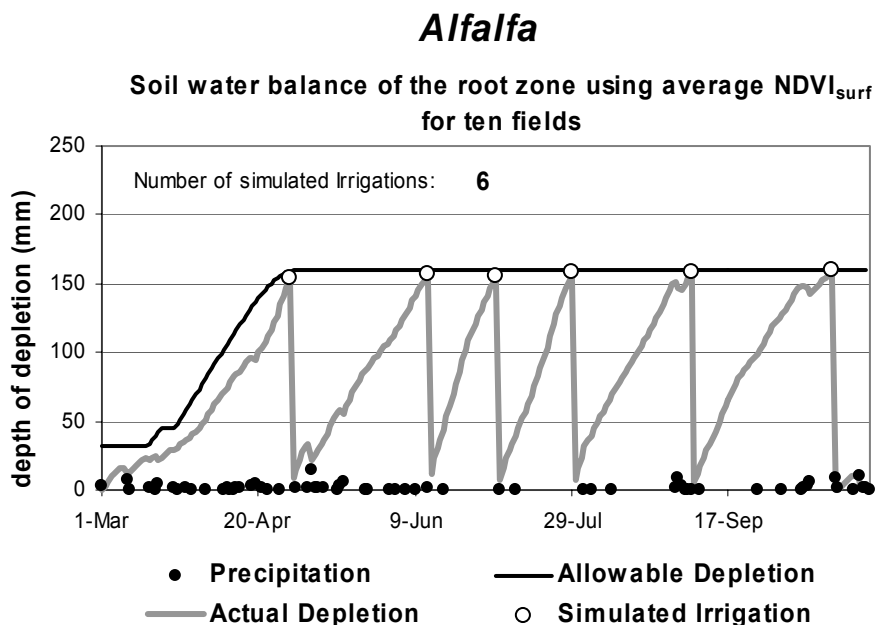


Figure 5.2-3 Soil water balance of the root zone and corresponding simulated irrigations using rooting characteristics specific to alfalfa.

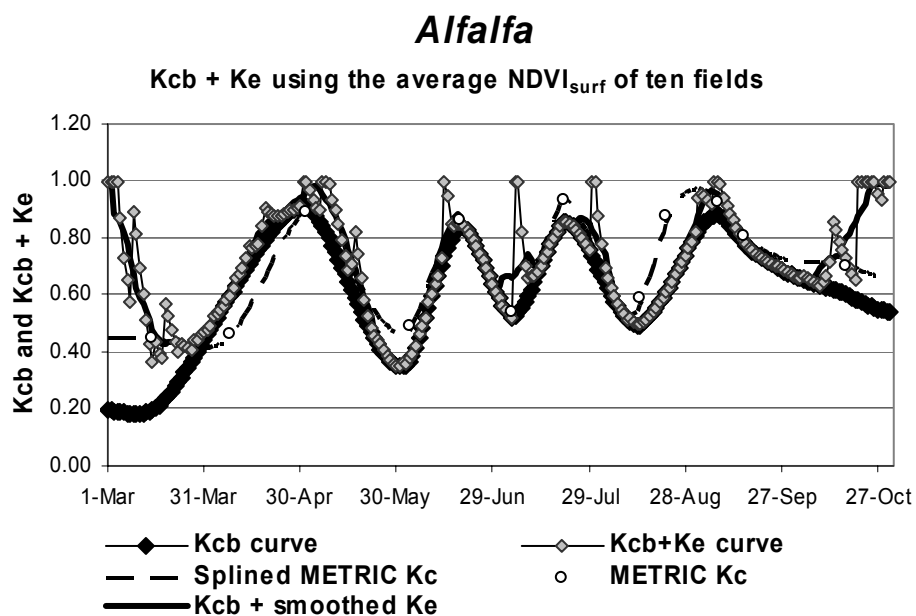


Figure 5.2-4 $K_{cb} + K_e$ curve generated using water balance model for alfalfa with crop specific characteristics ($K_{cb} +$ smoothed K_e curve: K_e smoothed using 10 day running average for visual curve comparison).

With the simulated irrigation events along with known precipitation, the seasonal $K_{cb} + K_e$ curve can be constructed (Figure 5.2-4). The spikes observed in the $K_{cb} + K_e$ curve represent evaporation from the soil surface immediately following wetting events. Also included in the figure is the K_c estimated from METRIC both on the image date as well as daily values estimated using the cubic spline of image date values. The $K_{cb} +$ smoothed K_e curve in Figure 5.2-4 is constructed by using a ten day running average on the daily K_e values before being added to the K_{cb} . This is done solely for visual comparison of the water balance model results with METRIC K_c curves. In the comparison of METRIC values with the daily values estimated by the water balance model for alfalfa, a relatively good agreement is observed.

The resulting seasonal ET estimation for alfalfa gave the highest overestimation of METRIC observed ET with a seasonal ratio of 1.02. The over estimation could be attributed to the frequency of remote sensing images and the consequent error associated with the inability to track the multiple cuttings precisely. Also as discussed in the parameter development section above, the water balance model as developed tends to predict more irrigation events for alfalfa crops due to the high vegetation cover early in the year. This was in part compensated for with the increased amount of allowable water depletion within the alfalfa root zone.

Beans

Beans are another common agricultural crop grown in southern Idaho. While many varieties exist, they all exhibit similar irrigation and agronomic characteristics. The average NDVI from ten randomly sampled fields can be seen in Figure 5.2-5. Beans typically grow to a height of 0.4 meters and have a shallow starting rooting depth of 0.1 meters up to approximately 0.9 meters. For beans the K_{cb} -NDVI relationship custom fitted for beans was utilized.

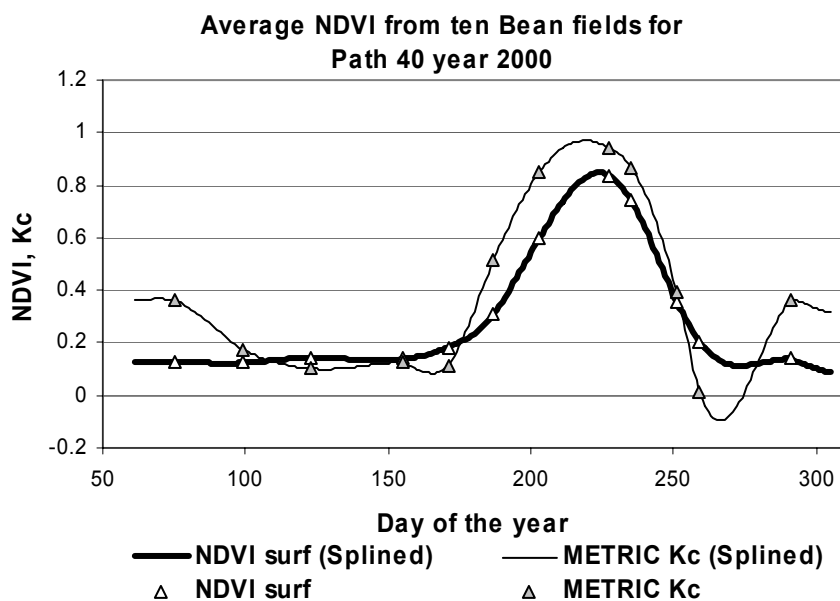


Figure 5.2-5 Average NDVI from ten bean fields along with the average METRIC Kc sampled from the same ten fields.

Conducting the soil water balance model on the average bean field yielded a total of 10 simulated irrigations (Figure 5.2-6). Also seen in Figure 5.2-6 is the short duration of the irrigation season for the bean crops. This follows the growth pattern seen in the seasonal variation of bean field NDVI. It is also noted that a distinct spike in the depth of allowable depletion occurs later in the year (early September) which corresponds to the water balance models increase in the MAD after bean crop harvest. This increase in MAD occurs to stop irrigation simulations by allowing a deficit, which in most cases lasted until the end of the study period with no additional irrigation simulations.

The long time periods of bare soil conditions would suggest that the use of a water balance model and accompanying K_e estimates from bare soil would be beneficial. However, the largest deviation from METRIC results was found for beans with an approximate 8% under estimation. The bean simulations also had a mean absolute percentage difference of 19.1% (only exceeded by Winter Wheat with $MAPD_{iff}$ of 19.7%). Bean simulations had a RMSD of 0.74 mm/day and a model efficiency of 0.92. However a visual average of $K_{cb} + K_e$ in Figure 5.2-7 compares relatively closely with the average K_c from METRIC over the entire growing season.

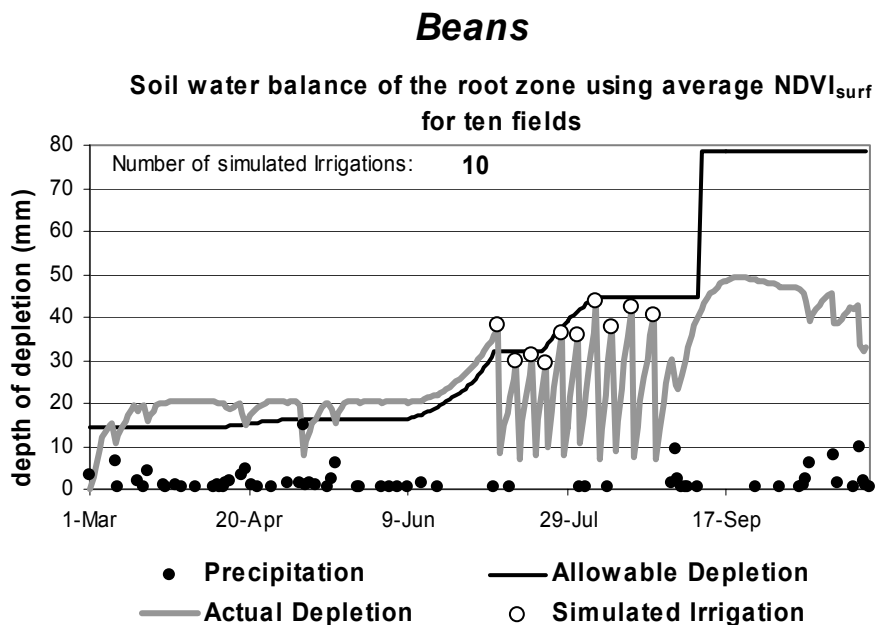


Figure 5.2-6 Soil water balance of the root zone for Beans using average field conditions.

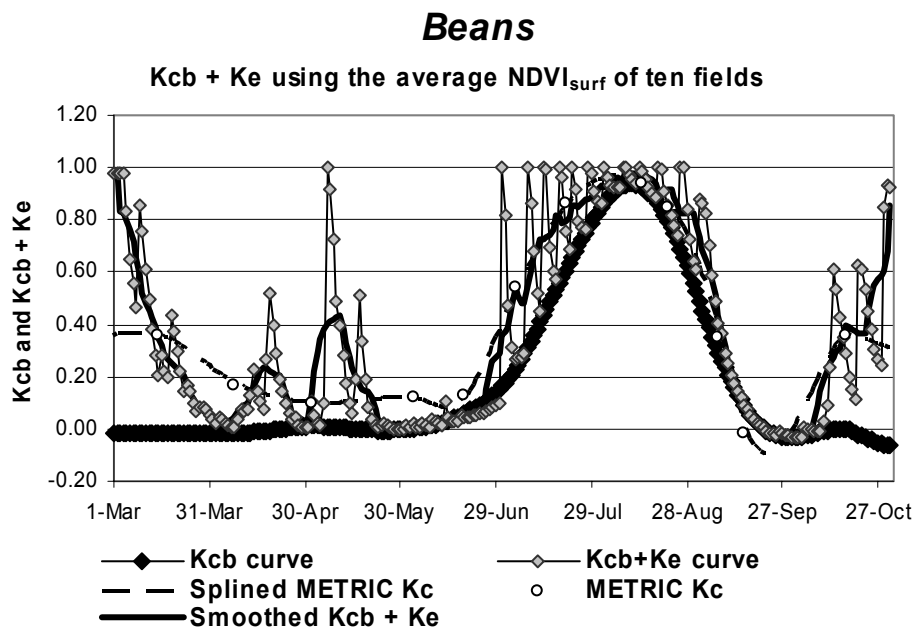


Figure 5.2-7 $K_{cb} + K_e$ curve for Beans constructed using custom (bean specific) K_{cb} -NDVI relationship from average NDVI of ten fields and simulated irrigations ($K_{cb} +$ smoothed K_e curve: K_e smoothed using 10 day running average for visual curve comparison).

Corn

Several varieties of corn crops are grown within the Magic Valley from silage corn used for dairies, field corn, to sweet corn for human consumption. Figure 5.2-8 shows the average NDVI from ten randomly sampled corn fields throughout the Magic Valley. No distinction between corn types was attempted. While corn can grow to heights above two meters the maximum height used in this analysis was 2 meters. The root depth used in the corn simulation ranged from 0.25 up to 1.7 meters. Also the custom K_{cb} -NDVI relationship developed specifically for corn was used in the following simulations.

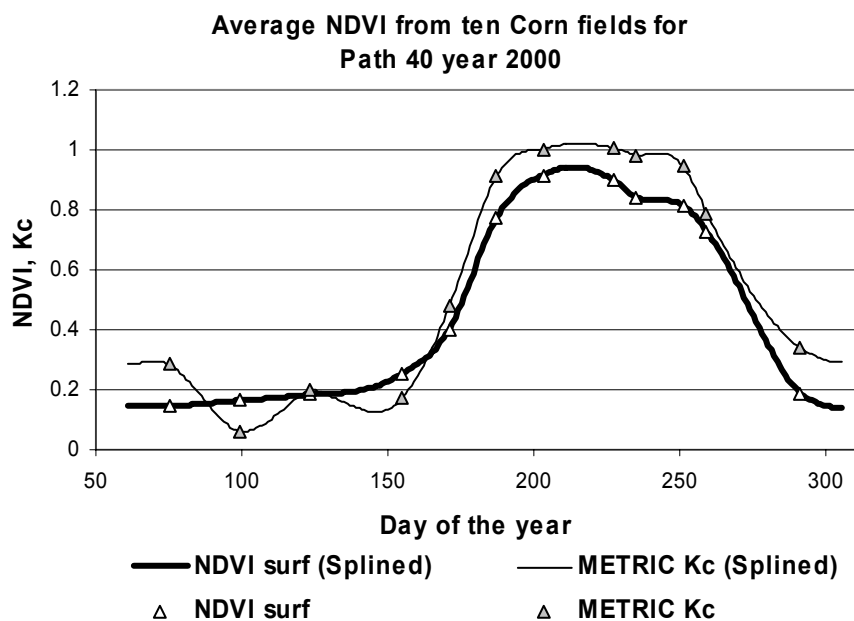


Figure 5.2-8 Average NDVI and observed METRIC K_c for ten randomly sampled Corn fields within the Magic Valley.

Simulations for the ten randomly sampled corn fields predicted an average of 7 irrigation events throughout the growing season. Seasonal ET estimates from corn compared very well to METRIC with a seasonal ration of 1.00. The corn model simulation also had the highest model efficiency of 0.99. Figure 5.2-10 shows good

agreement between the water balance model $K_{cb} + K_e$ curve and image date METRIC K_c . Early in the growing season ‘spikes’ in $K_{cb} + K_e$ due to precipitation correspond to METRIC observations. During full crop development similar correspondence is observed.

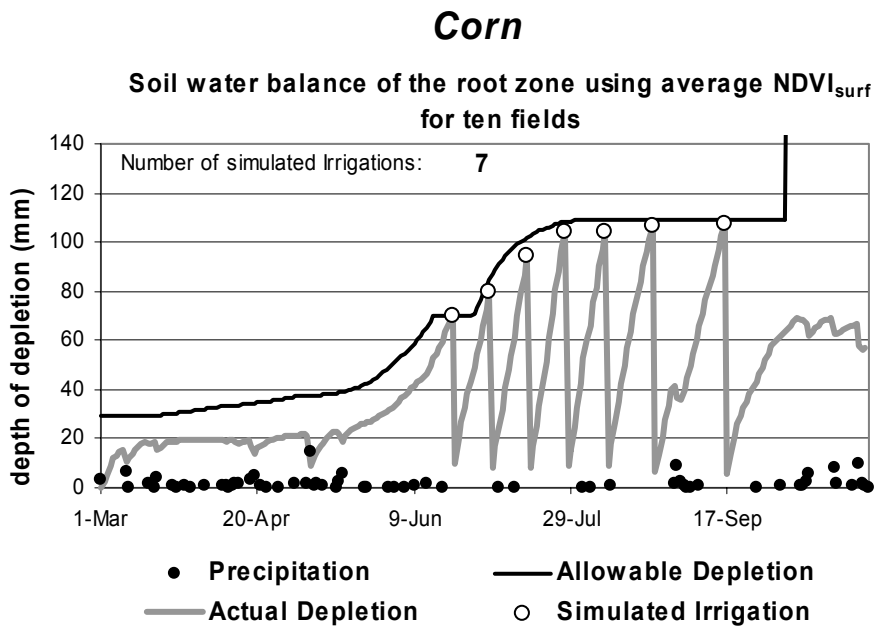


Figure 5.2-9 Soil water balance and simulated irrigation events for average Corn field constructed using average NDVI from ten randomly sampled corn fields.

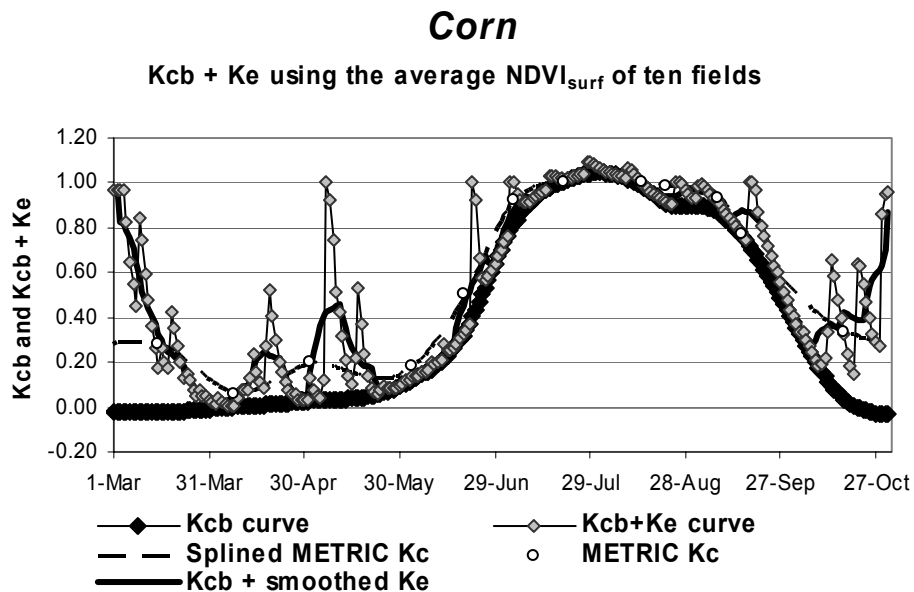


Figure 5.2-10 $K_{cb} + K_e$ curve for Corn constructed using custom (corn specific) K_{cb} -NDVI relationship from the average NDVI of ten fields and simulated irrigations ($K_{cb} +$ smoothed K_e curve: K_e smoothed using 10 day running average for visual curve comparison).

Potatoes

Southern Idaho is known throughout the world for its high quality potato production. The seasonal variation in NDVI can be seen below in Figure 5.2-11. Crop specific characteristics used for maximum crop height, and root depth were 0.6 and 0.1 to 0.6 meters respectively. The crop specific simulations for potatoes also utilized the K_{cb} -NDVI relationship developed specifically for potatoes.

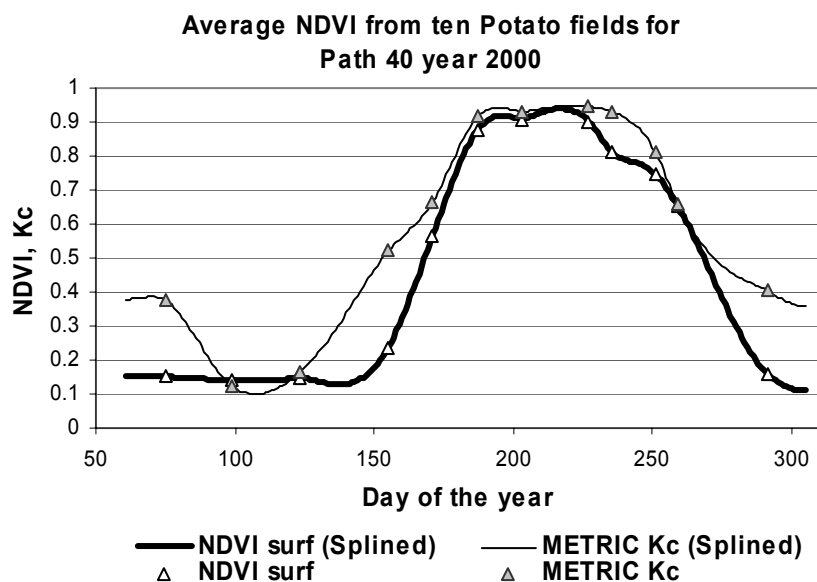


Figure 5.2-11 Average NDVI and METRIC Kc from ten randomly sampled Potato fields.

The 23 simulated irrigation events shown in Figure 5.2-12 may appear high but is typical of center pivot irrigation systems. It is not uncommon for potatoes in southern Idaho, irrigated by center pivots, to receive as many as 40 low volume irrigations (Dr. Brad King USDA-ARS, personal communication). This could in part suggest under estimation in seasonal ET from the water balance model, which was observed with approximately 3.4% under estimation.

The model standard deviation of 3.16 mm/day was observed for the potato simulation along with the model efficiency of 0.83. Potato simulation had a RMSD of 1.13 mm/day. The under estimation of seasonal ET could suggest the need to begin irrigation simulation at a lower K_{cb} threshold for potatoes. It is also apparent from Figure 5.2-12 that the first irrigation lags rapid root growth which again implies the need of earlier irrigation simulations. This can be seen in Figure 5.2-13 by the large underestimation of METRIC Kc around the June 3 image date corresponding to the period of rapid potato crop development. Most irrigators are most likely irrigating at this time of crop development which the water balance model fails to predict.

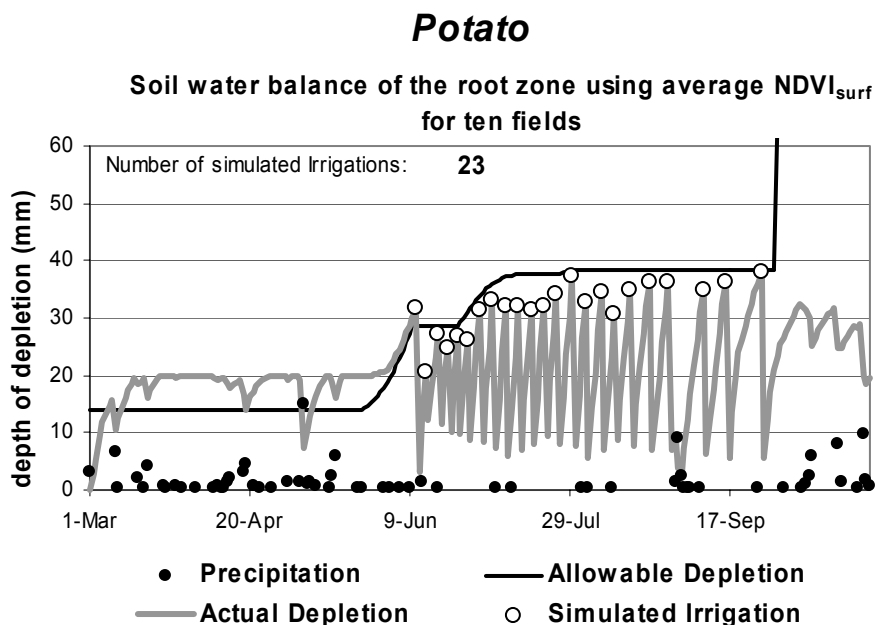


Figure 5.2-12 Soil water balance of the root zone and corresponding simulated irrigations for Potatoes using crop specific crop characteristics.

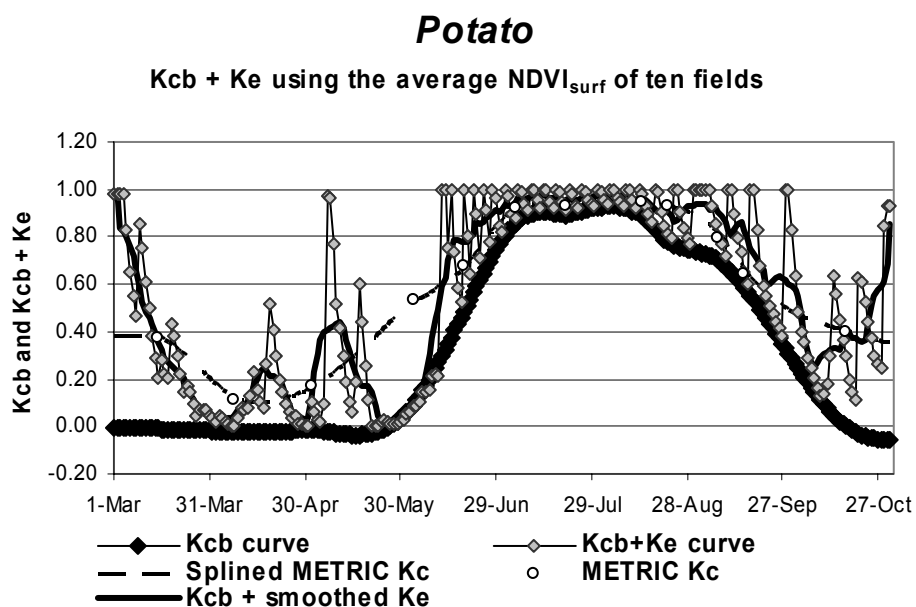


Figure 5.2-13 $K_{cb} + K_e$ curve for Potatoes generated using custom (potato specific) K_{cb} - $NDVI$ relationship from average $NDVI$ of ten fields and simulated irrigations ($K_{cb} + \text{smoothed } K_e$ curve: K_e smoothed using 10 day running average for visual curve comparison).

Sugar Beets

Sugar beets are another vital crop grown in Southern Idaho. Sugar Beets have similar characteristics as potatoes. The maximum plant height for sugar beets was set at 0.6 meters and the maximum root depth reaching 1.2 meters. Much of the lysimeter based research carried out with the USDA-ARS near Kimberly and corresponding with METRIC was conducted with sugar beets as the crop of interest (Wright, Allen et al., 2007b). Figure 5.2-14 shows the average NDVI of the ten sampled fields throughout the growing season. The general crop K_{cb} -NDVI relationship was used in sugar beet as it fit well to sugar beets in the development of the K_{cb} -NDVI relationships for each crop type.

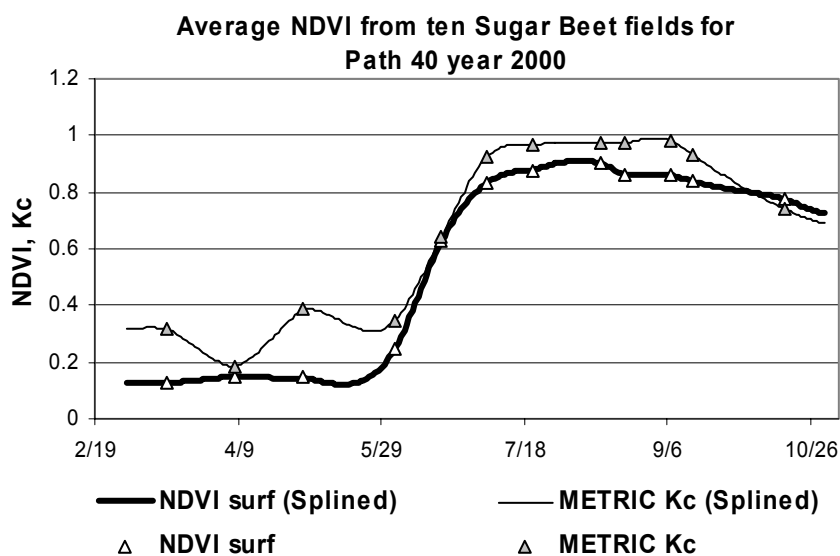


Figure 5.2-14 Average NDVI and METRIC K_c from ten randomly sampled Sugar Beet fields.

Sugar Beet simulations followed closely the results for potatoes. The overall seasonal ET ratio compared to METRIC was approximately 0.96. The mean bias error for the sugar beet simulation was only -0.13 mm/day and the RMSD was 0.58 mm/day.

Comparison of the seasonal $K_{cb} + K_e$ curve with the image date observations made with METRIC show relatively good agreement. Under estimation by the water model appears to be affected more by the timing of irrigation simulations than by the

frequency. Early season peaks in the $K_{cb} + K_e$ curve confirm METRIC observations when bare soil conditions exist.

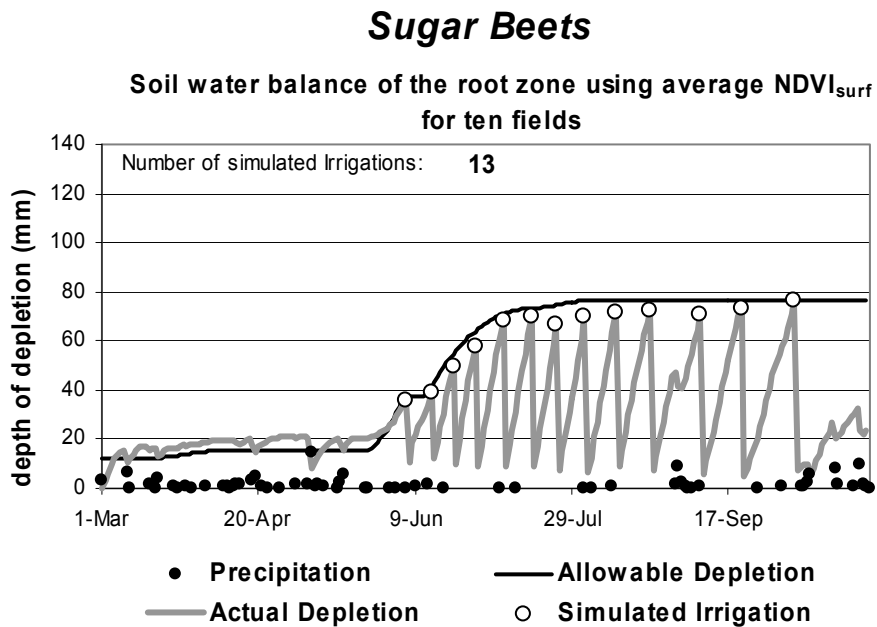


Figure 5.2-15 Soil water balance of the root zone with corresponding simulated irrigations.

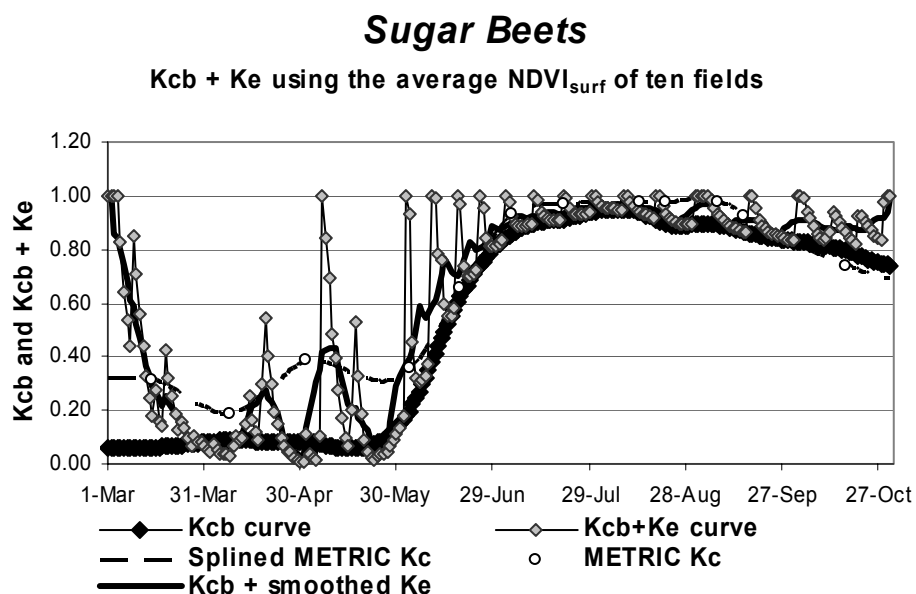


Figure 5.2-16 $K_{cb} + K_e$ curve generated using water balance model for Sugar Beets with crop specific rooting characteristics and the general K_{cb} -NDVI relationship ($K_{cb} +$ smoothed K_e curve: K_e smoothed using 10 day running average for visual curve comparison).

Spring Grain

Grain crops throughout the west are planted both in the spring as well as in the fall. Separate analysis is performed for grain crops planted for each of these time periods. Grains include the crops of barley, wheat, and no attempt was made to distinguish sampled fields between grain varieties. The average NDVI from ten randomly sampled fields is displayed in Figure 5.2-17. Spring grain crops typically grow to a maximum height of 1.0 meter and have rooting depths up to 1.5 meters. Spring grain simulations also used the K_{cb} -NDVI relationship developed for all crops within the Magic Valley.

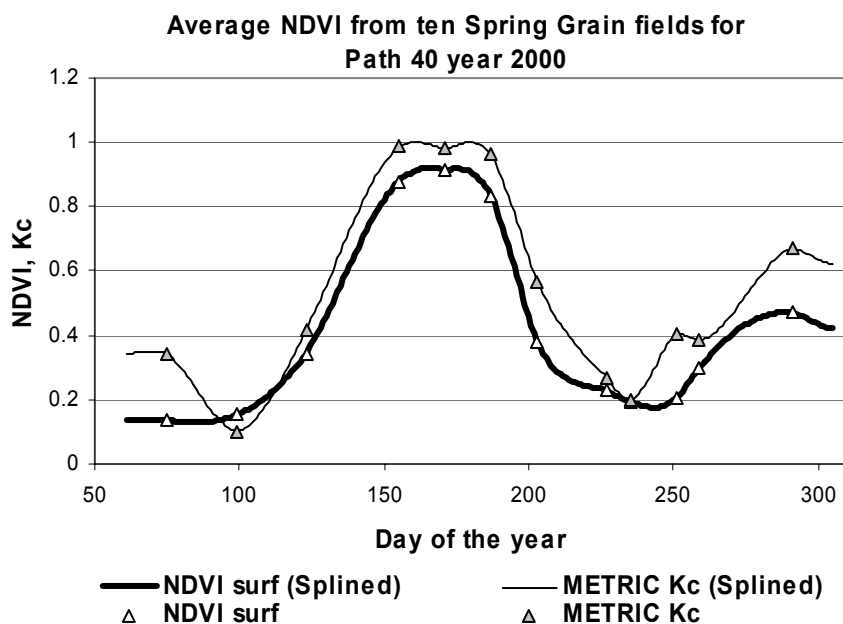


Figure 5.2-17 Average NDVI and METRIC K_c from ten randomly sampled Spring Grain fields.

Spring grain simulations provided under estimation of observed METRIC seasonal ET with a seasonal ratio of 0.96. The model for spring grain did have the second highest model efficiency of 0.97. The second lowest RMSD of 0.53 mm/day was also observed for the spring grain simulation.

With a total of 7 simulated irrigations, the constructed $K_{cb} + K_e$ curve compares the best with METRIC observations during the irrigation season. After the fields were harvested and irrigation ceased, differences between METRIC and the $K_{cb} + K_e$ model become more pronounced.

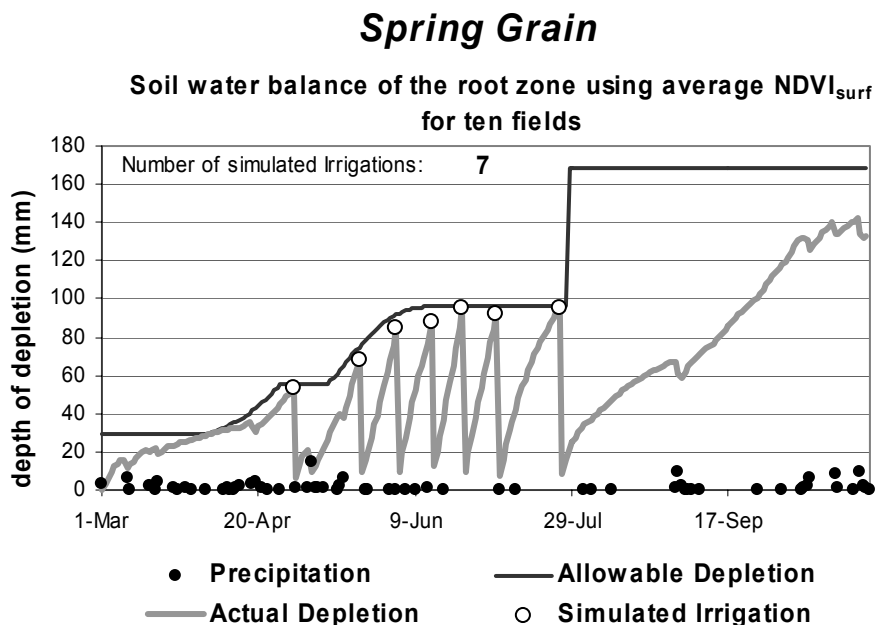


Figure 5.2-18 Soil water balance of the root zone with corresponding simulated irrigations.

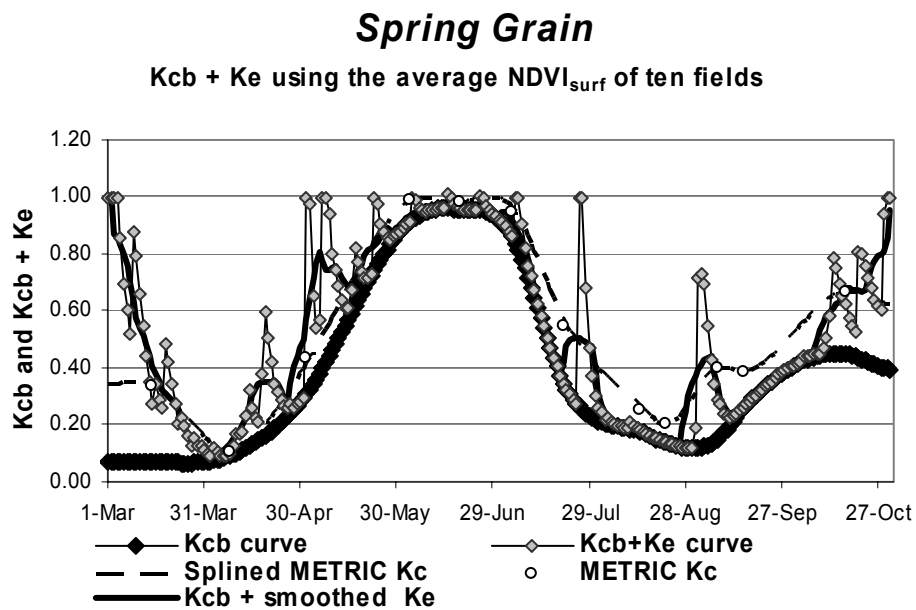


Figure 5.2-19 $K_{cb} + K_e$ curve for Spring Grain generated using water balance model with crop specific rooting characteristics and the general K_{cb} - $NDVI$ relationship (K_{cb} + smoothed K_e curve: K_e smoothed using 10 day running average for visual curve comparison).

Winter Grain

Winter grain is planted in late fall and typically emerges before winter temperatures cause it to go dormant throughout the winter months. Winter grain also reaches a maximum height of 1 meter and maximum root depths of 1.8 meters, slightly deeper than for grain planted in the spring. Figure 5.2-20 shows the seasonal variation in NDVI for the average of the ten fields sampled. Winter grain simulations also utilized the general K_{cb} -NDVI relationship fitted for all crops within the Magic Valley.

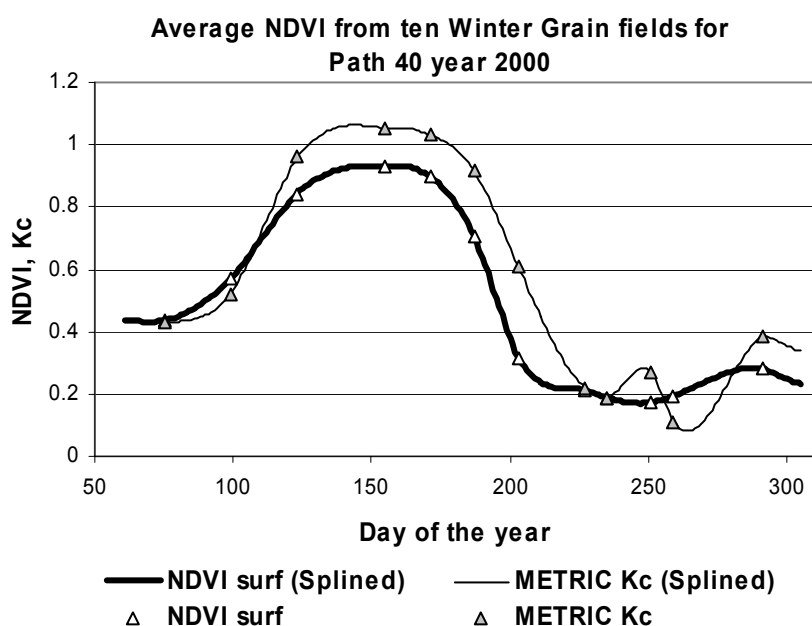


Figure 5.2-20 Average NDVI and METRIC K_c from ten randomly sampled Winter Grain fields.

The winter grain simulations performed similar to those for spring grain with a slightly larger deviation from METRIC with approximately 4.9% under estimation. Winter grain had a much higher RMSD than spring grain at 1.01 mm/day. The highest mean absolute difference of 0.77 mm/day was observed for winter grain simulations.

Similar to spring grain, $K_{cb} + K_e$ estimates deviate slightly from METRIC late in the season after irrigation simulations have ceased. The total of 8 simulated irrigations could be low and cause some of the under estimation in seasonal ET. Also, the first

simulated irrigation simulated is before the typical beginning of irrigations within the Magic Valley and can be attributed to the high K_{cb} detected early for winter grain.

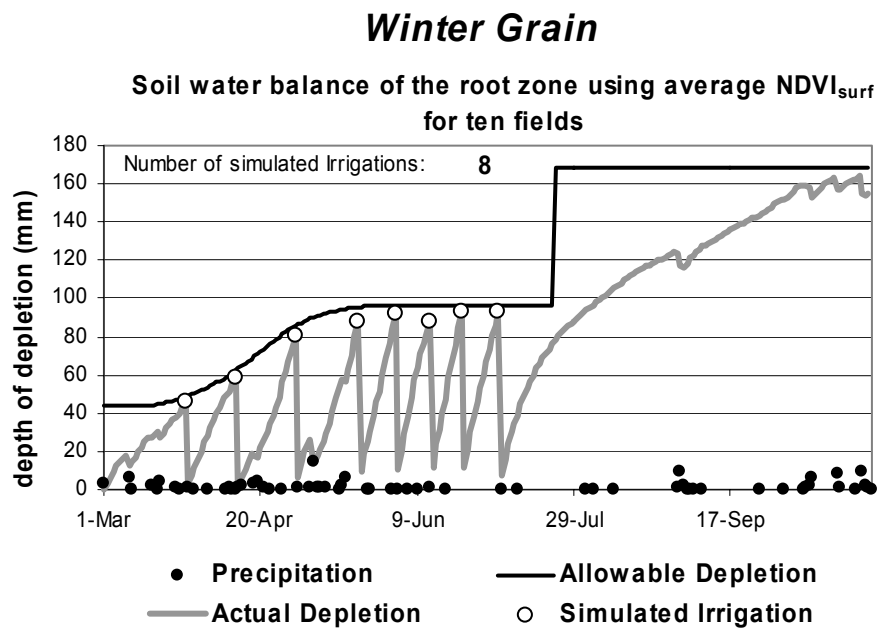


Figure 5.2-21 Soil water balance of the root zone and corresponding simulated irrigations.

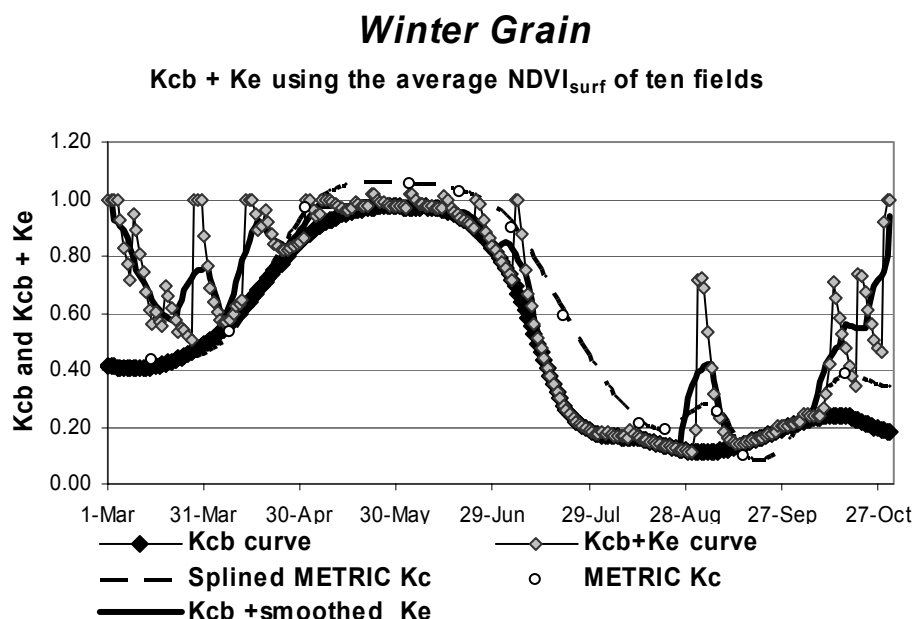


Figure 5.2-22 $K_{cb} + K_e$ curve for Winter Grain generated using water balance model with crop specific rooting characteristics and the general K_{cb} -NDVI relationship ($K_{cb} +$ smoothed K_e curve: K_e smoothed using 10 day running average for visual curve comparison).

5.3. Accuracy of Individual Field Simulations

The following discussion is made to analyze the performance of the water balance model when a single individual field, or pixel within a field, is considered with a custom crop specific K_{cb} -NDVI function and crop specific rooting depth and maximum plant height. Table 5.3-1 gives comparison results for all individual field simulations for each crop. With ten field simulations and twelve estimates (one for each image period) made for each field, a total of 120 ET estimates were available for comparison with METRIC observations.

Table 5.3-1 Summary of the accuracy of individual field simulations using specific crop characteristics and custom crop K_{cb} -NDVI curves (n = 120, 12 image sub-period estimates for 10 fields for each crop).

n=120 Crop	Stdev model (mm/day)	Model Efficiency (E)	RMSD (mm/day)	MADiff (mm/day)	MAPDiff (%)	MBE (mm/day)	r ²
Alfalfa	1.9	0.80	0.93	0.69	15.1	-0.05	0.80
Beans	2.6	0.75	1.38	0.89	33.3	-0.19	0.76
Corn	3.0	0.93	0.80	0.55	13.6	-0.07	0.94
Potatoes	3.0	0.78	1.37	0.76	17.8	-0.16	0.80
Spring Grain	2.9	0.88	1.09	0.78	21.3	-0.29	0.88
Sugar Beets	2.7	0.82	1.16	0.63	13.5	-0.11	0.83
Winter Grain	2.8	0.85	1.25	0.98	25.0	-0.29	0.87

****Note:** Evaluation was conducted using the average daily ET (mm/day) over each satellite sub-periods from the Kcb + Ke water balance model (predicted) and METRIC (observed) for March 1, 2000 to October 31, 2000

The analysis of all sampled fields for each crop type shows that simulations for individual corn fields would provide the best accuracy compared to METRIC observations. Figure 5.3-1 shows the comparison of the total 120 predicted ET estimates for corn to METRIC estimates which gave an r² of 0.94. Interestingly corn ET data estimated for the June 19 image date (noted in Figure 5.3-1) had the highest differences between METRIC and water balance model results. This date in June corresponds to the period of rapid growth for corn crops and the beginning of simulated irrigation events within the water balance model. Much of the difference observed between ET estimates could be largely influenced by prediction of irrigation events and how well those events mirror the actual irrigations for those individual corn fields. The simulations for individual bean fields had the lowest r² (0.76), and the highest mean absolute percentage difference of 33.3%. Beans also had the highest RMSD of 1.38 mm/day.

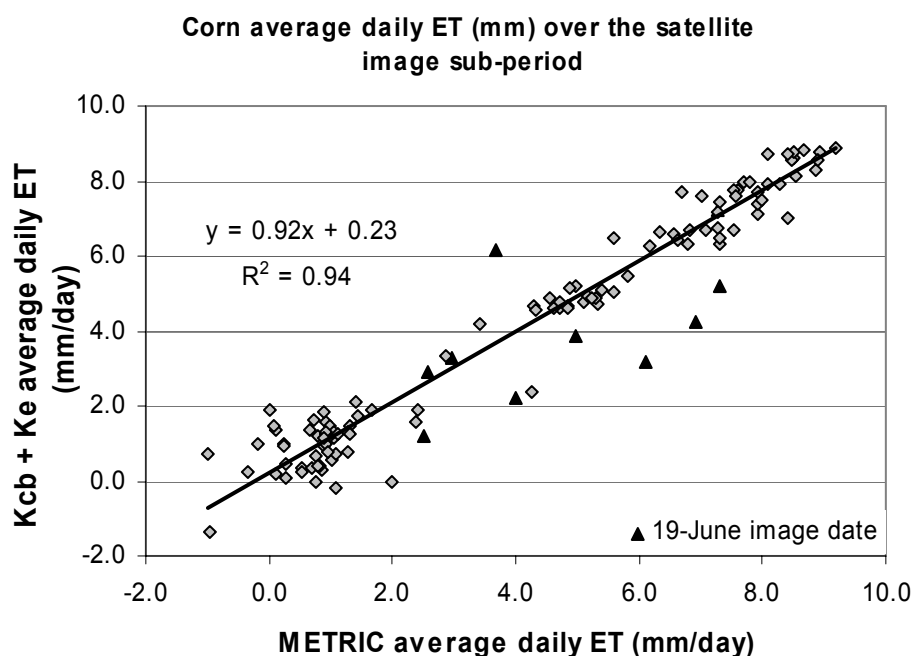


Figure 5.3-1 Comparison of predicted average daily ET to METRIC observed average daily ET for 10 individual Corn fields (n=120).

5.4. Average Field Condition Simulation using 3,754 Sampled Fields

This section presents the results of simulations on field conditions representing average crop conditions for the Magic Valley. The average field condition for each crop type was constructed by sampling image date NDVI values from a large number of fields for each crop type within the study area and taking the average NDVI of all fields to represent average conditions. This was carried out for all study crops. Simulations were then conducted using this average field and $K_{cb} + K_e$ curves constructed.

Table 5.4-1 displays the results for each crop simulation along with the total number of fields sampled for each crop analysis. Using average field conditions for each crop coupled with specific crop characteristics and custom K_{cb} vs NDVI relationships predicted ET similar to average observed METRIC ET from the same fields. METRIC estimates were calculated as the average of all individually sampled fields.

Water balance model predicted ET estimates were within 6% of METRIC for all crop types when compared over the entire growing season. Corn estimates gave the highest deviation from METRIC with 5.6% under estimation but had the highest r^2 of 0.97. Sugar Beets had the smallest RMSD of 0.50 mm/day.

Table 5.4-1 Average field condition (average crop defined by average NDVI over all sampled fields of that crop type) simulation using K_e from single irrigation simulation for average condition and crop specific characteristics.

n = 12		Seasonal	Stdev model	Model	RMSD	MADiff	MAPDiff	MBE	
Crop	# fields	Ratio	(mm/day)	Efficiency (E)	(mm/day)	(mm/day)	(%)	(mm/day)	r^2
Alfalfa	325	1.03	1.72	0.91	0.54	0.46	9.9	0.06	0.92
Beans	432	1.03	2.66	0.92	0.67	0.50	20.3	0.12	0.94
Corn	474	0.94	2.93	0.96	0.53	0.30	7.0	-0.18	0.97
Potatoes	717	0.99	2.98	0.90	0.84	0.51	13.7	0.07	0.93
Spring Grain	546	1.02	2.90	0.92	0.85	0.64	18.9	-0.05	0.92
Sugar Beets	516	1.00	2.61	0.96	0.50	0.34	7.5	-0.01	0.96
Winter Grain	564	1.02	2.90	0.89	1.05	0.78	21.1	-0.04	0.89

****Note:** Average crop simulation is conducted using average field condition which is estimated from the average NDVI from all sampled fields of that crop type for the entire growing season (1-Mar to 31-Oct). METRIC observations are the average ET of same fields for each crop type.

5.5. K_e Simulation Sensitivity

The amount of evaporation occurring over a given crop can play a large role in total ET, especially under bare soil conditions. When conducting a water balance model and associated irrigation simulations to single locations, the combined $K_{cb} + K_e$ curve can be extremely ‘spiky’ and may not represent actual conditions due to uncertainty in actual dates for irrigation. Furthermore, when conducting simulations for individual pixels within remotely sensed images, pixels within the same field may have drastically different simulated irrigation schemes.

One way to overcome this difference is to use an average K_e to be added to K_{cb} , for each crop type constructed from multiple irrigation simulations conducted for each crop under consideration. In this analysis the average K_e was generated for each crop by conducting ten field simulations and then averaging the K_e obtained from each irrigation simulation. This not only gives a more realistic K_e for each crop type but also has the effect of ‘smoothing’ spikes in the $K_{cb} + K_e$ curves. Figure 5.5-2 shows the resulting

'smoothing' of the K_e based on individual simulations such as shown in Figure 5.2-21. It is worth noting that K_e spikes from precipitation were not smoothed by the averaging, since precipitation was assumed to apply to each sampled field.

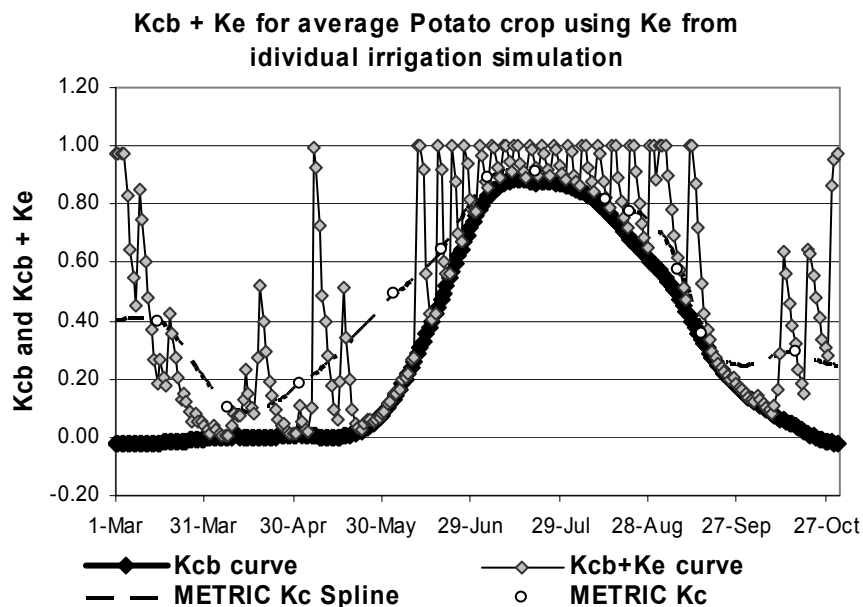


Figure 5.5-1 $K_{cb} + K_e$ curve for an average Magic Valley Potato field using K_e derived from one individual irrigation simulation and specific crop characteristics.

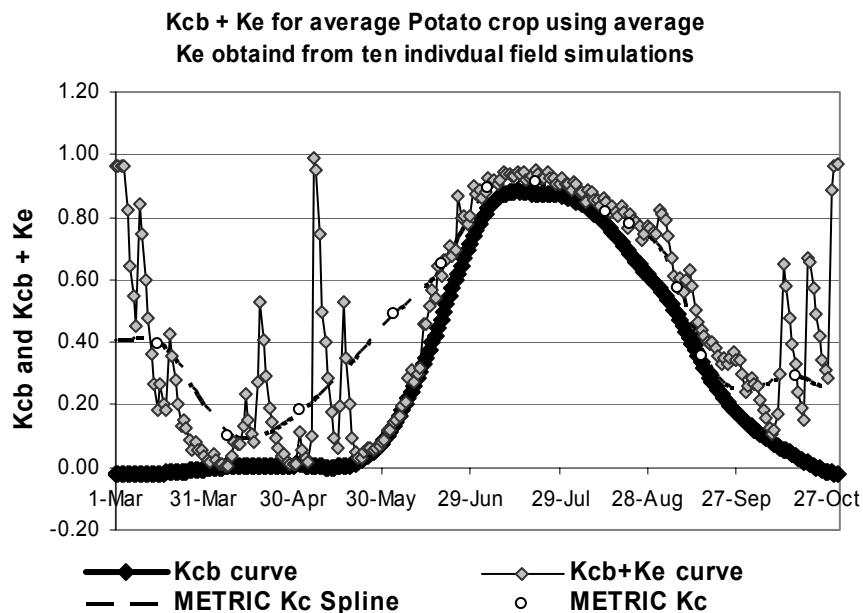


Figure 5.5-2 $K_{cb} + K_e$ curve for the average Potato field condition within the Magic Valley using K_e averaged from individual field irrigation simulations from ten fields, using specific crop characteristics.

The effects of using the average K_e from ten field simulations for each crop type and the resulting comparison with METRIC observations can be seen in Table 5.5-1. Again corn produces the largest under estimate for seasonal ET with an under estimation of 5.8% compared to the 5.6% under estimation found for corn with K_e from individual simulations. It is also noted that using the average K_e for each average field simulation reduced the RMSD for all crops considered. The only exception was for the corn simulation where the RMSD of 0.50 increased to 0.53 mm/day, and sugar beets which increased slightly from 0.50 to 0.51 mm/day.

This reduction in RMSD by using a K_e averaged for each crop can be attributed to the smoothed K_e which reduces daily variation in the overall $K_{cb} + K_e$ curve. The use of average K_e also increased model efficiency and decreased the mean absolute difference between model and observed METRIC ET in most cases. Overall the use of an average K_e obtained from individual simulations proves advantageous for simulations when crop classification is known.

Table 5.5-1 Average field condition simulation using specific crop characteristics for each crop and K_e averaged from individual simulations for ten fields for each crop type (average field condition is defined by averaging NDVI over all fields of each given crop).

n = 12 Crop	# fields	Seasonal Ratio	Stdev model (mm/day)	Model Efficiency (E)	RMSD (mm/day)	MADiff (mm/day)	MAPDiff (%)	MBE (mm/day)	r^2
Alfalfa	325	1.01	1.68	0.93	0.49	0.39	8.5	0.00	0.93
Beans	432	1.00	2.60	0.94	0.58	0.45	18.1	0.03	0.95
Corn	474	0.94	2.87	0.96	0.53	0.31	7.4	-0.21	0.97
Potatoes	717	0.99	2.90	0.90	0.84	0.47	12.5	0.02	0.92
Spring Grain	546	0.99	2.89	0.94	0.72	0.54	16.0	-0.12	0.94
Sugar Beets	516	0.99	2.59	0.96	0.51	0.35	7.8	-0.03	0.96
Winter Grain	564	1.00	2.89	0.92	0.89	0.69	18.6	-0.10	0.92

****Note:** Average crop simulation is conducted using average field condition which is estimated from the average NDVI from all sampled fields of that crop type. METRIC observations are the average ET of all sampled fields for each crop type.

6.0 CROP CLASSIFICATION FREE K_{cb} + K_e WBM

One of the major purposes of this study was to develop an ET estimation method from the short wave satellite data which does not depend on a crop classification of the area of interest. Detailed crop classification is both timely and expensive. The results of the water balance model were tested for simulations with and without crop classifications to assess any loss in accuracy due to a crop classification free approach.

6.1. Ten Field Simulations for Each Crop under Consideration

This section presents results of ten field simulations for each of the seven crops under consideration using the “classification free” general K_{cb} versus NDVI relationship. While a total of ten simulations were conducted for each crop type we will first present the results of the average field condition for each crop. The average field condition is characterized by performing the water balance model of a hypothetical field of the crop type under consideration (but using the ‘classification free’ K_{cb} -NDVI relationship), developed from the average NDVI values for each of the ten field observations per image date. This analysis gives a “pooled” set of observations, which can be used as an indicator, to examine the ability of the dual crop coefficient water balance model to replicate METRIC K_c and thus ET estimates for each of the studied crop types.

Table 6.1-1 shows the results of all “average crop” simulations for the randomly sampled fields. The ratio of the predicted seasonal ET to the METRIC observed seasonal ET was highest for the alfalfa crops at 1.17. Alfalfa also exhibited the lowest model efficiency ($E = 0.75$) as well as the largest mean bias error. The water balance model for the remaining crops produced seasonal ET estimates within 5% of METRIC. The water balance model conducted on Alfalfa did have the lowest standard deviation of model estimates of 1.60 mm/day. Interestingly, the total seasonal percentage of ET corresponding to evaporation was approximately 17% for the average alfalfa simulation (using average NDVI over ten randomly sampled fields) and ranged from 13% for winter grain up to 31% for bean crops using general crop characteristics and general K_{cb} -NDVI relationships. This is discussed in more detail in section 6.4.

Table 6.1-1 Summary of average field condition simulation using the universal (crop coefficient free) K_{cb} -NDVI relationship for ten sampled fields for each of the crop types considered.

n=12 Crop	Seasonal Ratio	Stdev model (mm/day)	Model Efficiency (E)	RMSD (mm/day)	MADiff (mm/day)	MAPDiff (%)	MBE (mm/day)	r^2
Alfalfa	1.17	1.60	0.75	0.91	0.72	15.88	0.66	0.90
Beans	0.97	2.41	0.92	0.74	0.58	21.8	-0.12	0.93
Corn	1.04	2.79	0.98	0.46	0.40	9.9	0.09	0.98
Potatoes	0.98	2.89	0.92	0.76	0.44	10.4	-0.02	0.93
Spring Grain	0.98	2.90	0.96	0.56	0.44	12.1	-0.15	0.97
Sugar Beets	0.98	2.75	0.96	0.55	0.41	8.7	-0.07	0.96
Winter Grain	0.96	3.02	0.91	0.98	0.72	18.3	-0.24	0.92

****Note:** Evaluation was conducted using the average daily ET (mm/day) over each satellite sub-period from the $K_{cb} + K_e$ water balance model (predicted) and METRIC (observed) for March 1, 2000 to October 31, 2000

One possible cause of the over estimation of ET from alfalfa can be attributed to the high number of irrigation events estimated using the water balance model and rooting characteristics for the average crop type. Figure 6.1-1 shows the total 21 irrigations simulated for the average alfalfa field using the general crop characteristics used for the classification free approach (max height = 0.6, max rooting depth = 1m). This is similar to the number predicted for each of ten individual field simulations but significantly higher than the typical number of irrigations for alfalfa within the Magic Valley when surface irrigation is practiced. The 21 irrigations are more representative of center pivot systems which are common in the Magic Valley.

Ordinarily, irrigation does not begin for alfalfa until mid April, whereas the model predicted irrigation as early as March 7. In this case delaying irrigations until April 15 would have reduced the seasonal ET estimates for alfalfa by approximately 5 %.

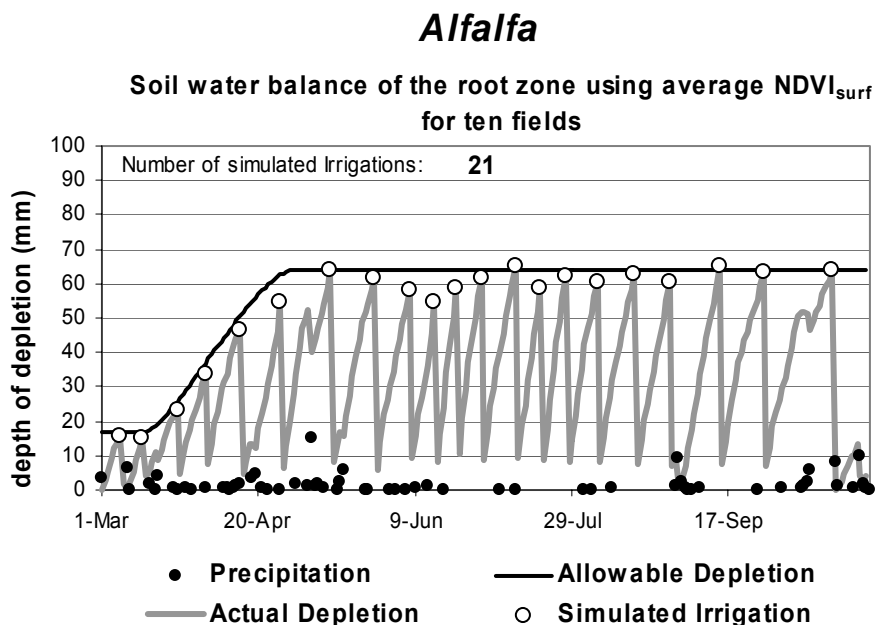


Figure 6.1-1 Soil water balance of the root zone for the average alfalfa field using general crop characteristics.

The high frequency in simulated irrigation events for alfalfa creates an extremely “spiky” $K_{cb} + K_e$ curve (Figure 6.1-2). With more irrigation, more water is available for evaporation and therefore predicted amounts increase. It was also observed that using the general crop characteristics coupled with the generic irrigation start/stop dates based on K_{cb} , ($K_{cb} > 0.25$) produced irrigation seasons for alfalfa over the entire study period of March 1 to October 31. The NDVI based K_{cb} for alfalfa was always greater than the K_{cb} threshold of 0.25 used as the indicator of irrigation season. Alfalfa was one of the two crops (winter grain simulations also predicted early irrigations) where irrigation season initiation prediction inaccuracies occurred and was compensated using the crop specific analysis discussed previously in chapter 5.

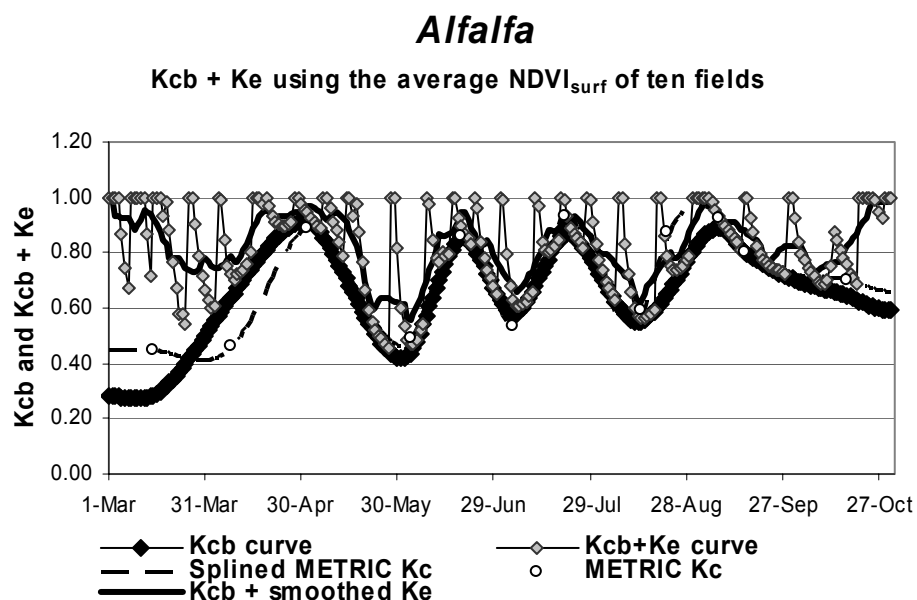


Figure 6.1-2 $K_{cb} + K_e$ for average alfalfa field constructed using water balance model. METRIC K_c is overlaid for comparison ($K_{cb} +$ smoothed K_e curve: K_e smoothed using 10 day running average for visual curve comparison).

Bean

Bean simulations using general crop characteristics and therefore the classification free approach actually performed better than simulations using the specific height and rooting depth characteristic for beans. The overall ratio of seasonal ET to the seasonal ET observed by METRIC was 0.97. The RMSD for the bean simulation was 0.74 mm/day. Examination of Figure 6.1-4 suggests reasonable agreement between seasonal $K_{cb} + K_e$ curves and METRIC K_c . It is seen however that under estimation can in part be attributed to the low number of irrigations.

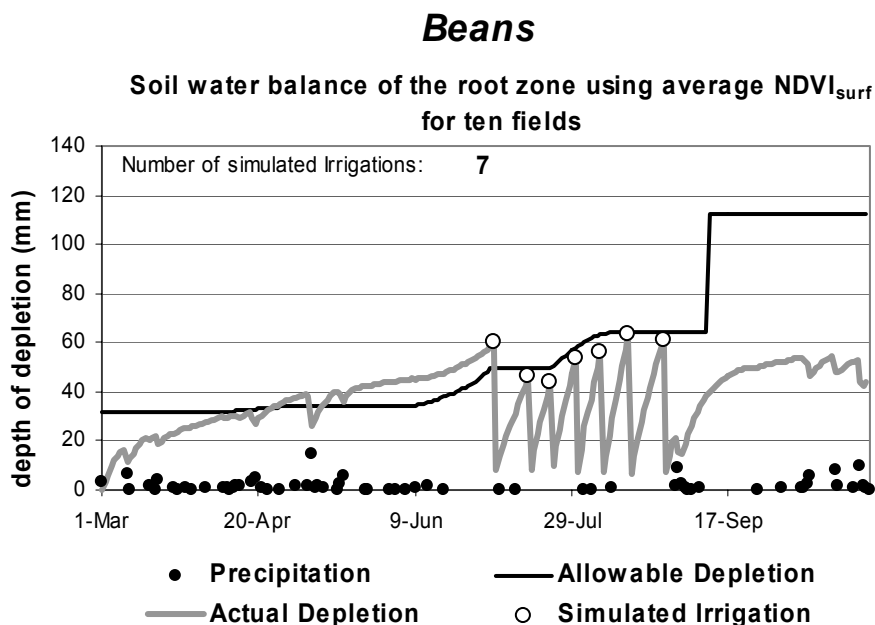


Figure 6.1-3 Soil water balance of the root zone and corresponding simulated irrigations using general crop characteristics.

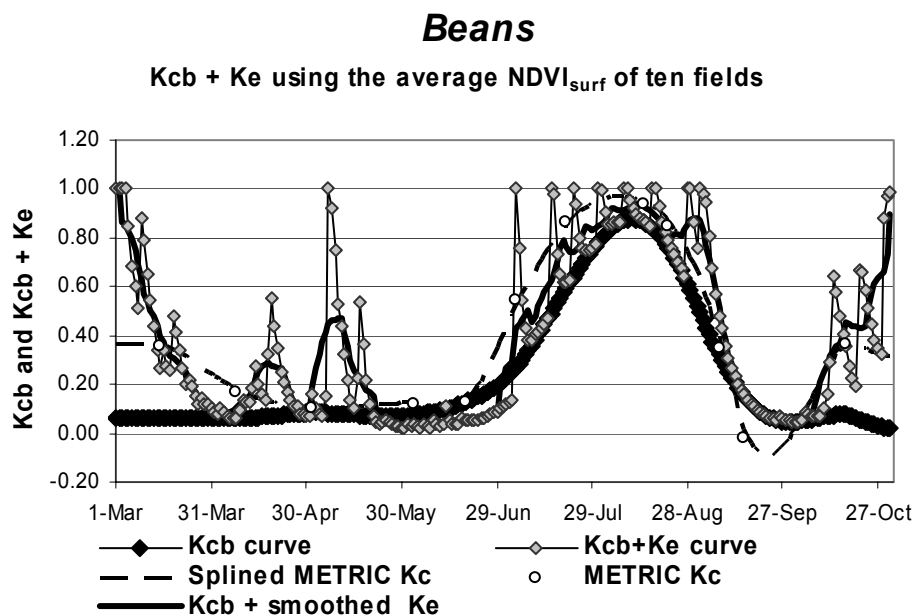


Figure 6.1-4 $K_{cb} + K_e$ curve for Beans generated using water balance model with general crop characteristics ($K_{cb} + \text{smoothed } K_e$ curve: K_e smoothed using 10 day running average for visual curve comparison).

Corn

Corn simulations using the general crop characteristics gave a seasonal ET ratio of 1.04 when compared to METRIC observed seasonal ET. This contrasts simulations for corn using specific corn characteristics which produced only 0.02% seasonal deviation from METRIC. Figure 6.1-5 also shows that the simulated number of irrigations increased from 7 to 13 when using general crop characteristics as opposed to corn characteristics (Figure 6.1-5 and 6.1-6 can be compared with Figures 5.2-9 and 5.2-10). This increase in irrigations creates a larger average K_e and therefore total crop coefficient. The resulting $K_{cb} + K_e$ curve can be seen in Figure 6.1-6.

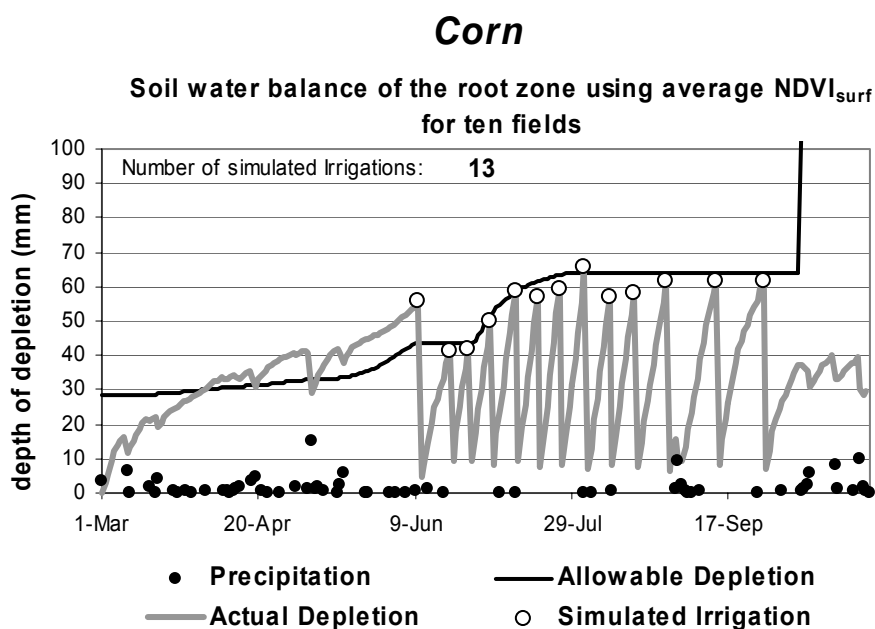


Figure 6.1-5 Soil water balance of the root zone for Corn using general crop characteristics.

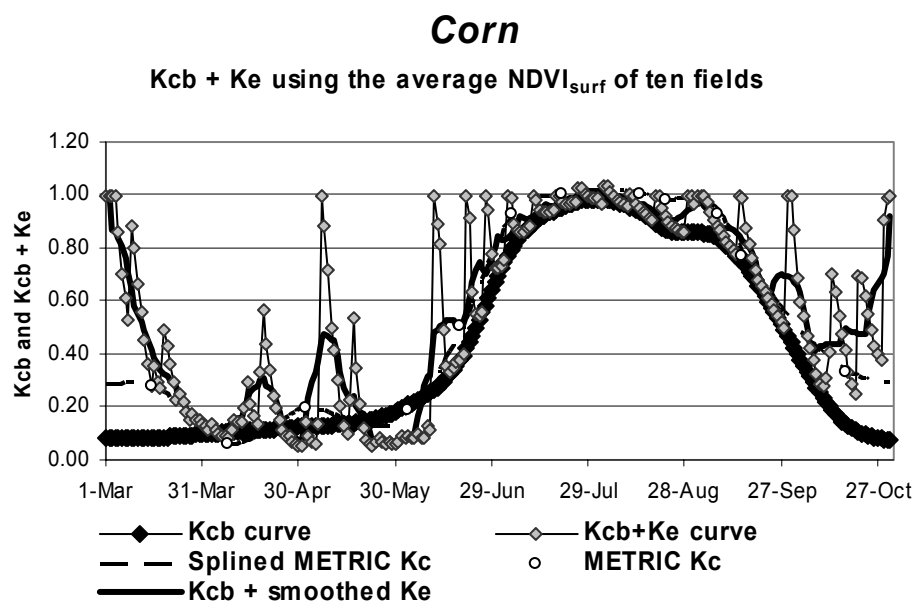


Figure 6.1-6 $K_{cb} + K_e$ curve for Corn generated using water balance model with general crop characteristics ($K_{cb} +$ smoothed K_e curve: K_e smoothed using 10 day running average for visual curve comparison).

Potato

General crop characteristics simulations for potatoes gave a seasonal ET ratio of 0.98 compared to METRIC and produced the smallest mean bias error of all simulations at -0.02 mm/day. The RMSD for the potato simulation using general crop characteristics was found to be 0.76 mm/day

Again as observed in simulations utilizing potato specific characteristics simulated irrigations appear to lag the start of rapid potato crop growth. Analysis of the $K_{cb} + K_e$ curve shown in Figure 6.1-8 shows that the first irrigation event is simulated approximately two weeks after the beginning of rapid crop growth. This coupled with the difference between water balance results and the METRIC K_c observation on June 3, suggest under estimation due to irrigation simulation. It seems that water balance model simulations lag the true start of the potato irrigation season within the Magic Valley. This problem could have been rectified by allowing irrigation for potatoes to proceed prior to

the $K_{cb} \geq 0.25$. However, in this particular simulation, it is assumed that the specific crop type is unknown.

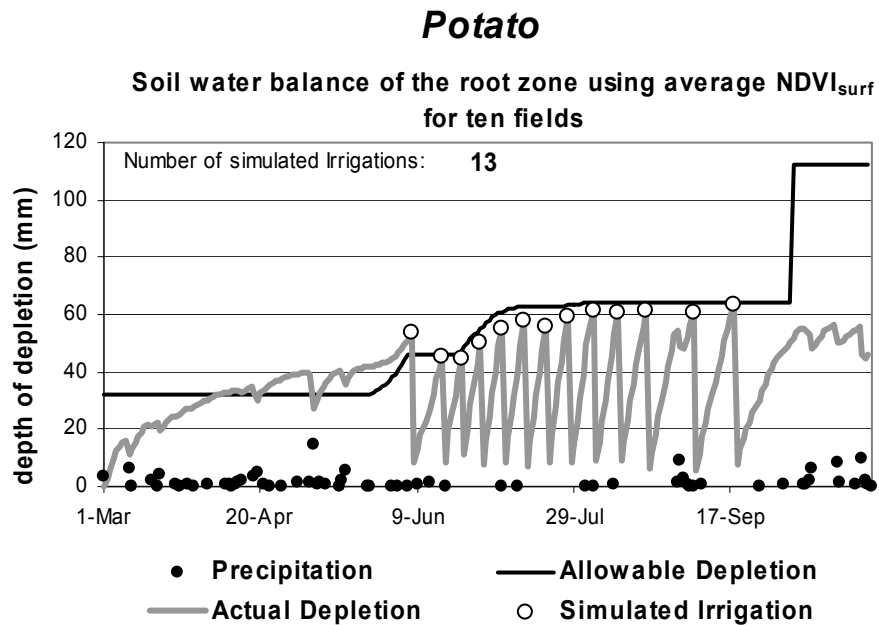


Figure 6.1-7 Soil water balance of the root zone for Potatoes using general crop characteristics.

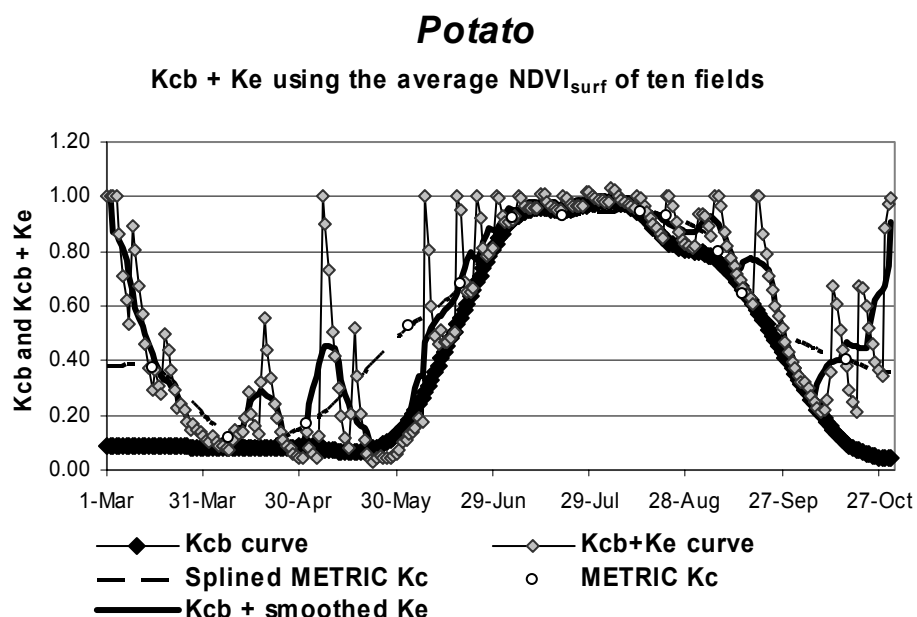


Figure 6.1-8 $K_{cb} + K_e$ curve for Potatoes generated using water balance model with general crop characteristics ($K_{cb} +$ smoothed K_e curve: K_e smoothed using 10 day running average for visual curve comparison).

Sugar Beets

Similar to simulations made with Potato fields the total seasonal deviation from METRIC ET decreased from -3.8% with sugar beet specific characteristics to -2.1% using the general crop characteristics. This can be attributed in part to the increase from 13 to 15 simulated irrigation events between the two simulations. The same lag between the start of rapid crop growth and the first simulated irrigation as with potato simulation suggest need for earlier irrigation simulation.

The RMSD for sugar beet simulations was the second lowest for all crop simulations with a value of 0.55 mm/day. Also the third highest r^2 was found for sugar beet simulations with a value of 0.96.

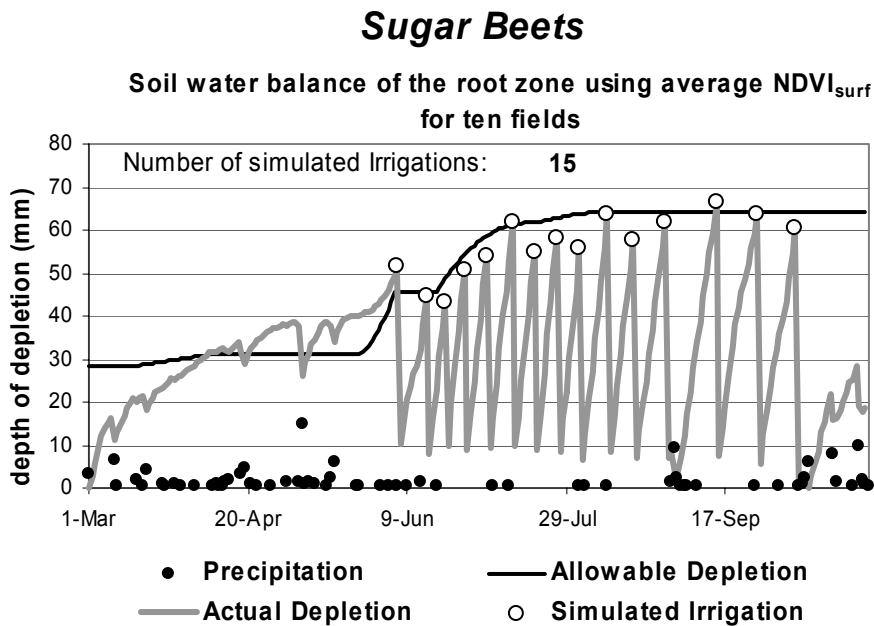


Figure 6.1-9 Soil water balance of the root zone for Sugar Beets using general crop characteristics.

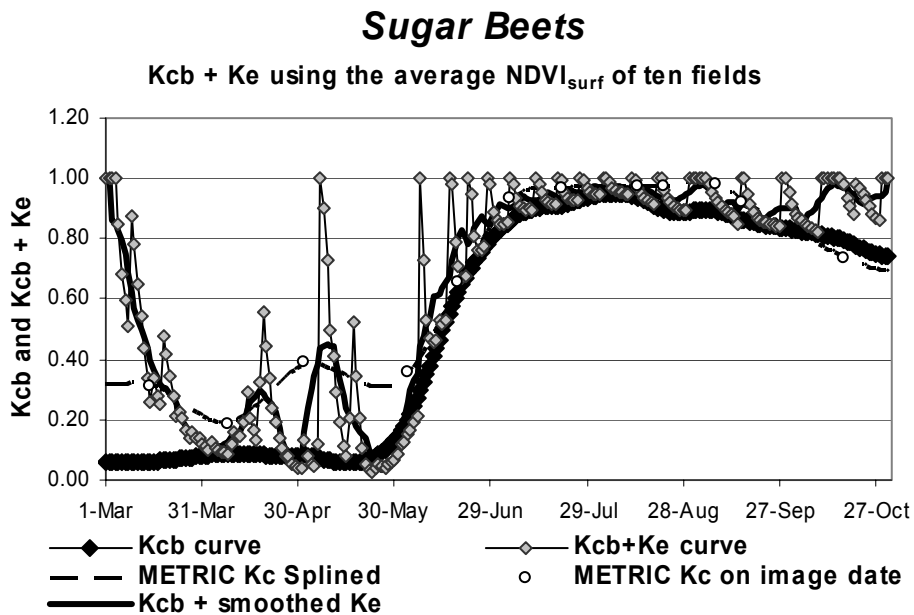


Figure 6.1-10 $K_{cb} + K_e$ curve for Sugar Beets generated using general crop characteristics ($K_{cb} +$ smoothed K_e curve: K_e smoothed using 10 day running average for visual curve comparison).

Spring Grain

As seen in Figure 6.1-11 a total of 11 irrigation events are simulated for the average spring grain field of the ten sampled fields when universal crop parameters are applied. Also a single irrigation is simulated late in the year as a result of an increase in vegetation growth seen in figure 6.1-12. This increase in vegetation could be due to replanting of many of the sampled fields with a winter grain crop, the growth of weeds, or 'nursed' alfalfa. The size of the last irrigation event is caused by the general assumption that the allowable depletion within the root zone increases to 70% of the available water after the crop is harvested. This increase eliminates further irrigations in most crops, but in this case where vegetation growth is observed and an additional irrigation simulated.

Even with the extra large irrigation simulated seasonal estimates of the water balance model still slightly under estimate METRIC estimates with a seasonal ratio of 0.98. Figure 6.1-12 also shows the majority of the under estimation occurring late in the season after the crop has been harvested. During this period of time it is possible that NDVI estimates may be artificially low due to the effect of crop residue left behind after the harvest. This residue can create difficulty in satellite based estimation of vegetation indices by altering the reflectance sensing by the satellite. This error in the NDVI estimation directly affects any estimate of ET based from NDVI. It is also possible that grain stubble was irrigated during August, following harvest, to moisten soil for cultivation (disking etc.). These events would be missed by the water balance model.

The overall RMSD for the spring grain simulation was 0.56 mm/day. The spring grain simulation also had the second highest model efficiency of 0.96.

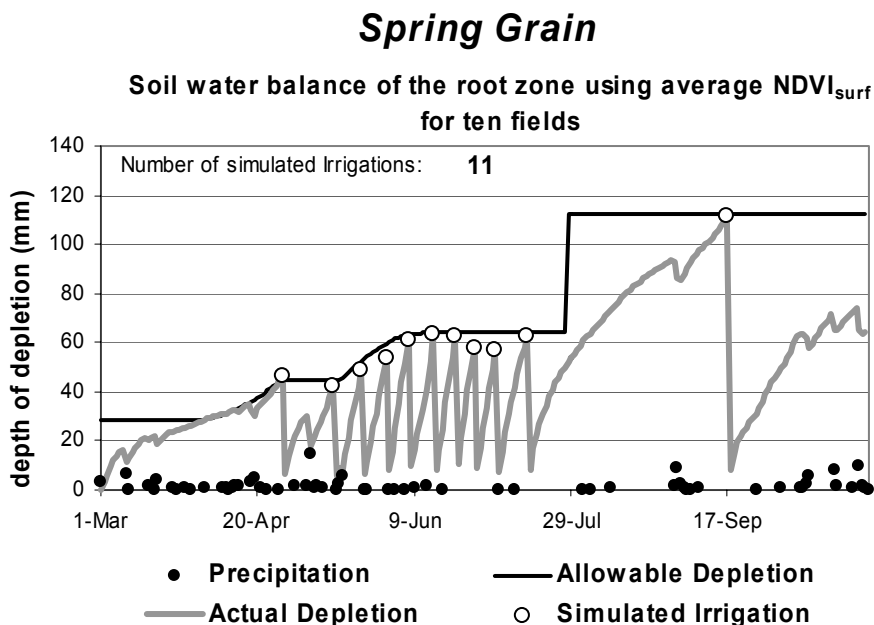


Figure 6.1-11 Soil water balance of the root zone for Spring Grain using general crop characteristics.

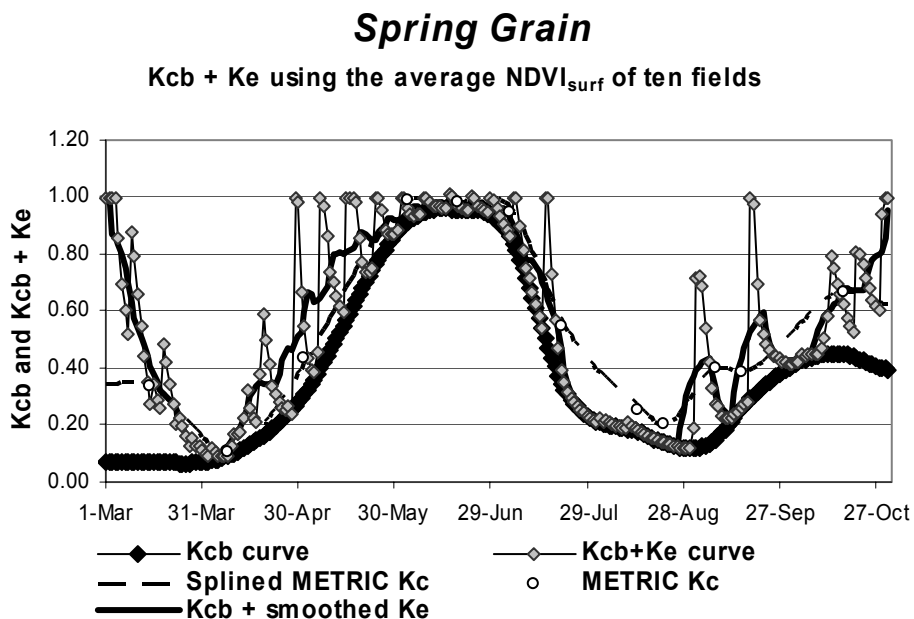


Figure 6.1-12 K_{cb} + K_e curve for Spring Grain generated using general crop characteristics (K_{cb} + smoothed K_e curve: K_e smoothed using 10 day running average for visual curve comparison).

Winter Grain

Winter grain simulations using the general crop characteristics provided similar results to simulations for spring grain as expected. Again most of the underestimation of ET observed from METRIC occurred late in the season after crops had been harvested (Figure 6.1-14) and the seasonal ET ratio was 0.96. This under estimation in seasonal ET from that observed by METRIC was the largest under estimation of all crops examined using the general crop characteristics.

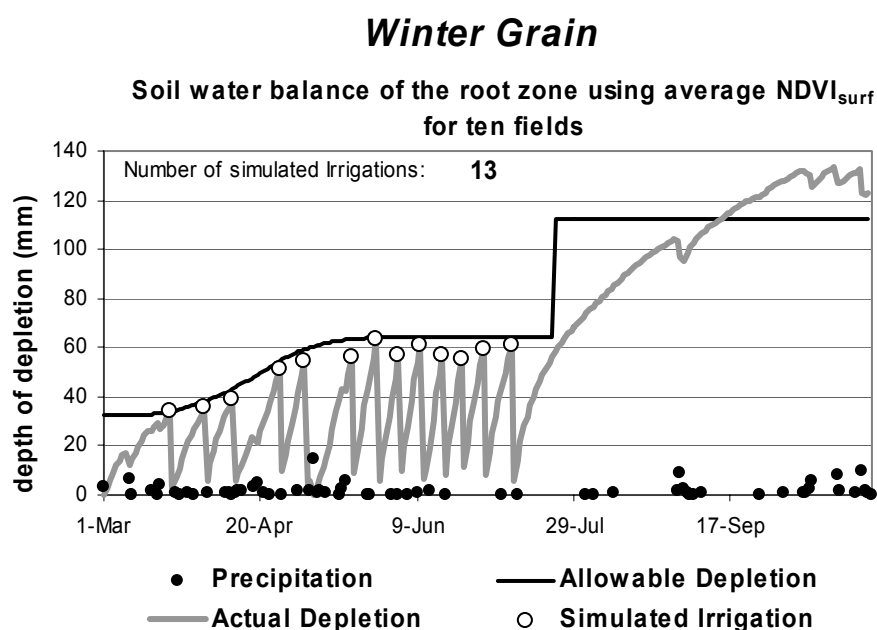


Figure 6.1-13 Soil water balance of the root zone for Winter Grain using general crop characteristics.

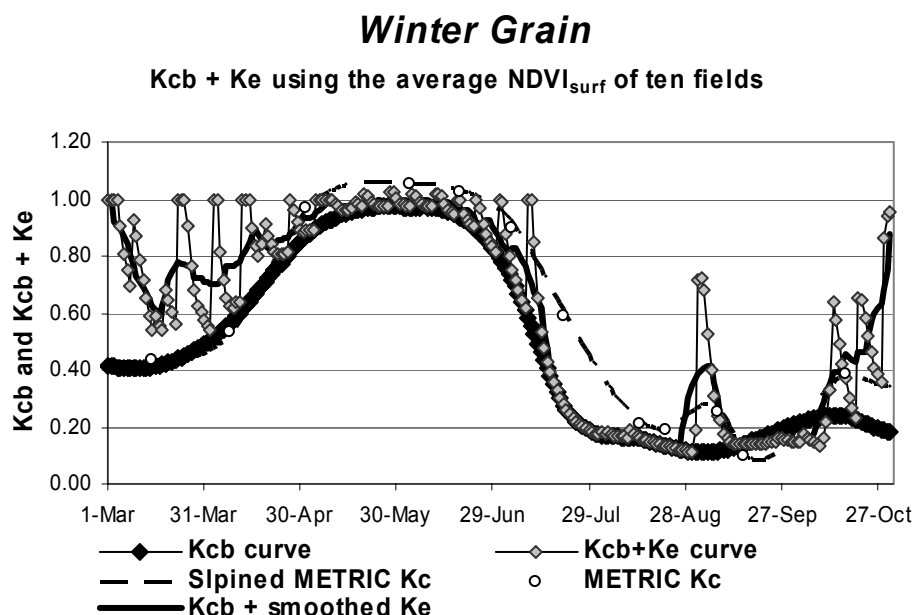


Figure 6.1-14 $K_{cb} + K_e$ curve for Winter Grain generated using water balance model with general crop characteristics ($K_{cb} +$ smoothed K_e curve: K_e smoothed using 10 day running average for visual curve comparison).

6.2. Individual Field Simulation using General Crop Characteristics

The use of a crop classification free approach has promise for accurate ET estimates from individual fields. General simulations for corn showed the highest accuracy (compared to METRIC) with an r^2 of 0.94 and the lowest mean absolute difference of 0.61 mm/day. The RMSD for the corn simulation was also the lowest for all crops with a value of 0.81 mm/day.

The largest discrepancies between water balance model results and METRIC observations were found in bean and alfalfa simulations with r^2 values of 0.77 and 0.78 respectively. The RMSD values obtained for beans of 1.36 mm/day was the highest of all crop simulations using the general crop characteristics. Potato and winter grain simulations yielded the second highest RMSD with values of 1.22 mm/day.

While the alfalfa model standard deviation was the lowest with a value of 1.8 mm/day, the lowest model efficiency of 0.70 and largest MBE of 0.59 mm/day, indicate

the poorest agreement with METRIC when looking at individual fields. This large discrepancy between water balance model and METRIC for individual alfalfa fields is due to the large variation in the actual field conditions among the high numbers of alfalfa fields present in a given area. Improvements in agreement were obtained using crop characteristics specific to alfalfa as discussed in section 5.

Table 6.2-1 Summary of individual field simulations for all crop types using general crop characteristics and general K_{cb}-NDVI relationship (10 field simulations for each crop with 12 image sub-period observations gives a total n = 120 for each crop type).

n=120 Crop	Stdev model (mm/day)	Model Efficiency (E)	RMSD (mm/day)	MADiff (mm/day)	MAPDiff (%)	MBE (mm/day)	r ²
Alfalfa	1.8	0.70	1.15	0.91	20.0	0.59	0.78
Beans	2.3	0.76	1.36	0.92	34.2	-0.16	0.77
Corn	2.7	0.93	0.81	0.61	15.0	0.09	0.94
Potatoes	2.9	0.82	1.22	0.73	17.2	-0.01	0.83
Spring Grain	3.0	0.88	1.06	0.75	20.4	-0.19	0.89
Sugar Beets	2.7	0.83	1.13	0.62	13.3	-0.07	0.84
Winter Grain	2.9	0.86	1.22	0.95	24.1	-0.22	0.87

****Note:** Evaluation was conducted using the average daily ET (mm/day) over each satellite sub-period from the K_{cb} + K_e water balance model (predicted) and METRIC (observed) for March 1, 2000 to October 31, 2000

6.3. K_{cb} + K_e WBM for Average Field Condition in the Magic Valley

To test the performance of the water balance model on average field conditions, the NDVI and METRIC K_c were sampled from a total of 3,574 fields throughout the Magic Valley. Simulations using the average field conditions, constructed using the average NDVI of all fields sampled of each crop type, were carried out using the general crop characteristics and then compared to the average METRIC ET estimates from all sampled fields of each crop type. Table 4.1-1 shows the total number of samples corresponding to each crop under consideration.

The average crop (field) condition within the Magic Valley was tested using the average NDVI from all sampled fields of all crop types and then simulations performed using the general crop characteristics and general K_{cb}-NDVI relationships. This was conducted as a crude representation of the ability of the water balance model to replicate

average ET estimates made by METRIC using a single water balance model simulation for each crop type.

With the exception of alfalfa and the average crop condition, water balance model simulations of seasonal ET were within 6% of METRIC observed seasonal ET. Here the ‘average crop condition’ reported in Tables 6.3-1 and 6.3-2, is constructed using the average NDVI sampled from all 3,574 fields sampled throughout the Magic Valley in the year 2000. This average crop condition, while ambiguous, is used simply to demonstrate an average simulation using the universal K_{cb} -NDVI relationship and general crop characteristics.

Improvement in the agreement of the water balance model to METRIC occurred for the average crop simulation when the average K_e from 10 simulations for each of the seven crop simulations (see section 5.5) was utilized, dropping the deviation from METRIC to within 4% for seasonal estimates, again excluding alfalfa and the average NDVI simulation (Table 6.3-2). While this type of average K_e utilized within the water balance would not be possible with the ‘classification free’ approach, it is presented here to show the improvement in water balance model results when a ‘smoothed’ K_e is available. Other methods of K_e smoothing would need to be explored for a true ‘classification free’ approach.

Table 6.3-1 Summary of average field condition simulations for all crops using general crop characteristics and K_e from one individual irrigation simulation per crop type using general K_{cb} -NDVI relationship (average field condition defined using NDVI averaged over all fields sampled for each crop type).

n = 12		Seasonal	Stdev model	Model	RMSD	MADiff	MAPDiff	MBE	
Crop	# fields	Ratio	(mm/day)	Efficiency (E)	(mm/day)	(mm/day)	(%)	(mm/day)	r²
Alfalfa	325	1.16	1.68	0.78	0.85	0.69	15.0	0.64	0.92
Beans	432	1.05	2.33	0.93	0.65	0.47	18.9	0.11	0.93
Corn	474	0.97	2.87	0.90	0.87	0.50	11.8	-0.09	0.91
Potatoes	717	1.05	2.82	0.93	0.71	0.52	13.9	0.22	0.94
Spring Grain	546	1.05	2.91	0.94	0.72	0.60	17.8	0.03	0.94
Sugar Beets	516	1.00	2.66	0.95	0.56	0.38	8.3	0.03	0.96
Winter Grain	564	1.06	2.89	0.91	0.97	0.75	20.4	0.11	0.91
Average crop	3574	1.20	1.76	0.85	0.71	0.59	17.8	0.59	0.97

****Note:** Average crop is estimated with the average NDVI and METRIC K_c from all 3,574 fields

****Note:** All comparisons are made between ET estimated by $K_{cb} + K_e$ WBM and results from METRIC as if METRIC is truth

Further evidence in the utility of incorporating average irrigation frequencies can be seen in Table 6.3-2 where simulations are made, again using general crop characteristics, incorporating the average K_e obtained from the ten individual field simulations presented above. It is noted here that individual field simulations used to construct the average K_e for this comparison also used general crop characteristics.

Table 6.3-2 Results for average field condition simulations using general crop characteristics and the K_e averaged from ten individual field simulations for each crop type using general K_{cb} -NDVI relationship.

n = 12 Crop	# fields	Seasonal Ratio	Stdev model (mm/day)	Model Efficiency (E)	RMSD (mm/day)	MADiff (mm/day)	MAPDiff (%)	MBE (mm/day)	r^2
Alfalfa	325	1.16	1.71	0.79	0.84	0.65	14.1	0.62	0.92
Beans	432	1.03	2.31	0.95	0.55	0.45	18.3	0.05	0.95
Corn	474	0.96	2.78	0.94	0.70	0.44	10.4	-0.16	0.94
Potatoes	717	1.03	2.77	0.93	0.72	0.48	12.8	0.14	0.94
Spring Grain	546	1.02	2.95	0.95	0.64	0.52	15.4	-0.03	0.95
Sugar Beets	516	0.99	2.63	0.95	0.55	0.36	8.0	-0.02	0.96
Winter Grain	564	1.02	2.92	0.93	0.86	0.67	18.2	-0.02	0.93
Average crop	3574	1.06	1.62	0.95	0.40	0.36	10.67	0.15	0.97

**Note: Average crop is estimated with the average NDVI and METRIC K_c from all 3,574 fields

**Note: All comparisons are made between ET estimated by $K_{cb} + K_e$ WBM and results from METRIC as if METRIC is truth

Using an average irrigation scheme provides seasonal ET estimates well within 4% of METRIC for average crop field conditions with the exception of alfalfa which retained it's 16% over estimation. Simulations for the average crop, including all sampled alfalfa fields, produced seasonal ET estimates within 6% of the average ET estimates from METRIC from all fields with an r^2 of 0.97.

6.4. Evaporation Fraction of total ET

The portion of total seasonal ET corresponding to evaporation can be quite large. Table 6.4-1 shows the fraction of seasonal evaporation to the total seasonal ET for simulations conducted on the average field condition for each crop within the Magic Valley.

Resulting seasonal evaporation fractions compare well with past work carried out within the Magic Valley by Allen et al, (2006) who found seasonal evaporation

percentages of 32% for beans and 19% for winter grain crops. Water balance model simulations using general crop characteristics and individual irrigation simulations (ten simulations per crop) for K_e , produced the highest estimates of evaporation in most cases. Potato and bean crops provided the exception with higher amounts of evaporation occurring in crop specific characteristic simulations (due to their actual root zone depletions being less than the all-crop average). Beans had the overall highest amounts of seasonal evaporation, which is expected given the more sparse crop cover characteristics for beans coupled with their short growing season, giving way to longer periods of bare soil conditions.

Table 6.4-1 Fraction of seasonal Evaporation to seasonal ET (March 1 to October 31) for simulations using the average field condition for the Magic Valley (Average field created using average NDVI from all sampled fields of a specific crop type).

Crop	General	General + Ave_Ke	Crop specific	Crop Specific + Ave Ke
Alfalfa	0.16	0.15	0.09	0.08
Beans	0.30	0.30	0.36	0.35
Corn	0.19	0.19	0.17	0.17
Potatoes	0.21	0.20	0.28	0.28
Spring Grain	0.21	0.19	0.19	0.16
Sugar Beets	0.16	0.15	0.15	0.15
Winter Grain	0.17	0.14	0.13	0.12

****Note:** General refers to simulations made using the general crop rooting and height characteristics and general (Classification free), and crop specific are simulations using customized K_{cb} -NDVI relationships and crop specific K_{cb} -NDVI relationship rooting and height characteristics for each crop type. The use of K_e averaged over ten individual field simulations per crop is denoted by + Ave_Ke

6.5. Loss or Gain of Accuracy with Classification Free Approach

The largest loss in accuracy associated with the crop type classification free approach was found with alfalfa simulations. This large disagreement between METRIC observations and estimates predicted by the water balance model using general crop characteristics can be attributed to several characteristics unique to alfalfa. As discussed previously, alfalfa crops are cut frequently throughout the growing season and the frequency of these cuttings for individual fields occurs essentially at random in a large population of fields. This can cause error in any NDVI based estimation due to the high variability in vegetation cover throughout the growing season. In addition the maximum

root zone for alfalfa of approximately 2 m (Table 4.3-2) is twice the average ‘general’ depth of 1 m. Therefore irrigations were scheduled about twice as often for alfalfa using the crop type classification free application as compared to typical surface irrigation schedules common within the Magic Valley. It is unclear, however; why the METRIC-based ET, which includes center pivot (high frequency) irrigated fields did not indicate these same effects.

Of the 70 individual fields sampled (ten fields for each of the seven crops under consideration), seasonal ET estimates using the general crop characteristics and general K_{cb} -NDVI relationship actually replicated METRIC seasonal ET more accurately, on average, than did the custom crop characteristic models with a seasonal MBE of only 1.4% versus -3.8% respectively. While this only represents a handful of field observations it does provide evidence for the usefulness of crop classification free simulations. Figure 6.5-1 shows the comparison of METRIC seasonal ET with seasonal ET estimated using the classification free approach. The high over estimation of alfalfa field simulations can also be seen in Figure 6.5-1.

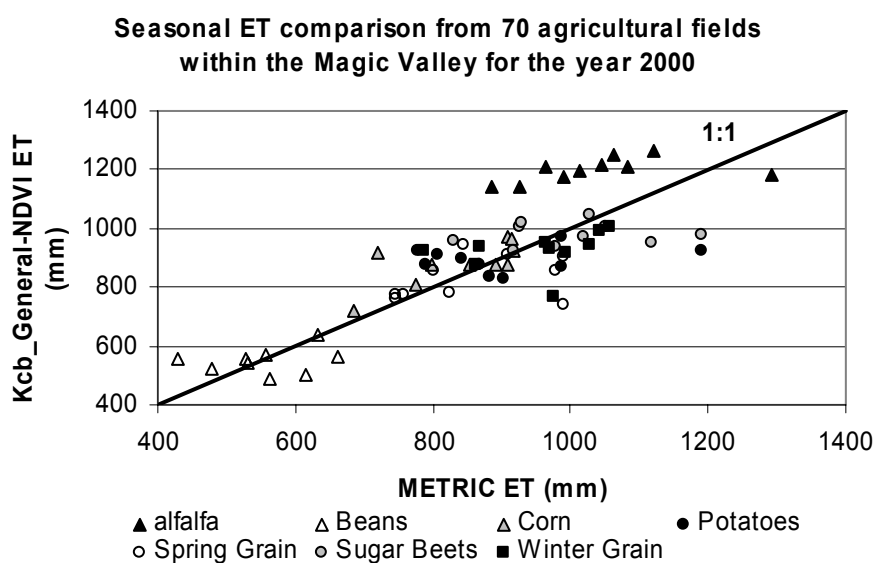


Figure 6.5-1 Seasonal ET estimates from METRIC compared with seasonal ET estimates using general K_{cb} -NDVI relationships and general crop characteristics.

7.0 COMPARISON OF ET ESTIMATES FROM $K_{cb} + K_e$ WBM AND K_{c_mean} METHODS

One question that arises in the examination of ET estimation methods based on vegetation indices is, Does the accuracy obtained by using an FAO 56 dual crop coefficient procedure (K_{cb} -NDVI relationship + K_e from water balance model) justify its use as opposed to a less intensive single crop coefficient procedure (K_{c_mean} -NDVI relationship)? In the K_{c_mean} procedure all impacts of evaporation from soil (K_e) are averaged, along with K_{cb} , into a single coefficient that is applied to all cases for a specific crop, or even all crops, if universal. Past work by Allen et al, (in preparation) developed ‘mean’ K_{c} -NDVI relationships and then performed ‘single’ crop coefficient procedures following the FAO 56.

The analysis of Allen et al, (pending) was conducted on a total of 3,420 agricultural fields within the Magic Valley. A universal relationship was fitted between the METRIC derived K_c (ETrF) and the at-surface NDVI for the sampled fields. In their analysis alfalfa crops were excluded from the K_{c_mean} -NDVI determination because of the random cutting schedules which occur among fields throughout a large area. The universal linear relationship found by Allen et al, (in preparation) for agricultural areas of the Magic Valley was as follows:

$$K_{c_mean} = 1.02 * NDVI_{surf} + 0.04 \quad (45)$$

Table 6.5-1 Sampled pixels used for the construction of K_{c_mean} -NDVI relationships by Allen et al, (in preparation) for crops within the Magic Valley for the year 2000.

Crop	# fields	Crop	# fields
Alfalfa	325	Sugar Beet	495
Bean	432	Spring Grain	536
Corn	451	Winter Grain	564
Potato	617	Total	3420

For comparative purposes this universal linear relationship was implemented on the 70 randomly sampled fields discussed in chapters 5 and 6 (10 fields for each of sthe

seven crops under consideration) and ET estimates compared to ET estimates made by the water balance model as well as METRIC ET observations. Table 6.5-2 presents the results of seasonal ET estimates based on the K_c_mean -NDVI relationship. Estimates made using the K_c_mean from NDVI gave the largest underestimation of seasonal METRIC ET observations of about 9% for spring grain fields and over estimation of seasonal ET as high as about 5% with alfalfa field simulations. It is noted that the development of the universal K_c_mean -NDVI relationship excluded alfalfa crops. If alfalfa is excluded from the comparison the largest deviation from METRIC observed using the $K_{cb} + K_e$ water balance model with general crop characteristics and general K_{cb} -NDVI relationships was 4 % overestimation of corn crops and 4 % underestimation in winter grain simulations (Table 6.1-1).

Table 6.5-2 Results of K_c_mean -NDVI relationship ET estimates from the average NDVI of ten randomly sampled fields of each crop type for March 1 to October 31 (same ten fields as discussed for water balance results in chapter 5 and 6).

n=12 Crop	Seasonal Ratio	Stdev model (mm/day)	Model Efficiency (E)	RMSD (mm/day)	MADiff (mm/day)	MAPDiff (%)	MBE (mm/day)	r^2
Alfalfa	1.05	1.80	0.92	0.53	0.37	8.17	0.16	0.93
Beans	0.96	2.13	0.90	0.83	0.65	24.2	-0.1	0.93
Corn	1.00	2.70	0.97	0.49	0.40	9.93	-0.08	0.98
Potatoes	0.93	2.92	0.95	0.63	0.41	9.55	-0.22	0.96
Spring Grain	0.91	2.90	0.97	0.49	0.37	10.11	-0.31	0.99
Sugar Beets	0.93	2.75	0.97	0.45	0.34	7.30	-0.26	0.98
Winter Grain	0.94	2.84	0.94	0.79	0.55	13.92	-0.28	0.96

****Note:** Evaluation was conducted using the average daily ET (mm/day) over each satellite sub-period from the K_c_mean -NDVI relationship developed by Allen et al, (in prep.) (predicted) and METRIC (observed) for March 1, 2000 to October 31, 2000

While seasonal ET estimates for water balance model simulations perform more accurately for most crops the r^2 values for the K_c_mean versus NDVI estimates are higher in most all crop simulations than for water balance model estimates. The lower r^2 for water balance model simulations is the result of differences on individual dates when irrigations are simulated but may not correspond to actual irrigations and therefore differ from ET estimates made by METRIC at that time (Figure 6.5-1). While the r^2 values presented in all tables are based on the average daily ET over image sub-periods, the effects of large daily variation in K_e is still seen. Because the K_c_mean ET estimates are directly related to NDVI, we would expect smaller ranges in daily ET estimates at any

given period. With the water balance model we would expect a large range of daily estimates early in the year when low NDVI and the K_e from irrigations or precipitation create spikes in $K_{cb} + K_e$ up to the maximum values and low ranges in estimates later in the year when NDVI is high (closer to the maximum K_c). Figure 6.5-1 shows crop coefficient curves generated for average potato crops using all K_c development methods discussed in this paper.

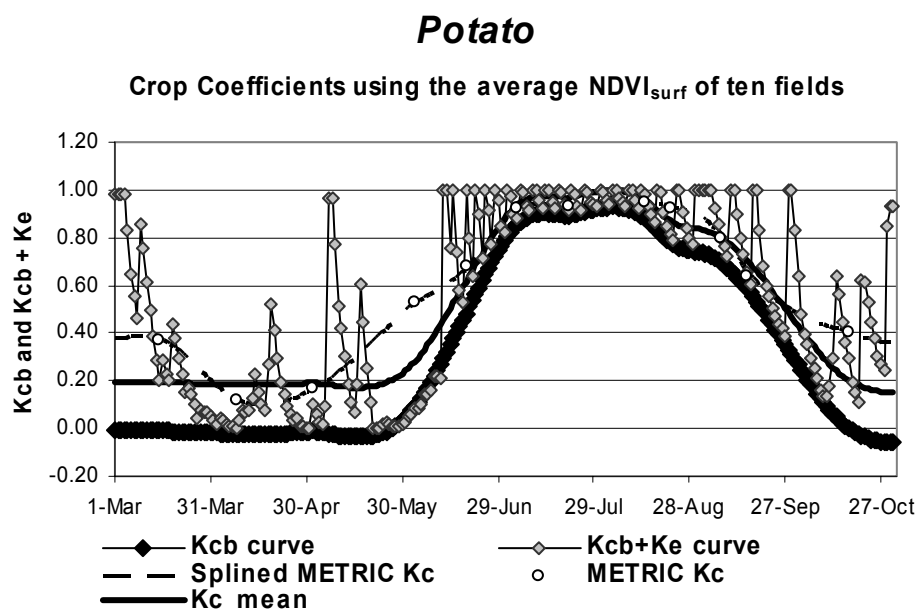


Figure 6.5-1 Comparison of daily crop coefficients for potato crops (average NDVI from ten randomly sampled potato fields) using various K_c estimation techniques within the Magic Valley for the year 2000.

The results of ET estimate simulations using average Magic Valley field conditions for each crop type are compared in Table 6.5-5. The MBE was lowest for crop specific water balance model simulations using crop specific K_{cb} -NDVI relationships with approximately zero MBE. General water balance model simulations resulted in the highest MBE of 0.15 mm/day but were reduced to 0.08 mm/day when attempts were made to incorporate a 'smoothed' K_e averaged over ten individual field simulations for each crop type. Again this type of smoothing would not be possible in a true crop

classification free approach but does show the value in using ‘smoothed’ K_e to reduce daily deviation in ET estimates from METRIC observations.

Table 6.5-3 Comparison of ET estimates from both general and crop specific water balance model simulations to ET estimates from K_c_mean -NDVI for average field conditions within the Magic Valley ($n = 84$, 12 image sub-period estimates for 7 crop types) Average field condition is using the average NDVI from all fields listed in Table 4.1-1 for each crop type.

n=84 Model	Stdev model (mm/day)	Model Efficiency (E)	RMSD (mm/day)	MADiff (mm/day)	MAPDiff (%)	MBE (mm/day)	r^2
General $K_{cb} + K_e$	2.7	0.92	0.75	0.56	14.7	0.15	0.93
General $K_{cb} + K_{e_ave}$	2.6	0.93	0.68	0.51	13.4	0.08	0.94
Custom $K_{cb} + K_e$	2.7	0.93	0.71	0.50	13.2	0.00	0.93
K_c_mean	2.6	0.96	0.53	0.39	10.3	-0.04	0.96

****Note:** Evaluation was conducted using the average daily ET (mm/day) over each satellite sub-periods from each model (predicted) and METRIC (observed) for March 1, 2000 to October 31, 2000. K_{e_ave} refers to the use of a K_e averaged over ten individual irrigation simulations, general simulations used general K_{cb} -NDVI relationships and Custom the crop specific K_{cb} -NDVI relationships.

The use of the dual crop coefficient based water balance model does appear to provide increased accuracy in seasonal ET estimates compared to ET estimates observed by METRIC. When crop classification is known water balance model estimates of seasonal ET can be obtained within 5% of METRIC observations. Water balance model simulations using general K_{cb} -NDVI relationships and general crop characteristics found seasonal ET estimates within 4% when excluding alfalfa field simulations (general water balance simulations gave up to 17 % over estimation of METRIC seasonal ET for alfalfa fields).

7.1. Analysis of Variance

The analysis of variance within each of the ET estimation techniques was made for a total of 840 (7 crops, 10 individual field simulations, 12 image sub-period average daily ET estimates) ET estimates made by each ET estimation model. The models tested were the $K_{cb} + K_e$ water balance model using general crop characteristics (Classification free), the $K_{cb} + K_e$ water balance model using crop specific K_{cb} -NDVI relationships and

specific crop characteristics, Kc_mean-NDVI ET estimation, and the observed METRIC ET estimates.

Histograms of all model results were compared and found to correspond to the assumption of approximate normal distributions. The main question to be answered by looking at the analysis of variance was to determine if the differences observed in ET estimates from each of the models were significantly different from observed ET estimated from METRIC processing. The primary hypothesis is that ET predictions made using water balance model techniques as well as Kc_mean-NDVI techniques provide similar results to METRIC observations and therefore can provide accurate ET estimates in the absence of thermal satellite imagery.

As expected the highest variance found between ET estimation model type were explained by the variances in crop type and image sub-period. Once variation due to crop type and image date sub-period were considered remaining variations in ET estimation was explained by estimation model method. This is at least in part expected when considering the wide range of conditions present from early spring to fall and between crop types. Table 7.1-1 gives the output of analysis of variance where attempt was made to exclude the main effect of image sub-period on model comparison by nesting the sub-period with the crop type. Statistically using the analysis of variance we are unable to conclude that all ET estimation models provide statistically similar results.

Table 7.1-1 Analysis of Variance output table generated in SYSTAT 11 testing average daily ET estimates of four model types.

Source	Type III SS	df	Mean-Square	F-ratio
MODEL\$	22.873	3	7.624	9.18
CROP\$	1526.723	6	254.454	306.354
SUBPERIOD (CROP\$)	21845.502	77	283.708	341.575
Error	2718.511	3273	0.831	

The next analysis conducted was a pair-wise comparison of average daily ET estimates made by each of the four methods. Table 7.1-2 presents the results of all pair-wise comparisons of ET estimates. It is apparent that based on comparisons of 840

average daily ET estimates (from the 70 randomly sampled fields) from each model that estimates made using the general water balance model and METRIC observations are not statistically different for these field observations.

Table 7.1-2 Games-Howell Test for pair-wise comparison of average daily ET estimates for each model considered (generated using SYSTAT 11).

MODEL\$ (i)	MODEL\$ (j)	Difference	p-value	95% Confidence Interval	
				Lower	Upper
Custom $K_{cb} + K_e$	Kc_mean	-0.006	1.000	-0.350	0.337
Custom $K_{cb} + K_e$	General $K_{cb} + K_e$	-0.170	0.588	-0.518	0.177
Custom $K_{cb} + K_e$	METRIC	-0.166	0.637	-0.526	0.194
Kc_mean	General $K_{cb} + K_e$	-0.164	0.599	-0.503	0.175
Kc_mean	METRIC	-0.159	0.649	-0.511	0.192
General $K_{cb} + K_e$	METRIC	0.004	1.000	-0.351	0.360

8.0 TESTING SPATIAL AND TEMPORAL APPLICABILITY

8.1. Path 40 year 2000

The following discussion presents the results of spatial $K_{cb} + K_e$ model simulations of ET for the entire Magic Valley for the year 2000. The twelve Landsat 5 and 7 images of Path 40 year 2000, previously discussed, were used to create seasonal ET estimates from the water balance model simulations. Crop specific simulations were first conducted using the 2000 crop classification and crop specific K_{cb} -NDVI relationships presented in chapter 4. The simulation used average daily K_e , obtained from the ten individual field simulations presented in chapter 5, for each crop type using the crop classification. Unclassified pixels were given daily K_e values averaged over all individual crop simulations. Using the K_e averaged over all fields for the unclassified pixels proved problematic as this added a higher K_e to non-agricultural (desert) pixels than would actually occur. This can be seen in the seasonal ET maps presented in Figures 8.1-1 and 8.1-2, where desert areas from the K_{cb} simulation had unrealistically high seasonal ET estimates. In practice, this could be removed by using land use type and $K_{cb} + K_e$ simulation for desert areas.

The visual comparison of the seasonal ET maps generated by both METRIC and the K_{cb} water balance model approach shows the largest differences in desert areas and water bodies. METRIC is able to sense evaporation occurring from water bodies where the K_{cb} approach (as applied here) can not. The inability of the K_{cb} model to assess evaporation from water bodies is a direct result of the use of the vegetation index. The NDVI of water bodies is negative which explains the low estimates of ET for water bodies by the K_{cb} water balance model approach. It is also noted the resolution of the short wave bands used to obtain NDVI are 30 X 30 m for both Landsat 5 and 7, while the thermal band used in METRIC processing has a 120 X 120 m resolution for Landsat 5 and a 60 X 60 m resolution in Landsat 7. The reduced resolution in the thermal bands creates the 'fuzzy' appearance of the METRIC ET map.

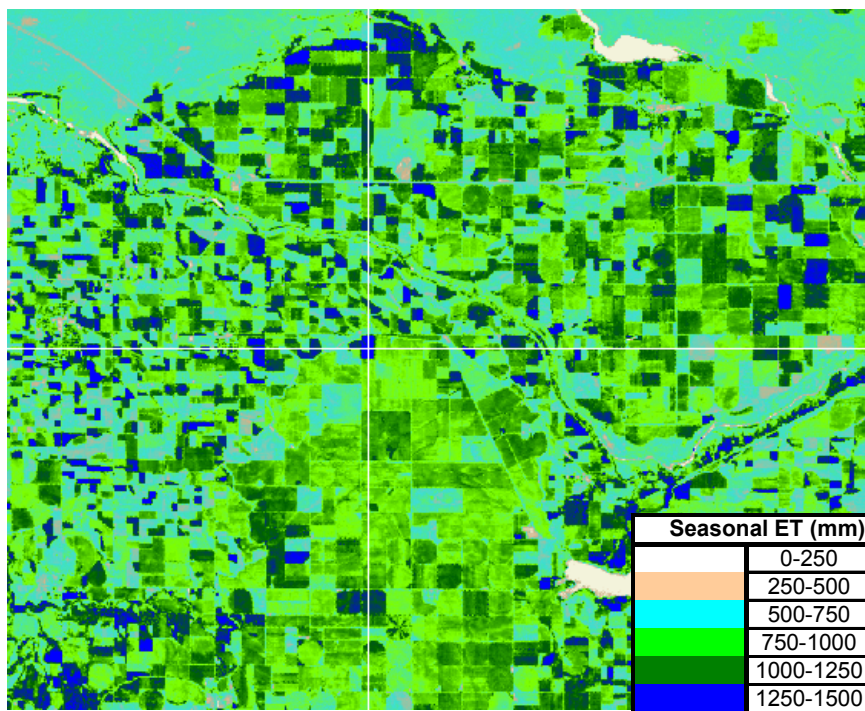


Figure 8.1-1 Seasonal ET map generated using K_{cb} -NDVI + K_e approach for the year 2000 (1-Mar to 31-Oct) within the Magic Valley near the communities of Murtaugh and Hansen Idaho.

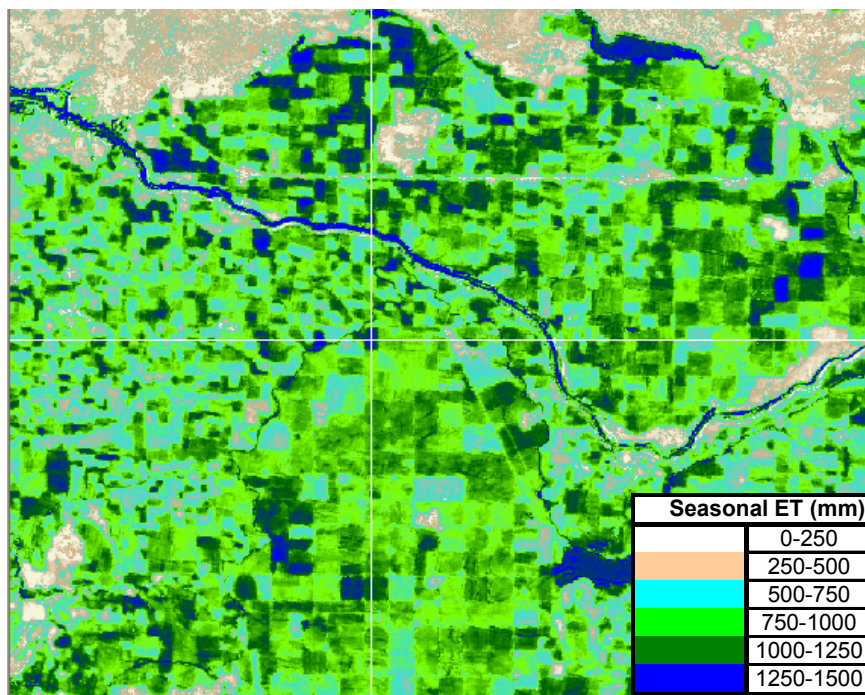


Figure 8.1-2 Seasonal ET map generated using METRIC processing for the year 2000 (1-Mar to 31-Oct) within the Magic Valley near the communities of Murtaugh and Hansen Idaho.

To test the results of the spatially distributed K_{cb} water balance model results a total of 8,521 agricultural pixels were sampled from within the Magic Valley. Table 8.1-1 gives the number of samples taken from each crop type under consideration. These sampled pixels represent pixels where no cloud cover was present on any of the twelve image dates (Figure 8.1-3).

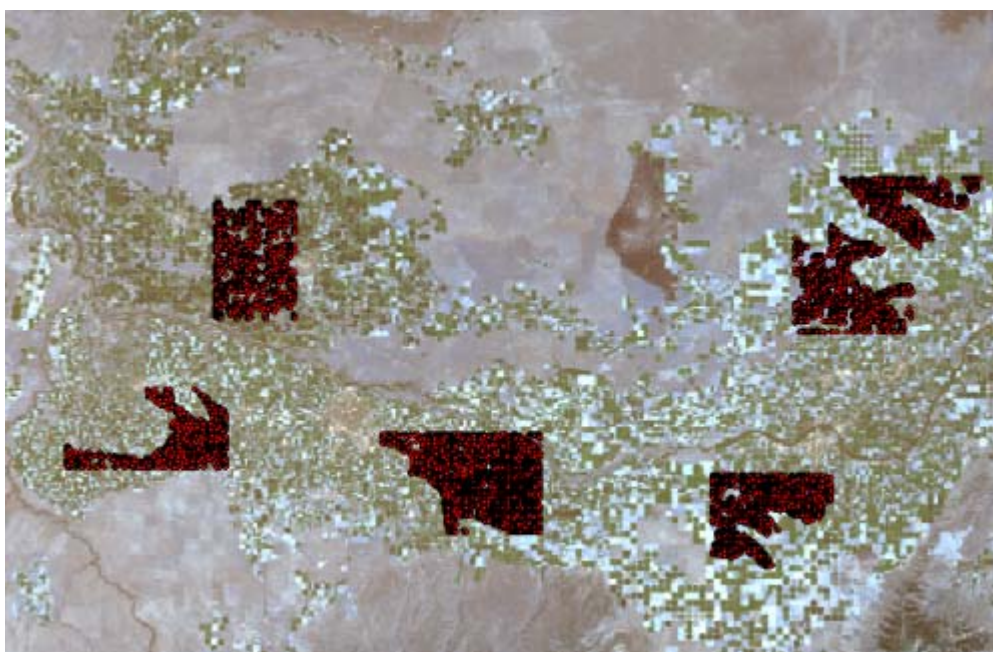


Figure 8.1-3 Cloud free sampled pixels within the agricultural area of the Magic Valley for the year 2000.

Table 8.1-1 Sampled "cloud free" fields for seasonal ET comparison for crops within the Magic Valley for the year 2000.

Crop	# Pixels	Crop	# Pixels
Alfalfa	526	Spring Grain	1354
Beans	1110	Sugar Beets	831
Corn	1255	Winter Grain	1059
Potatoes	2386	All crops	8521

Seasonal ET from each of the estimation methods were then sampled from all sampled pixels. Here it is important to note that while sampled pixels were filtered to ensure that no error was introduced by the presence of clouds, no attempt was made in this analysis, to avoid field edges and the accompanying error in METRIC estimates due to thermal pixel contamination. Table 8.1-2 gives the average deviation of $K_{cb} + K_e$ water balance model seasonal ET from METRIC seasonal ET. The average deviation for all sampled pixels regardless of crop type was only 1.3% from observed METRIC ET. The largest deviation was again found from alfalfa fields with an average deviation of 7.9%. Simulations for potato and corn crops performed the best with -0.5 and -0.6% deviations respectively.

Table 8.1-2 Percentage deviation in seasonal ET estimates of $K_{cb} + K_e$ water balance model from observed METRIC seasonal ET from 8,521 sampled pixels. Negative values represent under estimation of the water balance model compared to METRIC observations.

Crop	%dev from METRIC	Crop	%dev from METRIC
Alfalfa	7.9	Spring Grain	1.3
Beans	1.8	Sugar Beets	3.6
Corn	-0.5	Winter Grain	1.2
Potatoes	-0.6	All crops	1.3

While the average deviation of the crop specific water balance model ET estimates from METRIC observations is small, Figure 8.1-4 shows that for individual fields the deviation can be quite large. In some cases the deviation for individual fields was as high as 60% of METRIC observations. However, the next section discusses how much of this difference is attributed to thermal pixel contamination near field edges. This illustrates the need to utilize METRIC processing when thermal satellite information is available.

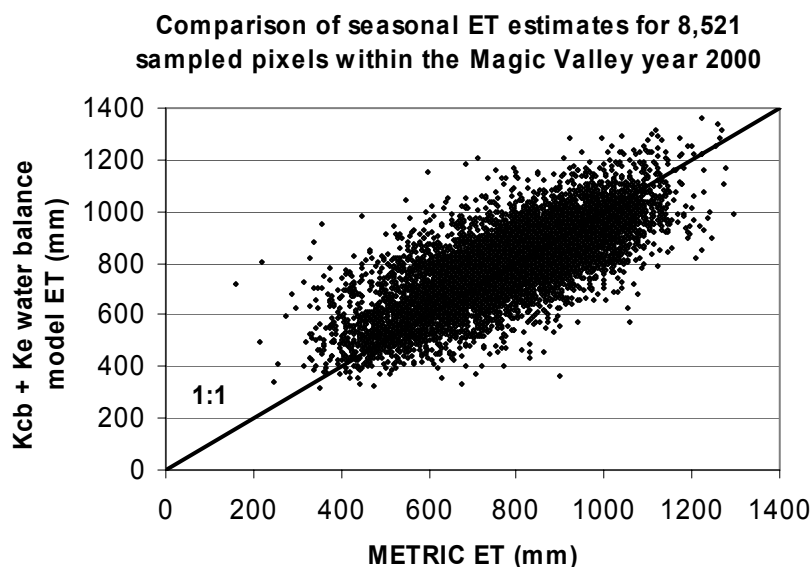


Figure 8.1-4 Comparison of seasonal ET estimates from the crop specific $K_{cb} + K_e$ water balance model and observed METRIC estimates no filtration of possible thermal contamination.

Because many of the sampled pixels were taken from field edges where thermal pixel contamination can cause METRIC ET estimates to deviate from the field-average (Tasumi et al. 2003, Allen et al. 2007a), the next analysis was performed using pixels sampled by Tasumi et al, (2003) where care was taken to select only pixels within fields away from thermal contaminated field edges (near the center of fields). All pixels in this analysis were also cloud filtered so that sampled fields had no cloud cover on any Landsat image dates. Table 8.1-3 lists the total number of fields sampled for each crop type representing cloud free locations.

Table 8.1-3 Sampled fields based on crop type within the Magic Valley for the year 2000. All sampled fields are taken well within field edges to avoid contamination by thermal pixels (thermal contamination can cause within-field bias in METRIC ET estimation), as well as filtered so that no cloud cover was observed for any of the Landsat image dates.

Crop	# fields	Crop	# fields
Alfalfa	241	Sugar Beet	285
Bean	228	Spring Grain	282
Corn	346	Winter Grain	258
Potato	409	Total	2049

Figure 8.1-5 shows the comparison of seasonal ET between METRIC and the crop specific $K_{cb} + K_e$ water balance model seasonal ET estimates. Comparison of figure 8.1-5 and Figure 8.1-4 show reduced scatter in results by excluding cloud and thermal pixel contaminated pixels (near field edges) in the ET analysis. In this case the average deviation between water balance model results and METRIC observations was reduced to -0.2 % for all sampled fields regardless of crop type (Table 8.1-4). Here the deviation from METRIC was reduced to about 0.5 % for alfalfa fields but was increased for bean crops to about 8 % over estimation.

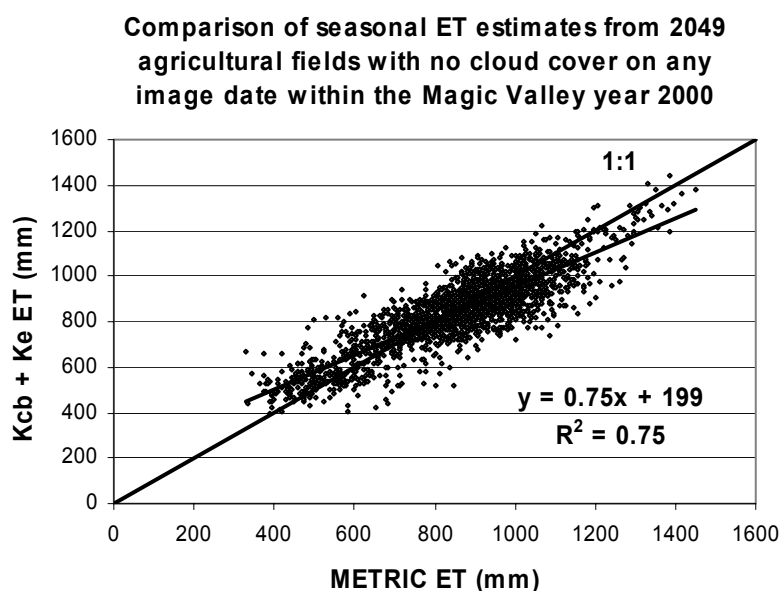


Figure 8.1-5 Seasonal ET comparison between METRIC and the custom K_{cb} -NDVI water balance model results using crop specific crop characteristics.

It is noted from Figure 8.1-5 that the actual relationship between water balance model seasonal ET estimates and METRIC observations is actually less than one to one. This difference occurs for several reasons. First, in conditions of low vegetation (bare soil or near bare soil) when an irrigation or precipitation event occurs, a large spike in the evaporation component (K_e) of ET is observed. Observations made by METRIC at these times sees the ‘average’ effect of this spike in ET, and therefore at low rates of ET the water balance model tends to predict higher rates of ET than METRIC (when averaged over a large number of pixels). Second, during full cover conditions (this time period accounts for the highest percentage of seasonal ET) METRIC is able to capture the effect

of wet soil surface beneath full cover vegetation, following precipitation or irrigation, which can increase the rates of ET about 5 % higher than the reference ET (ET_r).

METRIC applications within the Magic Valley has found peak K_c values of 1.1 which corresponds to a 10% higher ET rate than the reference (Tasumi et al. 2005). This in part explains why at high values of seasonal ET METRIC tends to predict higher ET than the water balance model estimates.

Table 8.1-4 Average deviation for METRIC seasonal ET estimates using the $K_{cb} + K_e$ water balance model with crop specific characteristics and custom K_{cb} -NDVI relationships for each crop. Negative values represent under estimation by the water balance model compared to METRIC observations.

Crop	% dev from METRIC	Crop	% dev from METRIC
Alfalfa	0.5	Spring Grain	-0.2
Beans	8.0	Sugar Beets	1.1
Corn	-5.6	Winter Grain	-1.3
Potatoes	-1.0	All crops	-0.2

9.0 AUTOMATIC ANCHOR PIXEL SELECTION

In determining ET, the METRIC process utilizes hot and cold anchor pixels to set boundary conditions for pixels exhibiting 0 or nearly 0 ET (hot pixel) and those with maximum ET (cold pixel). METRIC differs from other energy balance models by assigning the cold pixel to a well-irrigated crop within an agricultural field at full cover and assigning reference ET, ET_r , or some fraction of ET_r to that pixel. The SEBAL energy balance model often assigns the cold pixel temperature to that of local water body. The METRIC hot pixel candidate is also selected from agricultural areas but is associated with a dry, bare field where it can be assumed that ET is approximately 0. In cases where substantial precipitation has occurred within a week or so of the image, it is possible for the hot pixel to have some positive amount of ET. In these cases, it is necessary to conduct a daily soil water balance to estimate the amount of evaporation occurring from bare soil due to antecedent soil moisture.

NDVI and surface temperature are the two most important pieces of information in the identification of hot and cold pixels. From the energy balance equation it is seen that physically, ET will be highest when the sensible heat flux is the smallest.

$$H = R_n - G - ET \quad (46)$$

Furthermore, examination of the sensible heat flux equation shows that it will have the smallest value at low surface temperatures

$$H = \frac{\rho c_p (T_s - T_a)}{r_{ah}} \quad (47)$$

This coupled with the strong correlation between agricultural crops with high vegetation cover (high NDVI) and low temperature proves very useful in the determination of cold anchor pixels. Statistically out of the nearly 30 million pixels within a Landsat image we would expect to find a representative cold pixel within the top percentages of high NDVI and within the lowest percentages of surface temperature.

Similarly we would expect that statistically the hot pixel would lie within the hottest pixels within a given image, and because METRIC defines the hot anchor pixel as bare agricultural field exhibiting nearly zero ET, we would expect low values for NDVI ranging from 0 to 0.2. The hot anchor pixel will be more difficult to determine statistically from surface temperature due to the high amount of desert area found in the western United States. Desert areas tend to have a much higher surface temperature than surrounding agricultural areas (Allen et al 2006 and Lorite et al 2005) and therefore additional methods were analyzed to determine representative hot anchor pixels. Some interaction by the operator is probably necessary for hot pixel selection such as the delineation of an area of interest within an agricultural area where the user feels bare soil is present.

Other relationships were examined to find possible correspondence between the parameters albedo, estimated LAI and the hot pixel. Also because the hot pixel is assumed to be from a bare agricultural field with little or no ET, we would expect the soil to be dry. The ability to determine the amount of moisture within a given soil would be a valuable tool. While the remote sensing of soil moisture is best applied using the microwave portion of the electromagnetic spectrum, most satellites are not equipped with sensors within this wavelength.

9.1. Ts and NDVI statistics

To study the behavior of the hot and cold pixel conditions and to set up for the analysis of statistical selection of the METRIC model calibration “anchor” pixels, METRIC generated K_c , albedo, T_s , and NDVI values were sampled from all pixel locations exhibiting K_c near that of both the hot ($K_c = -.03$ to 0.03) and cold ($K_c = 1.02$ to 1.08) anchor pixels. This was accomplished using METRIC images for Path 39 year 2000, processed by the University of Idaho (Trezza et al, 2006 UI document) and using Trezza’s manually selected anchor pixels as target values.

By examining relationships between K_c , T_s , albedo, and NDVI from pixels exhibiting K_c ranges within the range of the hot and cold anchor pixels, strong

correlations between T_s , NDVI and K_c were observed. As expected the expert-user-defined cold anchor pixel had an NDVI within the highest percentage of all NDVI values. It is interesting to note however, that a broad range of NDVI (≈ 0.15 range) for pixels exhibited an ETrF near that of the cold pixel (Figure 9.1-1). The user defined hot pixel was located within the lowest NDVI, as expected, but again exhibiting a fairly large range in NDVI (≈ 0.20 range) at values of ET near zero.

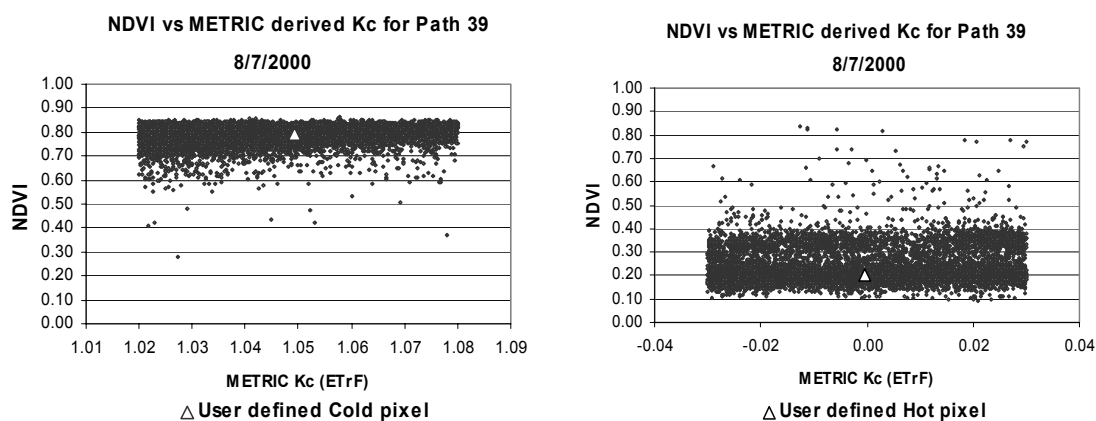


Figure 9.1-1 NDVI versus K_c analysis for fields sampled with in Path 39 exhibiting K_c (ie. ETrF) near that of the "cold anchor" pixel and the "hot anchor" pixel.

9.2. Statistical Selection of the Cold pixel

The analysis of the automatic selection of "anchor" calibration pixels used in METRIC was first conducted using Landsat path 39 data which covers the Aberdeen and American Falls areas of southern Idaho (Figure 9.2-1). A total of twelve Landsat 5 and 7 images were available for path 39 year 2000. All NDVI, METRIC ETrF, T_s , and other pertinent data were sampled near Aberdeen from METRIC processing conducted by Trezza (2006).

The establishment of an area of interest (AOI) from which to sample the T_s and NDVI data was found to be a vital component of the statistical process. Better results were achieved when the selected AOI was delineated well within an agricultural area with care to eliminate as much non-agricultural (desert, water bodies, etc) as possible. The AOI is drawn for an area where it is believed that both cold and hot anchor pixels

reside and should contain 10,000 to 30,000 acres (5,000 to 15,000 ha). The effect of AOI delineation on final results was more profound for the statistical selection of the hot pixel than for the cold pixel due to the bias in statistics caused by large amounts of dry desert; however both the cold and hot pixel were selected from the same AOI sampled data set. Figure 9.2-1 shows the agricultural AOI from which statistical analysis was conducted.

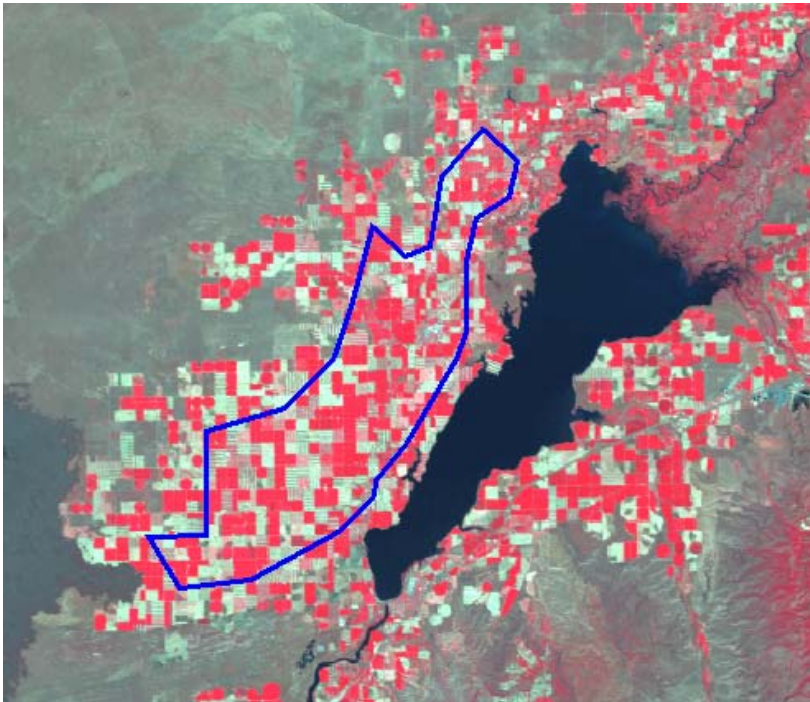


Figure 9.2-1 Path 39 study area near Aberdeen Idaho, water body shown is American Falls Reservoir, and area of interest (AOI) is outlined in blue.

To ensure accurate results, Landsat images were cloud masked for each image date (to eliminate cold pixels caused by clouds) and filtered for thermal contamination near field edges (where thermal pixels represented a mixture of conditions inside and outside fields and therefore were not suitable candidates). Thermal contamination was filtered using by calculating the coefficient of variation (CV) of NDVI between shortwave (30 meter resolution) pixels for all pixels within a thermal pixel within a given image (similar to Kustas et al., 2003). In this study a CV of 15 was used as the threshold value to ensure that thermal pixel selection was not near field edges or areas having non-uniform NDVI (Figure 9.2-2).

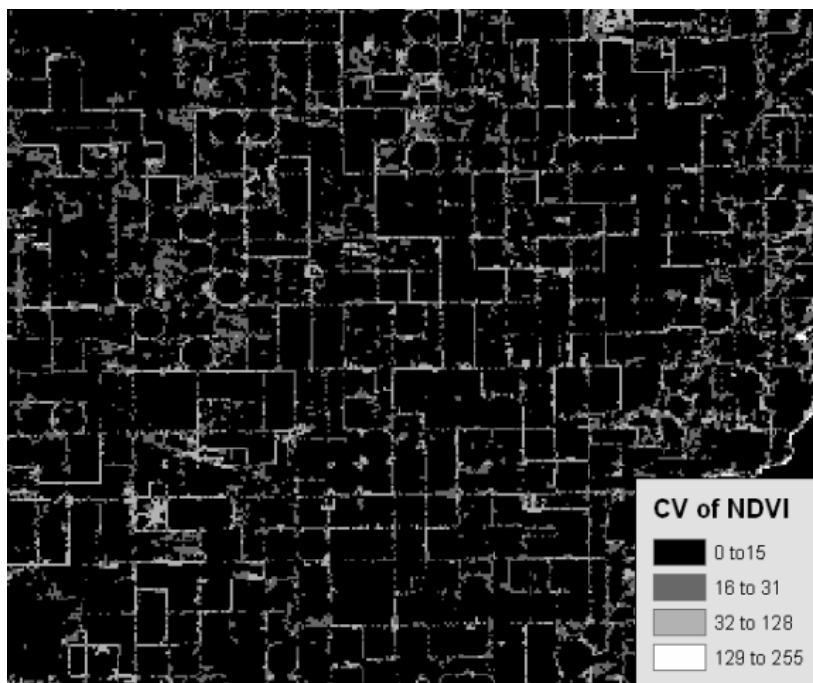


Figure 9.2-2 Coefficient of Variation in NDVI used to filter out edges of fields where contamination of Landsat data can occur due to the thermal pixel.

Samples were taken over the study area using a 245m by 330m grid. This included over 3,100 sample locations, which were then sampled for NDVI, METRIC K_c , T_s , and albedo. All data were then cloud and CV filtered as discussed above.

While various statistics were tested only the methodology associated with the selected statistics are presented. For a discussion of other statistics tested the reader is referred to appendix B. The selected statistical method for delineating both the cold and hot pixels was first proposed by R. Allen and C. Kelly, (2005, personal communication) and were investigated here. Following the cloud and CV filtering, statistical selection was performed on the remaining sampled points to identify statistically derived cold anchor pixels to be used in METRIC calibration as:

Cold Pixel Statistics

Using a defined AOI well within an agricultural area,

1. Select the top 5% of the highest NDVI

2. From the group made in step 1, select the coldest 20% of T_S
3. Take the average T_S of the reduced sample (step 2) as T_S of the cold pixel

The statistics described above were applied to each of the twelve image dates in Path 39. The image on May 3, 2000 had significant cloud cover over the study area and comparison on that date was not possible for the cold pixel. Figure 9.3-4 shows the comparison of the statistically derived T_S to the user defined T_S throughout the growing season. In this case the user defined cold pixel temperatures were determined by the University of Idaho METRIC team during the processing of Path 40 year 2000 (Trezza, 2001).

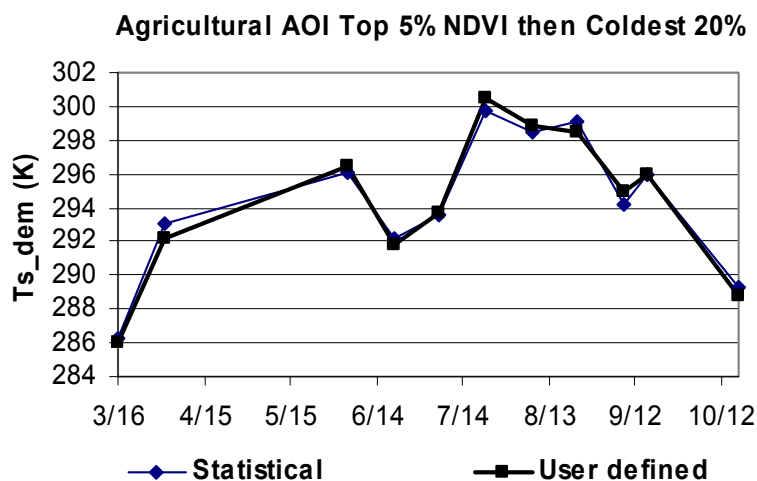


Figure 9.2-3 Comparison of user defined cold pixel temperature with statistically determined temperature for path 39, row 30 for year 2000.

The absolute difference between user defined and statistically determined T_S was never greater than 0.87 K (Table 9.2-1). The average seasonal absolute difference was found to be only 0.47 K. This average absolute error in T_S of 0.47 K, when inserted into the $dT = a \cdot T_S + b$ equation for the 11 images produced an average dT error of 0.27 K. This corresponds to an average seasonal error in sensible heat flux (H) of approximately 9 W/m^2 . This estimate in H was made using an average aerodynamic surface resistance (r_{ah}) for the cold pixel of 30 s/m. This is a representative r_{ah} for an agricultural pixel with a wind speed of approximately 2 m/s at two meter height above the ground surface, and is

used solely for comparative purposes to show the approximate error introduced by statistical anchor pixel selection. The mean ET flux over the 11 images averaged about 463 W/m² over the cold pixels so that the error in H caused by the error in T_{S_cold} was about 2 % of the ET at the cold pixel.

Table 9.2-1 gives the difference between statistically derived cold pixel temperatures and the user defined temperatures. With such small differences between the two Ts selection methods the possibility of using statistics to locate the Ts used for the cold anchor pixel in METRIC processing proves promising. The statistical process assumes that the AOI includes sufficient pixels where ETrF \approx 1.05, so that the cold pixel can be statistically identified. This may not be the case in winter and early spring, where full vegetation cover may not exist, or in non-irrigated areas in late summer. In this example, however; the estimate for March 16 was quite accurate due probably to some fields of winter wheat that were near full cover.

Table 9.2-1 Comparison of user defined Ts_dem and statistically derived Ts for the cold anchor pixel throughout the growing season for path 39, row 30.

Date	Ts_dem (Statistics)	Ts_dem (user)	T _s error (K)
3/16/2000	286.27	286.00	0.269
4/1/2000	293.10	292.23	0.867
6/4/2000	296.11	296.43	-0.322
6/20/2000	292.23	291.77	0.461
7/6/2000	293.54	293.72	-0.180
7/22/2000	299.70	300.51	-0.810
8/7/2000	298.46	298.86	-0.400
8/23/2000	299.06	298.53	0.523
9/8/2000	294.22	294.91	-0.683
9/16/2000	295.95	295.99	-0.036
10/18/2000	289.30	288.74	0.559

9.3. Statistical Selection of the Hot pixel

In the arid regions of the Western United States, agricultural areas are surrounded by vast amounts of desert. These desert areas can be at significantly higher temperatures than the hottest agricultural soils due to differences in soil structure, soil moisture, soil

heat flux, and shading of the surface by brush. The biggest difficulty in automatic hot pixel selection is therefore controlling the presence of and relative number of desert or otherwise very dry pixels within an image coupled with the corresponding higher temperatures. Often, large amounts of desert lead to statistical approaches yielding hot pixel temperatures higher than those expected from agricultural soils.

A histogram of an elevation (lapse) normalized surface temperature is shown in Figure 9.3-1. The large peak in the histogram from approximately 317 K to 330K represents the large number of high temperature desert pixels within the image. The bare, dry agricultural pixels in the early June image averaged about 314 to 317 K, with the user defined temperature for this image date of 315.2 K. It is apparent from such histograms that any statistical based method for anchor pixel selection must include measures to avoid the inclusion of large areas of desert pixels. This will insure that desert and similar (roadways) pixels will comprise a consistent percentage of the selected AOI.

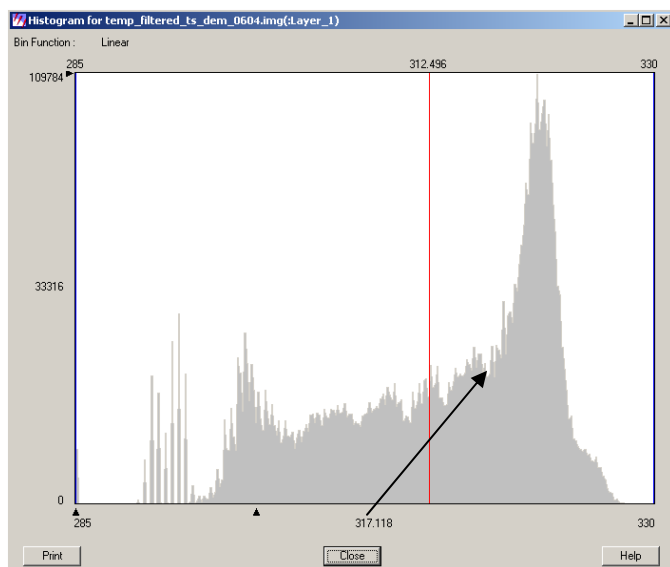


Figure 9.3-1 Temperature histogram for June 4, 2000 Landsat image (Created in ERDAS IMAGINE)

Early in the growing season differences in temperature between desert and agricultural areas are not large. At this time of year, before the irrigation season, desert soils in southern Idaho have similar moisture content as agricultural soils due to antecedent moisture and therefore exhibit similar temperatures. As the irrigation season

begins and progresses throughout the season, the relative difference between the temperature of the desert and agricultural fields increases due to essentially no rainfall. Figure 9.3-2 shows this progression throughout the growing season for the year 2000.

The plot shows the ratio:

$$ratio = \frac{(T_{s_{max}} - T_{s_{hot}})}{T_{s_{range}}} \quad (48)$$

where $T_{s_{max}}$ is the maximum surface temperature within the image, $T_{s_{hot}}$ is the temperature of the hot anchor pixel selected by an experienced METRIC user on the image date, and $T_{s_{range}}$ is the range of temperatures for the given image date. This analysis was conducted on a small AOI within the Aberdeen study area which included a combination of desert and agricultural areas.

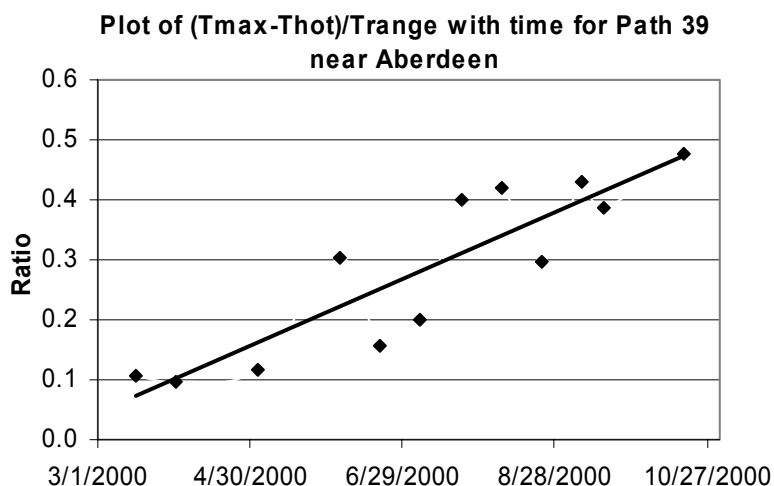


Figure 9.3-2 Relative difference between hot desert pixels and the hottest agricultural soils throughout the growing season for Path 39 year 2000.

Presumably the maximum temperature represents the temperature of the hot desert areas and the user defined hot anchor pixel represents the temperature of bare agricultural fields. The relationship shown in Figure 9.3-2 suggests that as the season progresses desert areas get hotter and hotter due to lack of wetting events and other factors (desert soil characteristics and vegetation shielding of the surface, Allen et al., 2007a), thus creating a larger difference from agricultural soils which receive frequent irrigations.

It is this phenomenon which makes the automatic selection of the hot anchor pixel difficult. In order to overcome this, two strategies are considered; careful delineation of the AOI to exclude hot desert pixels, and an adjustment to statistics for periods later in the season when the difference between desert and bare agricultural soils is more prevalent. The statistical delineation proposed by R. Allen and C. Kelly (2005, UI, personal communication) for the hot pixel is:

Hot pixel statistics

1. Select the lowest 10% of NDVI
2. Then select the hottest 20% of T_S from step (1)
3. Take the average T_S of the remaining sample from step (2) as T_S for the hot pixel

It is noted again that the statistics described above are carried out on the same data analyzed for the cold pixel selection, sampled from the AOI of Figure 9.2-1. As expected a larger deviation from the user defined T_S was found for the analysis of the hot pixel. Figure 9.3-3 shows this deviation throughout the growing season. As expected, later in the season, as the temperature of non-agricultural (desert, non-irrigated etc) pixels increases, the statistical procedure tends to over estimate the actual temperature of the hot pixel (bare, dry agricultural fields). Here the seasonal average deviation in temperature was approximately 2.2 K. This difference in temperature would produce an average error in the dT function of 0.9 K which, when using an average r_{ah} at the hot pixel of 20 s/m, produces an average error in the sensible heat flux (H) of 46 W/m². Some of the error in H associated with this difference in hot pixel T_S is compensated for during the METRIC calibration process (Allen et al., 2006). However, the error in $T_{S_{hot}}$ would tend to ‘stretch’ the resulting ET surface over drier areas and would estimate too high of ET for the ‘true’ dry agricultural soil condition. The average error of 46 W/m² averages about 10 % of the average ET_r at the time of satellite overpass. It is also noted that the lower value of r_{ah} for the hot pixel than the cold pixel (20 versus 30 s/m) reflects the effect of boundary layer instability over the hot dry soil therefore reducing r_{ah} .

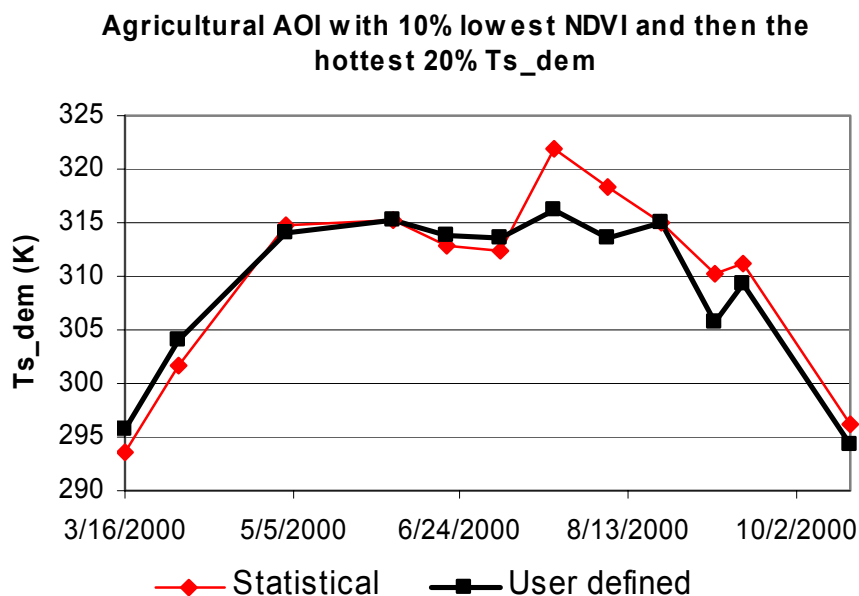


Figure 9.3-3 Comparison of statistically determined T_S for hot pixel and user defined T_S for path 39, row 30, year 2000.

9.4. Path 40 year 2000

Testing of the spatial applicability and transferability of the statistical anchor pixel selection method was carried out by conducting the derived statistical method on Path 40 images for the year 2000. The large agricultural area of the Magic Valley within Path 40 made it possible to analyze additional techniques used for the automatic pixel selection process. An area of interest was selected within the Magic Valley near the location of the weather station used for weather data. The selected AOI can be seen in Figure 9.4-1.

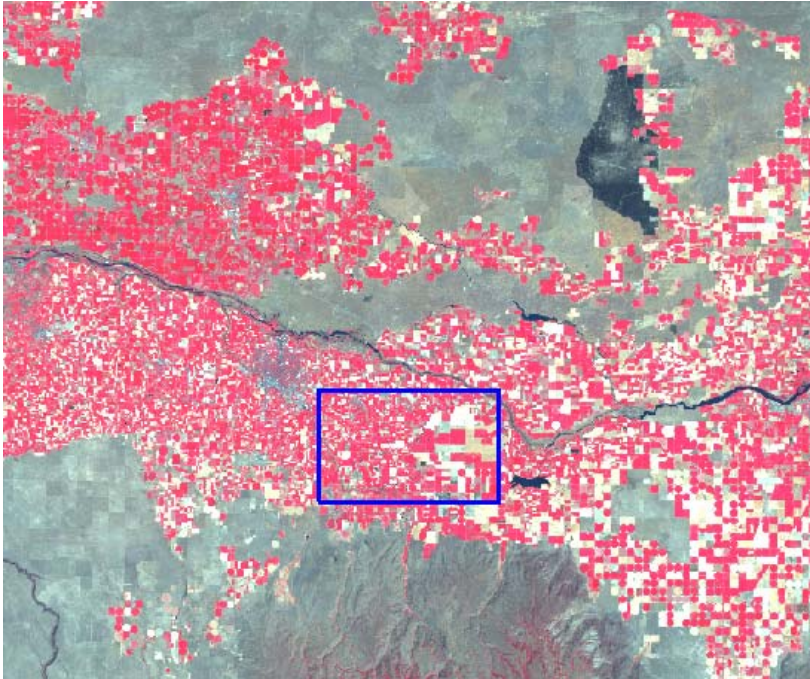


Figure 9.4-1 Area of interest (outlined in blue) established within the Magic Valley for the testing of the Automatic anchor pixel selection process.

The area of interest within Magic Valley was drawn so that boundaries of the AOI corresponded to roadways which in most cases are constructed on a mile by mile grid. Sampling grids were then established so that grid densities, in both the horizontal and vertical direction, were multiples of 200 meters. As seen in Figure 9.4-2 this provided the highest number of sampled pixels occurring within individual fields. This provided a total of over 5,000 pixels for the statistical analysis. All filtering of sampled data and statistics discussed above for Path 30 year 2000 were then applied for Path 40 year 2000 and the results are discussed below. Additional locations and methods (shapes) of AOI delineation were also tested as summarized in Appendix C.

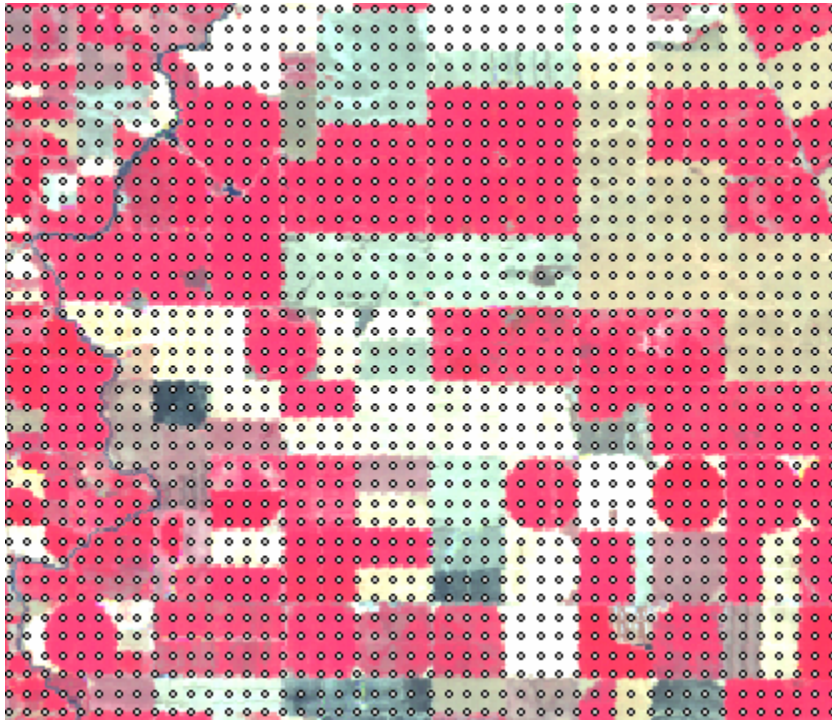


Figure 9.4-2 Grid density for AOI delineation for Path 40 year 2000.

Statistics for the cold pixel in Path 40 year 2000 provided similar results to those discussed above for Path 39 year 2000. Figure 9.4-3 shows the deviation in selected temperatures for the two methods throughout the growing season. The average absolute deviation was approximately 0.8 K with the highest deviation occurring on the first image date with an over estimation of approximately 1.8 K. The error on the first date, March 15, was due to the presence of few fields having ETrF of 1.05 which is required for the cold pixel. Using the dT relationship ($dT = a \cdot T_s + b$) where the coefficients a and b were determined previously for each image date during the original METRIC processing (Tasumi, 2003), this difference in temperature would produce an approximate error of 0.25 K in dT. This error produces an average error in the sensible heat flux (H) of 8 W/m^2 which was 1.7 % of the average ET flux ($\approx 480 \text{ W/m}^2$) for the cold pixel. Again this is assuming an average aerodynamic resistance (r_{ah}) of approximately 30 s/m for a cold vegetated pixel.

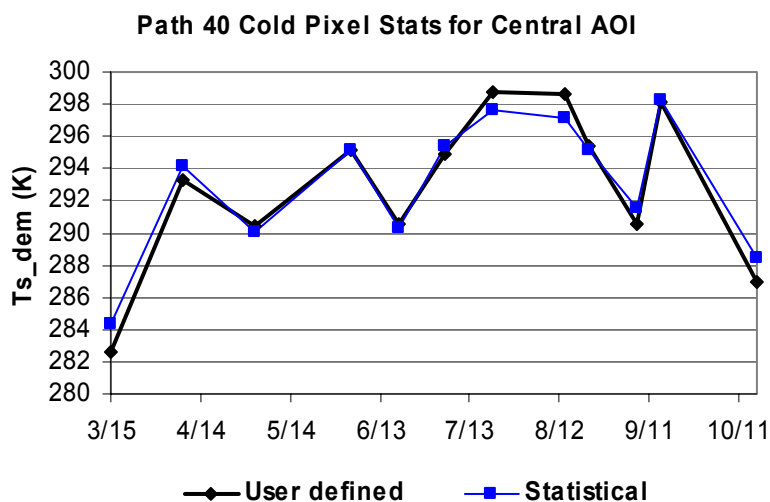


Figure 9.4-3 Comparison of user defined cold pixel and statistically defined for Path 40 year 2000 (User defined T_s from UI METRIC processing, Tasumi 2003).

The statistical selection of the hot anchor pixel used for METRIC calibration also provided similar results to those found in Path 39 year 2000. While the absolute deviation was slightly lower in the Path 40 analysis with a value of approximately 2 K/image, we again observe higher overestimation as the season progresses (Figure 9.4-4). The average difference in temperature would cause approximately 0.65 K of error in the dT at the hot pixel temperature which produces an average error in H of approximately 33 W/m^2 or 7 % of the average ET_r ($\approx 473 \text{ W/m}^2$).

With the increased overestimation in statistical TS observed in both Path 39 and Path 40 simulations, additional methods were pursued to improve the statistically derived hot pixel temperature. As discussed in section 9.3, the temperature difference between agricultural fields and non-agricultural fields (desert, non-irrigated pixels etc) increases throughout the growing season. As much of this phenomenon can be attributed to the occasional wetting of agricultural areas through irrigation (including bare soils), methods were sought to consider the influence of wetting events received by non-agricultural pixels through precipitation.

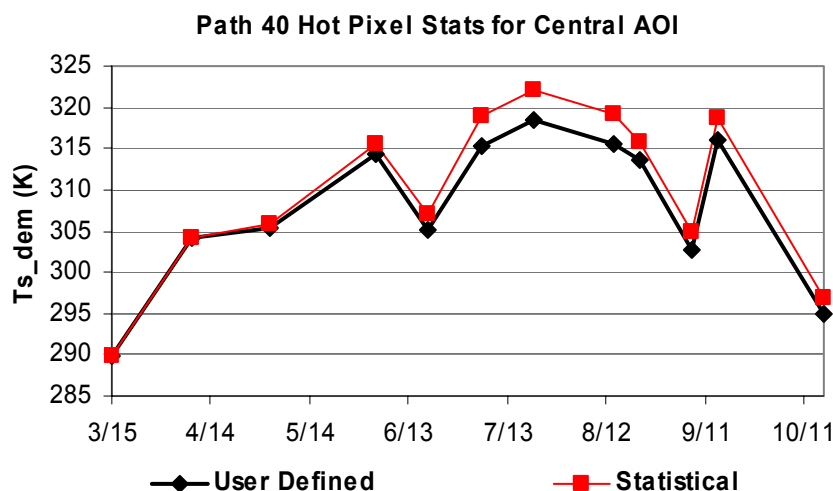


Figure 9.4-4 Hot pixel temperature comparison between experienced user defined and statistically derived Ts.

The lack of wetting events in non-agricultural (desert) areas during mid to late summer creates the larger difference between the temperature of desert and agricultural soils. In the FAO 56 manual Allen et al., (1998) found that this lack of well-watered conditions can cause differences in weather data collected over non-agricultural areas and data collected over agricultural (reference surface) areas. In that work they presented the use of the ratio of precipitation to reference ET (ET_r) as an indicator to correct weather data obtained from areas deviating from the reference surface conditions. Figure 9.4-5 shows the relationship between differences in minimum air and dew-point temperature measurements recorded at a range of weather stations and monthly precipitation/ ET_r ratios. As seen in the figure when more precipitation events (wetting events) occur and the ratio of precipitation to reference ET increases, the difference between measured daily minimum air temperature and dew-point temperature gets smaller and smaller. This is because, as discussed in Allen et al., (1998), the higher precipitation brings the non-agricultural areas closer to the reference surface which is defined as well watered, actively growing (and therefore transpiring) healthy vegetation.

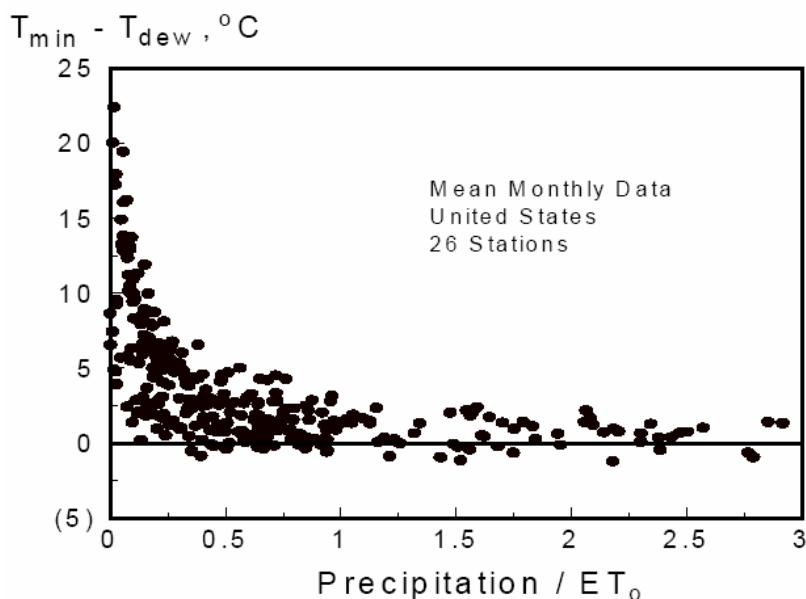


Figure 9.4-5 Difference between monthly minimum temperatures and dew point temperatures plotted against the ratio of monthly precipitation and monthly reference ET (Taken from FAO 56 Annex 6, Allen et al., 1998).

Following Allen et al., (1998) the amount of precipitation occurring over the study area was utilized to adjust the statistically derived temperature of the hot pixel using a precipitation/ ET_r ratio. Both the precipitation and ET_r were summed over the 60 days prior to each image date to reflect the long term relative antecedent precipitation and slow diffusive evaporation. The ratio of the 60 day summed precipitation to the 60 day summed ET_r was then plotted against the difference between the statistically determined surface temperature and the user defined temperature for the hot pixel. Figure 9.4-6 shows the result of this comparison for path 40 as well as the linear relationship fitted to the data. Weather data were taken from the Twin Falls Agrimet station. The breakpoint of no bias correction when $P/ET_r > 0.2$ suggests that when 60 day precipitation exceeds $0.2ET_r$ during the same period, residual evaporation from desert soils causes them to behave like agricultural soils.

Statistically derived hot pixel temperatures were then adjusted using the linear relationship displayed in Figure 9.4-6. As seen in Figure 9.4-6 no adjustment is made for precipitation/ ET_r ratios above approximately 0.2 and equation 44 was utilized to compute an r^2 of 0.80. Figure 9.4-7 shows the resulting comparison of the user defined TS for the

hot pixel and the statistically determined (following precipitation/ ET_r adjustment) throughout the growing season.

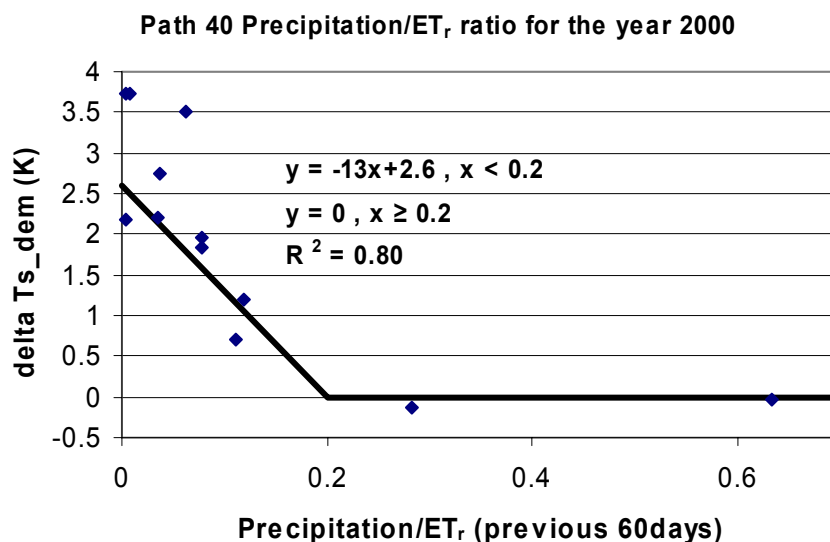


Figure 9.4-6 Comparison of the Precipitation/ ET_r ratio for the 60 days immediately preceding Image dates to the difference between statistically derived T_s and the user defined T_s of the hot pixel (Weather data measured near Kimberly Idaho).

Using the precipitation/ ET_r adjustment procedure produced promising estimates of hot anchor pixel temperatures. The use of the precipitation adjustment reduced the total absolute error from 2 K to only 0.55 K. This corresponds to an average error similar to the error found in the cold pixel analysis of only 0.2 K in dT , which would produce an average error in the sensible heat flux (H) of approximately 9 W/m^2 at the hot pixel. This error represents only 2% of the average ET_r at the time of satellite images.

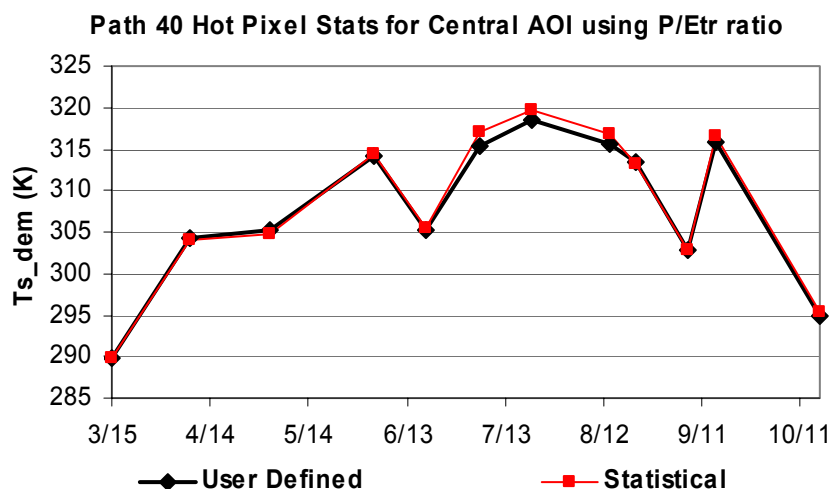


Figure 9.4-7 Hot pixel selection comparison with statistical method coupled with use of P/ETr ratio for correction due to desert heating.

9.5. Application of Statistically Derived Anchor Pixels for METRIC Processing

The estimates of error associated with the statistical selection of METRIC anchor pixels, discussed above were made using the calibration coefficients derived in the original METRIC processing of Path 39 and Path 40 for the year 2000. However; the actual calibration constants would change based on the selection of the cold and hot anchor pixels. To further test the use of statistically derived anchor pixels for the METRIC calibration process, images for the year 2000 for Path 40 were reprocessed using the statistically derived anchor pixels and the resulting ETrF images compared with the original ETrF images processed by Tasumi, (2003) and reprocessed by Burnett and Allen, (2007, personal communication).

The statistically derived temperatures for both cold and hot anchor pixels were associated with actual pixels within each Landsat image, prior to the METRIC processing. This was accomplished by applying a color scheme to the temperature image created from Landsat data as shown in Figure9.5-1 that identified T_S 'bands' that contained the $T_{S_{hot}}$ and $T_{S_{cold}}$ values.

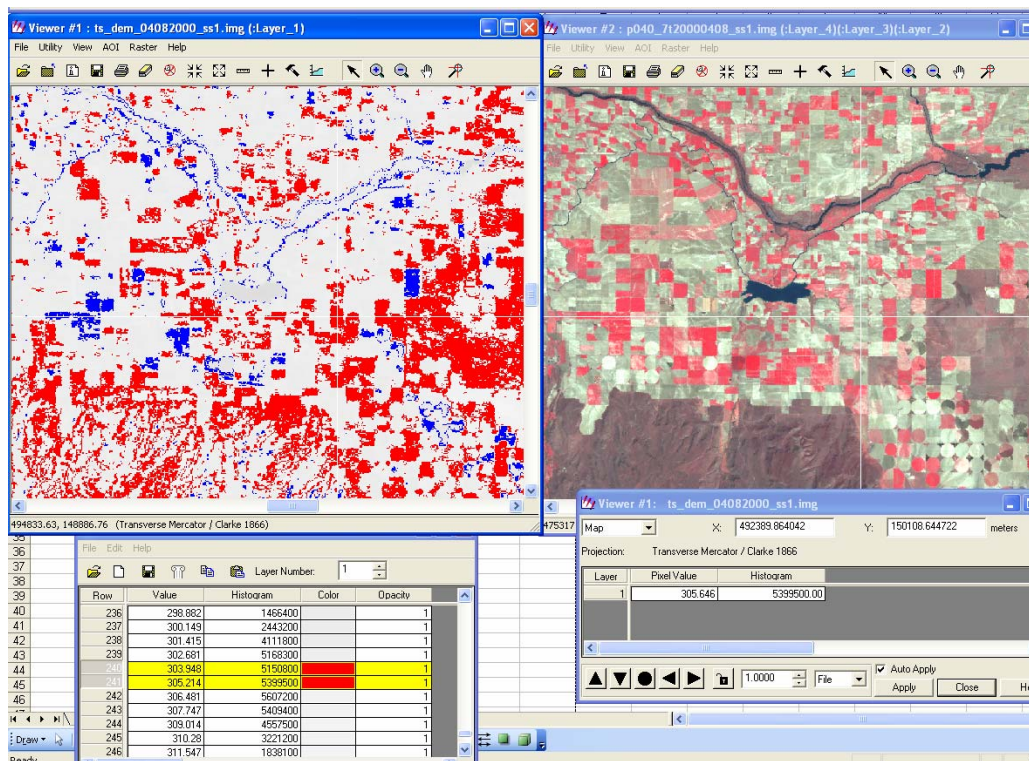


Figure 9.5-1 Surface temperature image colorization for the selection of individual pixels used as the cold and hot anchor pixels for METRIC processing of Path 40 year 2000.

In Figure 9.5-1 both the surface temperature (left image) and a false color composite of the original Landsat 7 image (right image) are displayed. Surface temperature pixels colored in blue exhibited temperatures within the range of the statistically derived cold pixel and red pixels the temperature range of the hot pixel. Cold and hot anchor pixels were selected using this information as well as the albedo and NDVI for each image date. Anchor pixels were selected from pixels within 0.2 K of the statistically determined temperatures for both the cold and hot pixel. Initially the pixel selected for the cold pixel was required to exhibit high NDVI (greater than ≈ 0.8) and an albedo within the range of 0.2 to 0.25. The hot pixel was also selected which exhibited low NDVI (less than ≈ 0.15), and an albedo between 0.18 to 0.25. Each of these criteria were used in all METRIC processing to best describe the conditions exhibited by well watered crop surfaces (cold pixel) and bare dry agricultural soils (hot pixel).

However, the accuracy of ET estimates (relative to manual calibration) using statistically derived T_S for the cold and hot anchor pixels was found to be highly dependent upon the albedo of the pixel selected for the cold anchor pixel. The first simulations of METRIC using statistically derived cold and hot anchor pixels where albedo was selected for the cold pixel with values ranging from 0.2 to 0.25, found overestimation of seasonal ET compared to METRIC user calibrated ET estimates (user defined METRIC calibration chose albedo ranging from 0.16 to 0.24). The over estimation in seasonal ET represented approximately 3 to 6% of the total seasonal reference ET (ET_r). Closer analysis of ETrF images for all image dates indicate that the accuracy associated with statistically calibrated METRIC processing depending heavily on the albedo of the chosen cold anchor pixel.

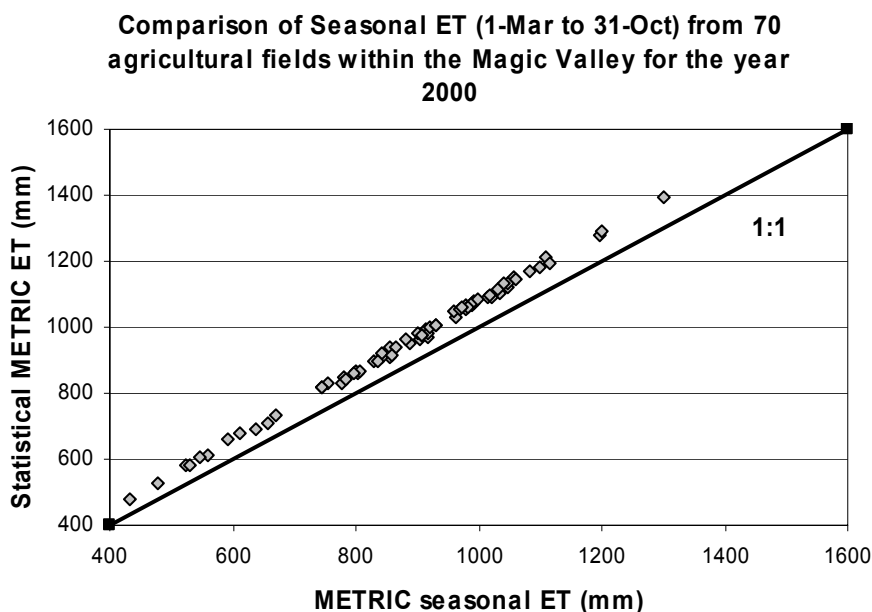


Figure 9.5-2 Seasonal ET comparison for 70 agricultural fields within the Magic Valley between standard METRIC processing and the statistically calibrated METRIC processing for the year 2000 with the albedo for the cold pixel used in the statistical calibration method ranging from 0.2 to 0.25.

As discussed previously in chapter 3 surface albedo is the ratio of reflected radiation from the surface to the shortwave radiation incident at the ground surface.

Higher values of albedo for a given pixel within an image represent less energy at the surface available for ET. At first glance one might therefore expect METRIC simulations using higher albedo values for the cold pixel to predict less ET than if low albedo values are used. This is not the case however because by selecting a cold anchor pixel with a high albedo you are in turn causing all other pixels with characteristics similar to the cold pixel but having lower albedo to have higher ET (larger than the $1.05*ET_r$ established for the cold pixel) than the reference. Figure 9.5-3 shows this ‘stretching’ of the ET near the cold pixel, where we see that for high ETrF the difference between the user calibrated METRIC and statistically calibrated METRIC gets more negative (increased over estimation) when the cold pixel albedo used for the statistical method is larger than the albedo used in standard calibration.

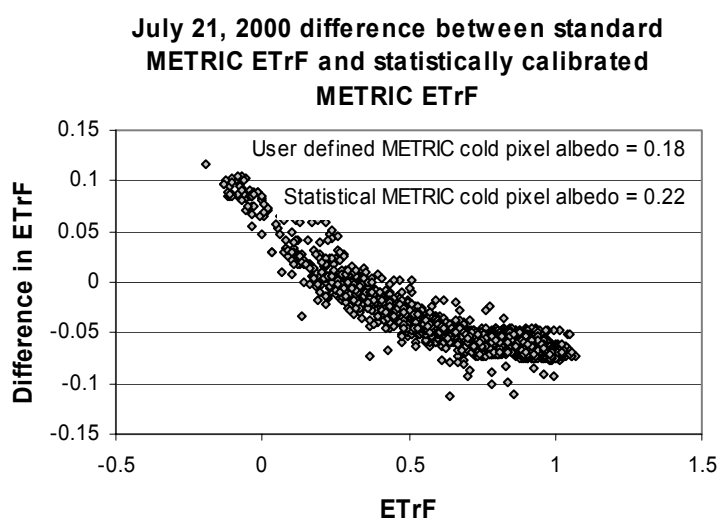


Figure 9.5-3 Difference in ETrF images using standard METRIC processing and METRIC calibrated by statistical selection of cold and hot anchor pixels for late July image.

This increase in over estimation under these conditions (higher albedo at the cold pixel for the statistical method) further effects the ET estimation as the larger difference is applied to higher ETrF values ($ET = ETrF*ET_r$). In the processing of both calibration methods it was observed that for the September 15, 2000 image date the albedo of the

cold pixels were nearly identical (manual calibration vs. statistical). On that image date the difference between ETrF images was very small compared to all other image dates (Figure 9.5-4). The range in differences in ETrF images was from 0.01 to -0.005 (total range of 0.015) compared to differences ranging from 0.1 to -0.1 (total range of 0.2) observed with the July 21, 2000 image (Figure 9.5-3).

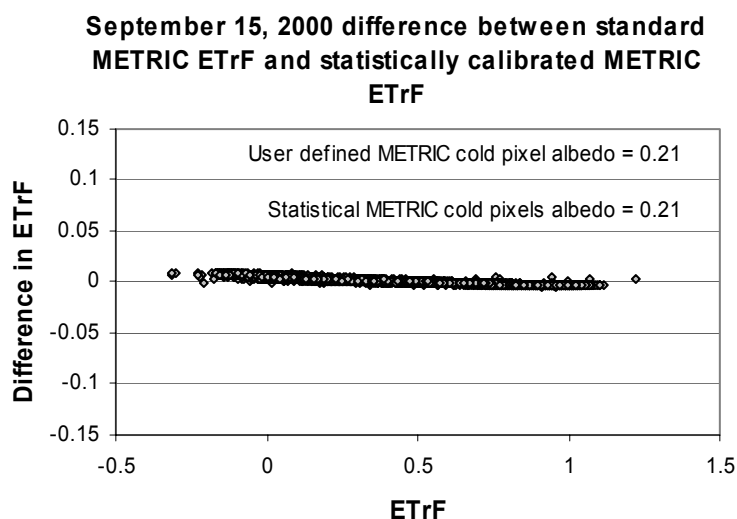


Figure 9.5-4 Difference in ETrF images using standard METRIC processing and METRIC calibrated by statistical selection of cold and hot anchor pixels when albedo at the cold pixel condition and the hot pixel condition were the same.

The effect of using an albedo at the cold pixel with a value less than the value used in METRIC standard user calibration is seen in Figure 9.5-6. It was observed that the albedo (albedo of cold pixel of 0.25) used in the statistical calibration at the cold pixel on June 3, 2000 was much larger than the user calibrated cold pixel albedo of 0.19. Differences between ETrF images under these conditions are seen in Figure 9.5-5. METRIC for this image date was reprocessed using the statistical calibration procedure with an albedo at the cold pixel of 0.17. Figure 9.5-6 shows that by choosing a cold anchor pixel closer to the albedo of the user calibrated cold pixel drastically reduces the range in differences between ETrF images (0.2 to 0.03 difference in ETrF). Also by

selecting the anchor pixel which had an albedo at the cold pixel less than that of the user calibration method gave only under estimation for that image date.

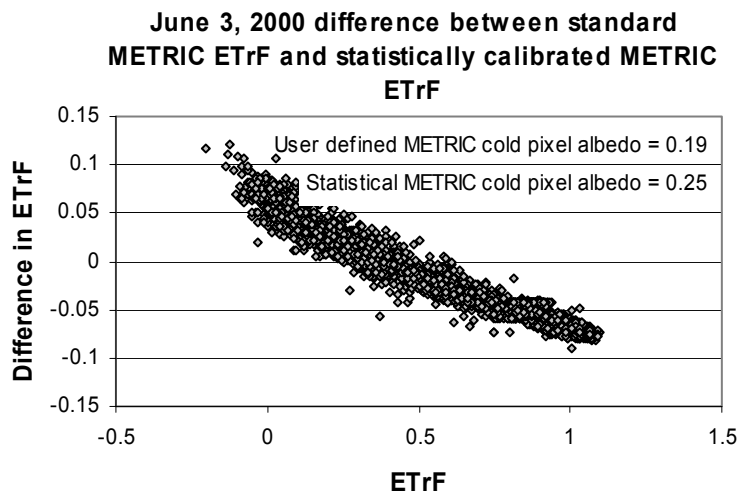


Figure 9.5-5 Difference in ETrF images using standard METRIC processing and METRIC calibrated by statistical selection of cold and hot anchor pixels when albedo at the cold pixel condition was higher for the statistical calibration method.

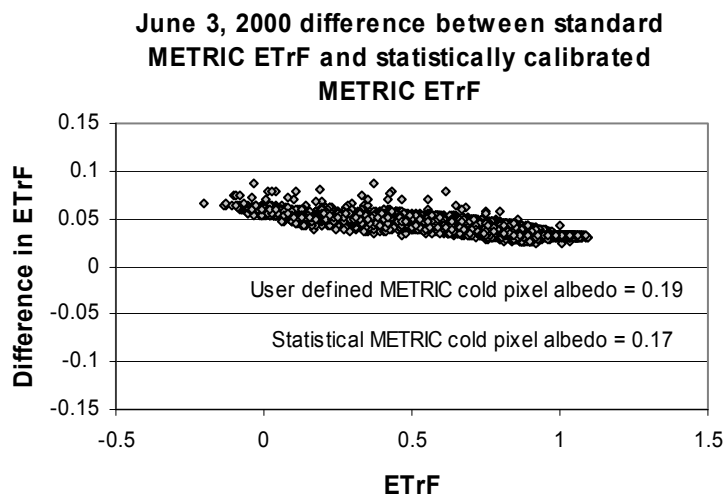


Figure 9.5-6 Difference in METRIC methods when albedo at the cold pixel is selected so that it is lower than the albedo of user defined METRIC processing when albedo at the cold pixel condition was slightly smaller for the statistical calibration method (same pixels sampled as in Figure 9.5-5).

All twelve image dates were reprocessed using the statistically determined temperatures of the cold and hot anchor pixels as but using cold pixels exhibiting albedo values more closely related to those selected in the standard METRIC processing by Tasumi et al (2003, reprocessed by Allen and Burnett in 2007). The hot pixels used in this case were the same as those defined previously using the statistical selection process (albedo ranging from 20 to 26). Tables displaying temperature, albedo, NDVI, and other pertinent data of the cold and hot anchor pixels can be seen in Appendix D. Figure 9.5-7 shows the comparison of resulting seasonal ET estimates from the same agricultural fields presented in Figure 9.5-2.

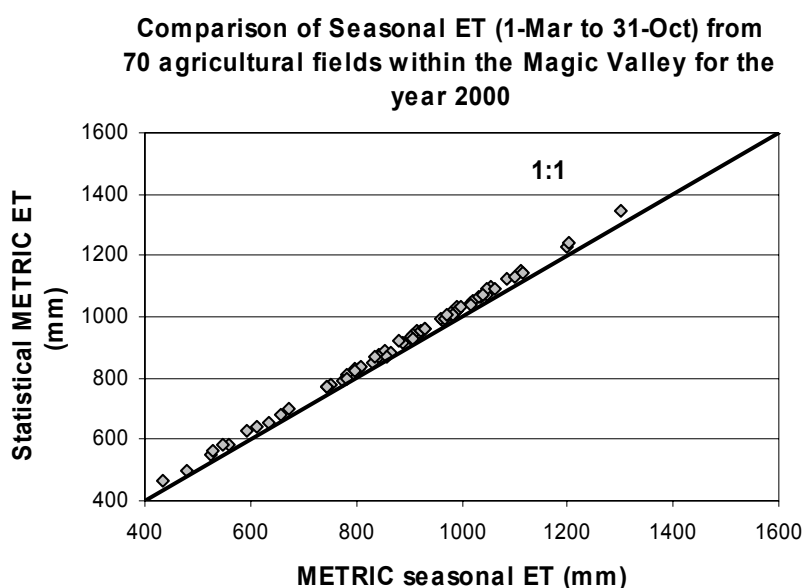


Figure 9.5-7 Seasonal ET comparison between standard METRIC processing and METRIC processing using statistical calibration for 70 agricultural fields within the Magic Valley for the year 2000.

While over estimation was still observed, the over estimation represents only 0.2 to 2.9 % of the total seasonal ET_r for the same time period (March 1 to October 31). Even with albedo selected within 0.05 of the cold pixel albedo for standard METRIC processing over estimation in seasonal ET was still observed. This could be in part explained by the fact that the largest over estimation occurs at high ET_r when statistically selected albedo at the cold pixel is higher than the standard user defined cold

pixel albedo, and this condition occurred for all July and August images when most crops are actively growing (and therefore at high ETrF, ET).

10.0 CONCLUSIONS AND RECOMENDATIONS

10.1. Conclusions

Large scale monitoring of seasonal ET fluxes from the agricultural areas of southern Idaho is currently accomplished using Landsat satellite imagery and Mapping Evapotranspiration at high Resolution with Internalized Calibration (METRIC). The overall objectives of this study were to 1) develop and test an evapotranspiration (ET) estimation method combining crop coefficients from satellite-based vegetation indices with water balance techniques for estimating the evaporation component of ET and 2) to examine methods for the automatic selection of the anchor pixels used in the METRIC calibration process.

The use of K_{cb} -NDVI relationships coupled with procedures for estimating evaporation using water balance model techniques can assist water managers in the estimation of seasonal ET fluxes over agricultural areas of southern Idaho, when thermal satellite information is not available to supply more accurate energy balance based techniques. Reasonable estimates of seasonal ET can be obtained from universal K_{cb} -NDVI relationships for agricultural areas thus; crop classification may not be required.

The largest advantage of the vegetation index based water balance model is that the model does not rely on thermal satellite information. The availability of high resolution thermal satellite data used in the more precise energy balance based ET estimation methods, has been jeopardized by the failure of Landsat 7 in 2003. Seasonal ET estimates using the satellite based K_{cb} -NDVI relationship coupled water balance models were within $\pm 5\%$ of ET observations from the energy balance based METRIC model, for most crops within the Magic Valley of southern Idaho. Estimates of seasonal ET using the rooting specific to each crop type as well as crop specific K_{cb} -NDVI relationships better replicated METRIC observations in most cases.

Statistical procedures can assist METRIC users in the selection of anchor pixels used in the internal calibration process. This calibration process is a vital component in METRIC applications if realistic estimates of ET are to be obtained. This statistical

procedure can reduce the uncertainty in ET estimates associated with the subjective user defined calibration for inexperienced users or users with varying levels of background in ET fluxes and radiation physics.

Comparison of statistically calibrated METRIC results to standard user calibration, found that the albedo of the anchor pixels, used in the calibration process, can significantly alter the accuracy of ET estimates. Sensitivity analyses of albedo values confirm the need of narrowing the range of albedo values exhibited by anchor pixel candidates.

10.2. Recommendations

Water Balance Model

Some additional analyses will be needed in the future to establish the applicability of the techniques discussed in this thesis for locations outside of southern Idaho. Future work should include the application and verification of these techniques for other agricultural crops as well as desert areas. The calibration process involved in crop specific simulations can be refined to better capture the effects of irrigation event and water management practices over the large areas contained within satellite images. This can be achieved by considering additional methods for irrigation season delineation, which would better mirror the actual irrigation season for crops such as potato and beans, that have very low K_{cb} values early in the year (simulated irrigation season tended to lag actual season), and grain crops that exhibit low NDVI late in the year when transpiration and irrigation can still occur (simulated irrigations tended to stop prior to typical irrigations for these crops).

In many cases simulated irrigations tended to mirror irrigation frequency typical for surface irrigation systems. A high percentage of the irrigation systems within the Magic Valley are center pivots which typically have a higher irrigation frequency than other irrigation methods. Capturing the effects of the large number of high frequency

irrigation systems within the Magic Valley could account for some of the underestimation of the water balance model compared to METRIC observations.

Future work should also examine additional methods for smoothing the evaporation component of ET to be added to the transpiration component since, in reality, the timing of this component is unknown. In this study smoothing was achieved by conducting multiple simulations for multiple individual fields based on crop type. Other possible methods include, but are not limited to, the use of averaging the evaporation component over simulations made for various NDVI ranges. The use of the water balance model may be useful, when coupled with METRIC, to ‘fill-in’ ET estimates during periods between image dates when rainfall occurs.

Statistical calibration

The statistical selection of anchor pixels used in METRIC calibration was fully tested for the year 2000 with path 40, row 30 Landsat 5 and 7 images which corresponds to the Magic Valley in southern Idaho. Future work should focus on the testing of statistical methods outside of southern Idaho to test the transferability of the procedure to areas with different crop and land use types (varying types on non-agricultural pixels, desert). Currently the University of Idaho is testing METRIC applications in Colorado and Nebraska.

The statistical calibration procedures presented in this thesis are based upon the surface temperature and amount of vegetation (NDVI) exhibited by the anchor pixels. Initial assumptions as well as final results suggest that other energy balance parameters such as surface albedo play a large role in the calibration accuracy of ET estimates from statistically calibrated METRIC processing.

REFERENCES

- AgriMet “Agrimet Crop Coefficients.” U.S. Bureau of Reclamation, Pacific Northwest Region, http://www.usbr.gov/pn/agrimet/cropcurves/crop_curves.html (accessed Oct 23, 2006)
- Allen, R.G., M.E. Jenson, J.L. Wright, and R.D. Burman. (1989) “Operational Estimates of Reference Evapotranspiration” *Argonomy Journal*. Vol 81, No4 pp 650-662.
- Allen, R.G., L.S. Pereira, D. Raes, and M. Smith. (1998). “Crop Evapotranspiration.” FAO Irrigation and Drainage Paper 56, Food and Agricultural Organization of the United Nations, Rome.
- Allen, R.G., A. Morse, M. Tasumi, R. Trezza, W.G.M. Bastiaanssen, J.L. Wright, and W. Kramber. (2002) “Evapotranspiration from a Satellite-Based Surface Energy Balance for the Snake River Aquifer in Idaho”. Proc., USCID/EWRI Conf. On Energy, Climate, Environment, and Water, San Luis Obispo, Calif.
- Allen, R.G. and J.L. Wright. (2002) “Conversion of Wright (1981) and Wright (1982) alfalfa based crop coefficients for use with the ASCE Standardized Penman-Monteith Reference Evapotranspiration Equation.”
- Allen, R. G., A. J. Clemmens, C. M. Burt, K. Solomon, and T. O’Halloran. (2005) “Prediction Accuracy for Projectwide Evapotranspiration Using Crop Coefficients and Reference Evapotranspiration” *Journal of Irrigation and Drainage Engineering*, ASCE. Vol. 131 No1 pp 24-36.
- Allen, R.G., M. Tasumi, R. Trezza. (2006) “METRIC Mapping Evapotranspiration at High Resolution” Applications Manual. University of Idaho. Kimberly Idaho
- Allen, R.G., W.O. Pruitt, D. Raes, M. Smith, and L.S. Pereira. (2005) “Estimating Evaporation from Bare Soil and the Crop Coefficient for the Initial Period Using Common Soils Information” *Journal of Irrigation and Drainage Engineering ASCE*, Vol. 131, No.1, Feb. 1, 2005 pp 14-23.

- Allen, R. G., Pereira, L. S., Smith, M., Raes, D., and Wright, J. L. (2005). "FAO-56 dual crop coefficient method for estimating evaporation from soil and application extensions." *Journal of Irrigation and Drainage Engineering*.
- Allen, R.G. and C.W. Robison (2006 revised 2007) "Evapotranspiration and Consumptive Irrigation Water Requirements for Idaho." University of Idaho technical report submitted to the Idaho Department of Water Resources.
- Allen, R.G., M. Tasumi, A. Morse, R. Trezza, (2007a) "Satellite-Based Energy Balance for Mapping Evapotranspiration with Internalized Calibration (METRIC) – Model"
- Allen, R.G., M. Tasumi, A. Morse, R. Trezza, W. Kramber, I. Lorite and C. W. Robinson. (2007b) "Satellite-Based Energy Balance for Mapping Evapotranspiration with Internalized Calibration (METRIC) – Applications"
- Allen, R.G., M. Tasumi, , R. Trezza, J.L. Wright, I. Lorite and C. W. Robinson A. Morse. (in preparation) "Satellite-based ET mapping for agricultural water management (2): Estimating evapotranspiration by NDVI"
- Bastiaanssen, W.G.M. (1995). "Regionalization of Surface Flux Densities and Moisture Indicators in Composite Terrain: A Remote Sensing Approach Under Clear Skies in Mediterranean Climates. PhD. Dissertation, CIP Data Koninklijke Bibliotheek, Den Haag, The Netherlands. 273p.
- Bastiaanssen, W. G. M., M. Meneti, R.A. Feddes, and A.A.M. Holtslag. (1998) " A Remote Sensing Surface Energy Balance Algorithm for Land (SEBAL): 1. Formulation." *Journal of Hydrology.*, 212-213, 198-212.
- Bastiaanssen, W. G. M., E.J.M. Noordman, H. Pelgrum, G. Davids, B.P. Thoreson, and R.G. Allen. (2005) "SEBAL Model with Remotely Sensed Data to Improve Water-Resources Management under Actual Field Conditions". *Journal of Irrigation and Drainage Engineering*. Vol 131, No 1. pp.85-93.

- Choudhury, B.J., Ahmed, N.U. Idso, S.B., Reginato, R.J., and Daughtry, C.S.T. (1994).
 “Relations between evaporation coefficients and vegetation indices studies by model simulations.” *Remote Sensing of the Environment.*, Vol 50, pp1-17.
- Haboudane, D., J.R. Miller, E. Pattey, P.J. Zarco-Tejada, I.B. Strachan. (2004)
 “Hyperspectral Vegetation Indices and Novel Algorithms for Predicting Green LAI of Crop Canopies: Modeling and Validation in the Context of Precision Agriculture”
Remote Sensing of Environment. ELSEVIER. Vol. 90 pp 337-352.
- Harrison, L.P. (1963). “Fundamental Concepts and Definitions Relating to Humidity.”
 In A. Wexler, (ed) *Humidity and Moisture*. Vol. 3. Reinhold Publishing Company, New York, NY.
- Hunsaker, D.J., P.J. Paul, E.M. Barnes, and B.A. Kimball. (2003) “Estimating Cotton Evapotranspiration Crop Coefficients with a Multispectral Vegetation Index.”
Irrigation Science 22: 95-104
- Hutson, Susan S., N.L. Barber, J.F. Kenny, K.S. Linsey, D.S. Lumia, and M.A. Maupin. (2004) “Estimated Use of Water in the United States in 2000”. U.S. Geological Survey Circular 1268. U.S. Department of the Interior.
- Jacob, F., A. Olioso, X. Fa GU, Z. SU, and B. Seguin. (2002) “Mapping Surface Fluxes using Airborne Visible, Near Infrared, Thermal Infrared Remote Sensing Data and a Spatialized Surface Energy Balance Model.” *Agronomie* Vol 22 pp 669-680.
- Jensen, J.R. (2005) “Introductory Digital Image Processing A Remote Sensing Perspective” Pearson Prentice Hall New Jersey
- Jensen, M.E. (1968) “Water Consumption by Agricultural Plants.” 1-22 In: Kozlowski, T.T. (ed). *Water Deficits and Plant Growth*, Vol. II, Academic Press, New York., 401pp.
- Kustas, W.P., M.S. Moran, K.S. Humes, D.I. Stannard, J. Pinter, L. Hipps, and D.C. Goodrich. (1994) “Surface Energy Balance Estimates at Local and Regional Scales

- Using Optical Remote Sensing from an Aircraft Platform and Atmospheric Data Collected Over Semiarid Rangelands”. *Water Resources Research*, 30(5), 1241-1259.
- Kustas, W.P., J.M. Norman, M.C. Anderson, A.N. French. (2003) “Estimating Subpixel Surface Temperature and Energy Fluxes From the Vegetation Index-Radiometric Temperature Relationship.” *Remote Sensing of Environment* Vol. 85 pp. 429-440.
- Lorite I. and R.G. Allen (2005) “Crop Classification in Magic Valley Including Kc and Irrigation Method Analysis”. University of Idaho, Kimberly Research and Extension Center.
- Morse, A., W.J. Kramber, R.G. Allen, M. Tasumi (2004) “Use of the METRIC Evapotranspiration Model to Compute Water Use by Irrigated Agriculture in Idaho.” *Proceedings of the 2004 IGARSS Symposium, Anchorage, AK.*
- Neale, C.M.U., Bausch, W.C., and Heerman, D.F. (1989) “Development of reflectance based crop coefficients for corn.” *Transactions of the ASAE* 32(6):1891-1899.
- Norman, J.M. W.P. Kustas, and K.S. Humes. (1995) “A Two-Source Approach for Estimating Soil and Vegetation Energy Fluxes in Observations of Directional Radiometric Surface Temperature. *Ag. And For. Meteorology.* 77:263-293
- Payero, J.O., C.M.U. Neale, and J.L. Wright (2004) “Comparison of Eleven Vegetation Indices for Estimating Plant Height of Alfalfa and Grass” *Applied Engineering in Agriculture ASAE.* 20:3:385-393
- Qualls R. and W. Brutsaert (1996). “Effect of Vegetation Density on the Parameterization of Scalar Roughness to Estimate Spatially Distributed Sensible Heat Fluxes.” *Water Resources Research*, 32(3), 645-652
- Rocchio, Laura. April 17, 2007 NASA Press release. “Precious Resources: Water & Landsat’s Thermal Band” http://landsat.gsfc.nasa.gov/news/news-archive/soc_0011.html (accessed April 2007)

- Tasumi M. (2003) "Progress in Operational Estimation of Regional Evapotranspiration Using Satellite Imagery" PhD Dissertation Biological and Agricultural Engineering, University of Idaho
- Tasumi M., R.G. Allen, R. Trezza, and J.L. Wright (2005) "Satellite-Based Energy Balance to Assess Within-Population Variance of Crop Coefficient Curves" Journal of Irrigation and Drainage Vol. 131, No. 1, pp94-109
- Trezza R. (2002) "Evapotranspiration Using a Satellite-Based Surface Energy Balance with Standardized Ground Control" PhD Dissertation Biological and Agricultural Engineering, Utah State University
- Wright, J.L. and M.E. Jenson (1972). "Peak Water Requirements of Crops in Southern Idaho." Journal of Irrigation and Drainage. Div., (ASCE), 96(IR1): 193-201
- Wright, James L. (1982) "New Evapotranspiration Crop Coefficients" Journal of Irrigation and Drainage. Div. (ASCE), 108:57-74.
- Wright James L. (1990) "Evapotranspiration and Water Requirements" ASCE, New York.

APPENDIX

A. Comparison of K_{cb} Curves with Literature

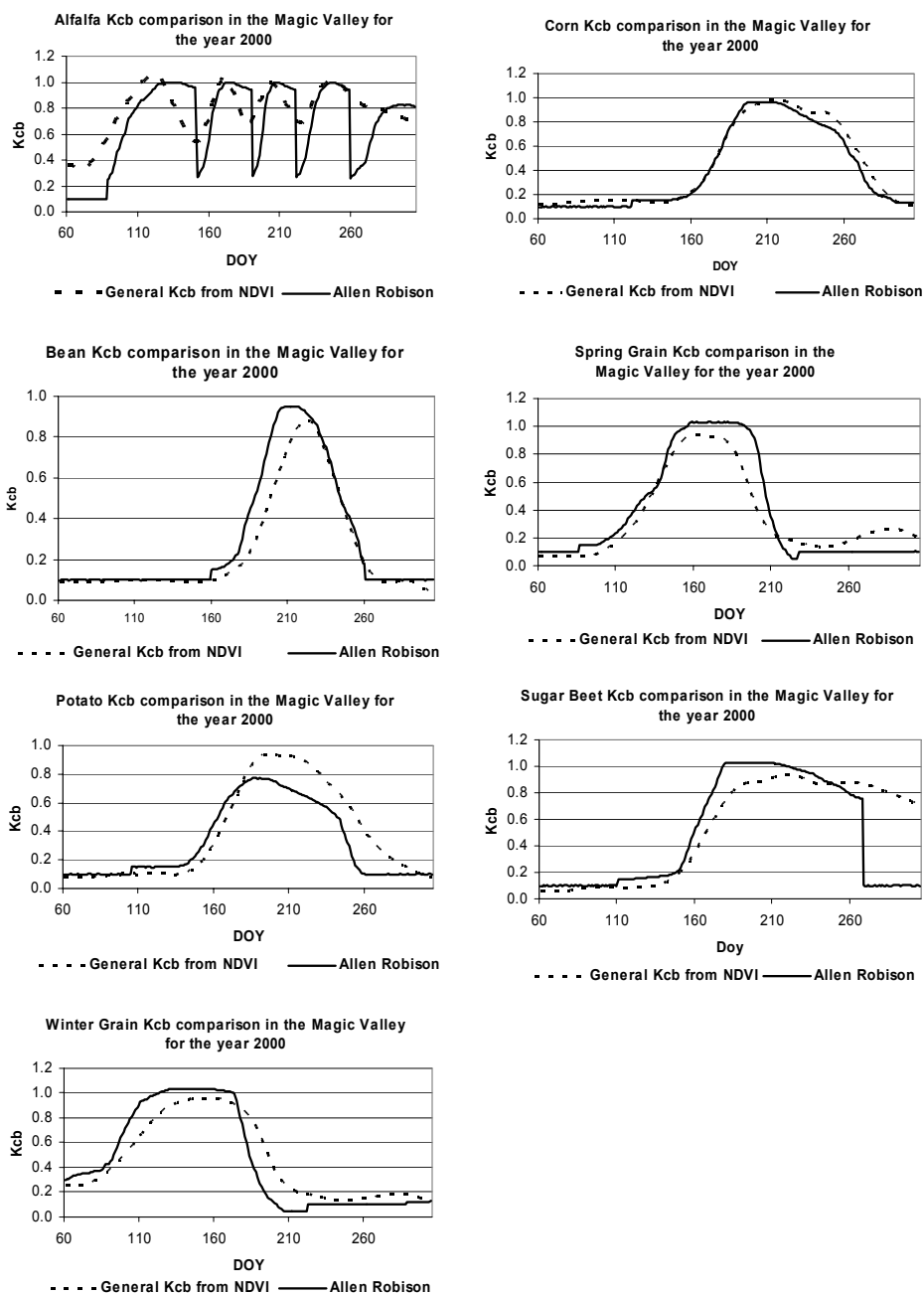


Figure 10.21 Comparison of General K_{cb} curves from NDVI with Allen and Robison (2007).

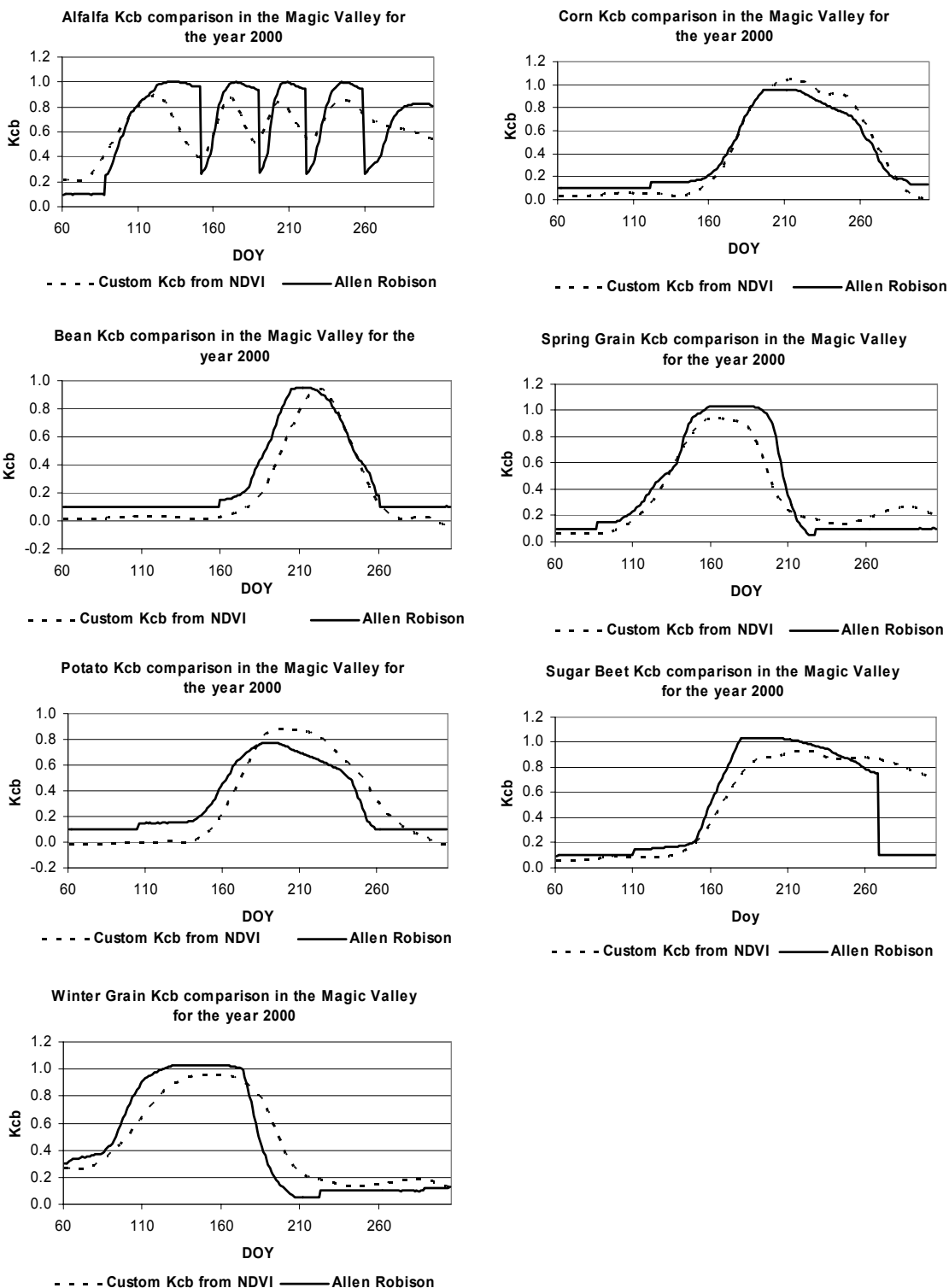


Figure A.2 Comparison of crop specific K_{cb} curves developed from NDVI to Allen and Robison (2007)

B. STATISTICS FOR “COLD” PIXEL SELECTION

The Study area is the agricultural area surrounding American Falls reservoir near Aberdeen in southern Idaho. Landsat images corresponding to the path 39 and row 30 were used for the analysis. Three sample sites were created within the Aberdeen study area and sampled using a 100 X 100 point grid. This gave a combined data set of 30,000 pixels for analysis. Separate sample areas were created to maximize the number of pixels that would be evenly spaced and within agricultural areas. The IMAGINE created grid yields X and Y coordinates such that 100 evenly spaced grid points were located in both the x and y direction of each sample area. The goal of the first search was to delineate AOI's that included approximately 10% desert pixels. The three AOI generated can be seen in the figure below. The three sample areas included a total surface area of 230 square miles (area 1 = 70 mi², area 2 = 42 mi², and area 3 = 118 mi²).

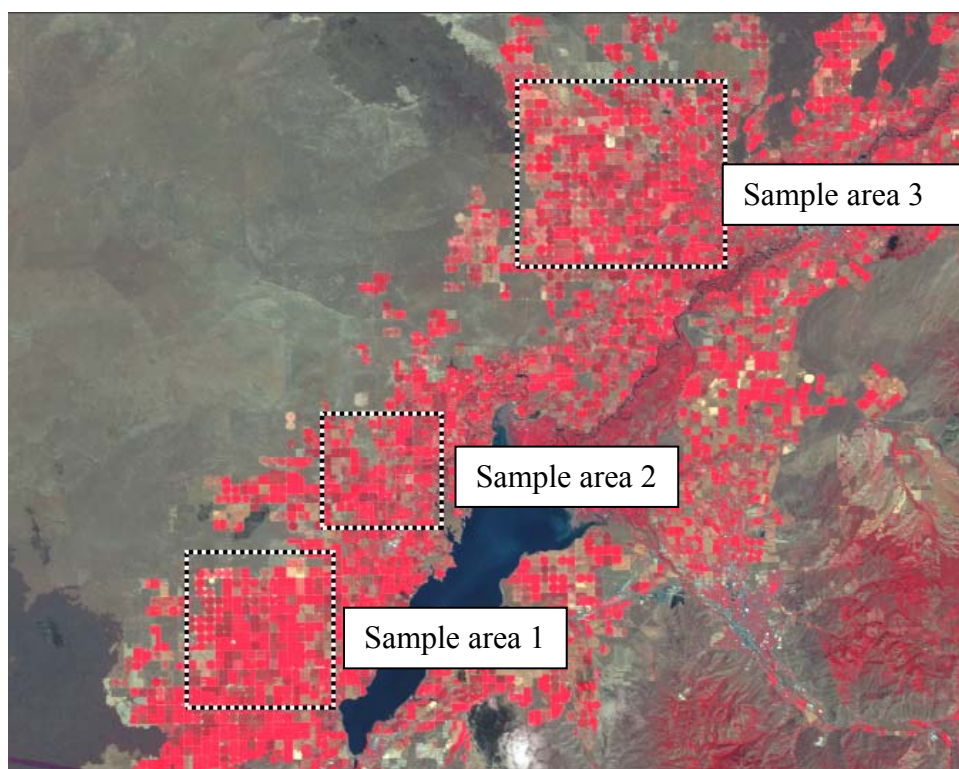


Figure 10.2B.1 Rectangular AOI's (outlined in dashed black and white) for the statistical selection of cold and hot anchor pixels for path 39, row 30, year 2000.

Several different Statistical calculations were carried out to examine locating a representative cold pixel within the image. As described above, Landsat images were sampled for the year 2000 over path 39 row 30. The information used in the analysis included NDVI, Ts_dem, and ETrF images generated using the METRIC model developed by Dr. Allen and the University of Idaho. The first method was to follow the statistics determined by Carlos Kelly, under the guidance of R.G. Allen and M. Tasumi.

Methodology 1

1. Select pixels with the top 5% of highest NDVI values
2. From the selected top 5% NDVI select the coldest 20% of Ts_dem
3. From the resulting sample take the average Ts_dem as the Statistically derived Ts_dem for the cold pixel

Variations in this procedure process were then conducted by altering step 2 as described above. The two additional variations of step two are as follows:

1. From the selected top 5% NDVI select the pixels with temperature in the range of the lowest 10 to 30%
2. From the selected top 5% NDVI select the pixels with temperature in the range of the lowest 20 to 40%

Methodology 2

Next the statistics were altered slightly to examine a slightly different range in NDVI. This was done by rejecting the highest values of NDVI and then conducting similar temperature analysis as above. The methodology can be seen bellow.

1. Select pixels with the top 5 to 10% of highest NDVI values
2. From the selected top 5% NDVI select the coldest 20% of Ts_dem

3. From the resulting sample take the average Ts_dem as the Statistically derived Ts_dem for the cold pixel

Variations in this procedure process were then conducted by altering step 5 as described above. The Two additional variations of step 5 are as follows:

1. From the selected top 5 to 10% NDVI select the pixels with temperature in the range of the lowest 10 to 30%
2. From the selected top 5 to 10% NDVI select the pixels with temperature in the range of the lowest 20 to 40%

Results

The two methods explained above yielded a total of six solutions for the cold pixel statistically determined Ts_dem. Graphs displaying the amount of variation between the statistically determined Ts_dem cold and the user defined Ts_dem cold can be seen below. Analysis of the total amount of absolute deviation from the user defined Ts_dem and the statistically determined Ts_dem for the cold pixel, suggests that the final methodology presented by Allen et al. (2004) provides the best statistical method for replicating the user defined Ts_dem for these image dates. It is important to note that the statistics presented below (Table B.1 column 4) do not match those presented for the path 39 results presented in Figure 9.2-1 and discussed in section 9.2 of this text, because resulting statistics of Table B.1 were obtained from the three AOI's shown in figure B.1. Also the sampled pixels from for this analysis were not filtered for the coefficient of variation (CV) of NDVI (thermal contamination) as were the data presented in Figure 9.2-1.

Table 10.2B.1 Difference in cold anchor pixel temperature statistically determined and user defined for six different combinations of statistical selection processes.

Highest NDVI Coldest Ts_dem Date	Top 5% NDVI			Top 5 to 10% NDVI		
	10 to 30% Ts error (K)	20 to 40% Ts error (K)	20% Ts error (K)	10 to 30% Ts error (K)	20 to 40% Ts error (K)	20% Ts error (K)
3/16/2000	1.32	2.20	-0.14	2.96	3.89	1.35
4/1/2000	2.16	3.20	1.31	4.96	5.63	3.84
5/3/2000*	-2.38	-2.15	-2.74	-0.50	-0.18	-0.62
6/4/2000	0.43	0.74	0.03	0.57	0.90	0.18
6/20/2000	0.67	0.91	0.33	1.81	1.76	1.91
7/6/2000	1.03	1.04	0.92	0.19	0.47	-0.22
7/22/2000	-0.49	-0.25	-0.80	-0.29	-0.01	-0.67
8/7/2000	0.58	0.93	0.03	0.33	0.72	-0.17
8/23/2000	1.62	1.84	1.43	2.42	2.56	2.38
9/8/2000	-0.39	-0.13	-0.79	1.31	1.34	1.30
9/16/2000	0.93	1.14	0.64	1.25	1.54	0.88
10/18/2000	1.13	1.49	0.46	1.91	2.21	1.25
Average error (K/image)	0.90	1.16	0.57	1.50	1.75	1.18

* This early May image was omitted from the analysis due to significant cloud cover over the study area (average error excludes 5-3-2000)

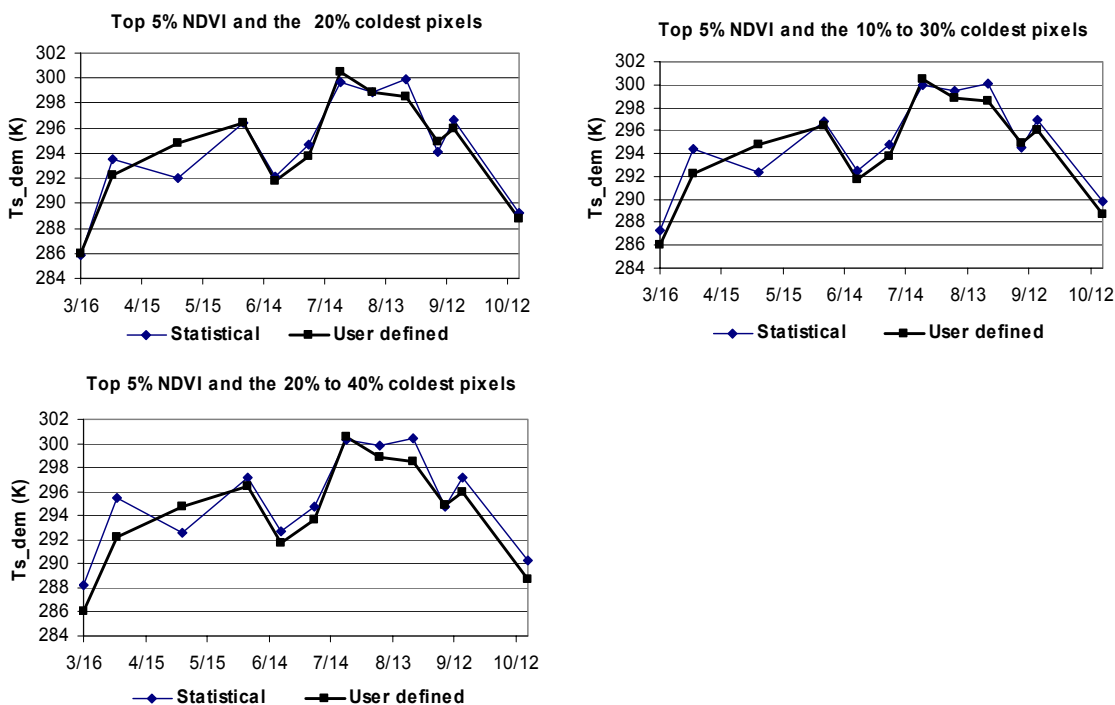


Figure 10.2B.2 Comparison of varying statistics for cold pixel selection looking at the highest 5% of NDVI.

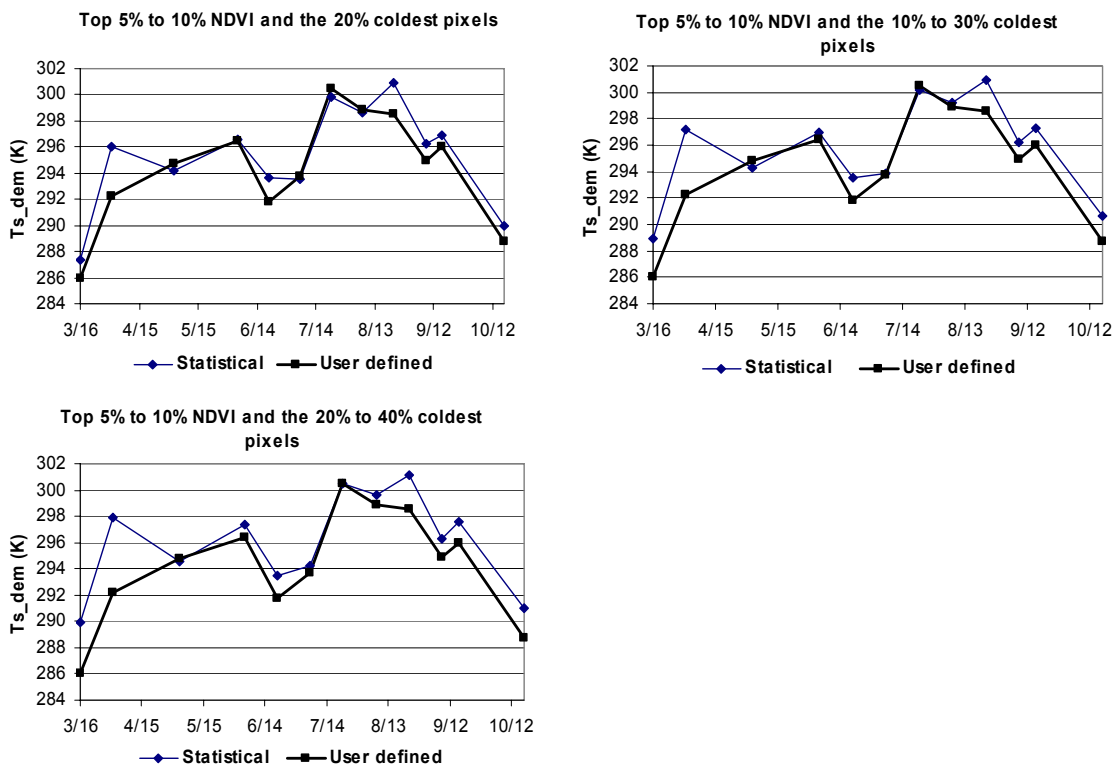


Figure B.3 Comparison of results from several statistical methods for the selection of cold anchor pixels looking at the highest 5 to 10% NDVI.

The largest difference between statistically derived values and those determined by the user were observed in the April 1st and May 5th images. Further investigation showed that the user defined cold pixel for the image data 5/03/2000 was located far from the study area west of Burley Idaho. Also on this date the image had significant cloud coverage over the two upper sample sites and therefore only 10,000 pixels from Sample area 1 were used. Examination of the Ts_dem image also showed that for this date a significant number of fields in the Aberdeen area were at a much cooler temperature than in the Burley area where the user defined cold pixel was located. The combination of these observations led to the inability of the statistical methods to replicate this user defined Ts_dem , and in some cases some doubt on the accuracy of the user defined calibration.

Cold pixel Conclusions

From the above analysis we conclude it best to stay with the statistics previously determine by Kelly et al. The statistics are repeated below.

1. Select pixels with the top 5% of highest NDVI values
2. From the selected top 5% NDVI select the coldest 20% of Ts_dem
3. From the resulting sample take the average Ts_dem as the Statistically derived Ts_dem for the cold pixel

C. SENSITIVITY TO AOI DELINEATION

One of the major objectives in obtaining a statistical method for the selection of cold and hot anchor pixels is to have a method which provides consistent results between different users. Results of this study indicate that the delineation of an area of interest (AOI) from which to sample and perform statistics was the most important for the hot anchor pixel selection methods. The first simulations conducted in this study used carefully selected AOI delineated within agricultural areas, at least 1 mile from non-agricultural (desert, city etc.) pixels. Figure C.1 shows the carefully selected AOI's which excluded major cities within the Magic Valley.

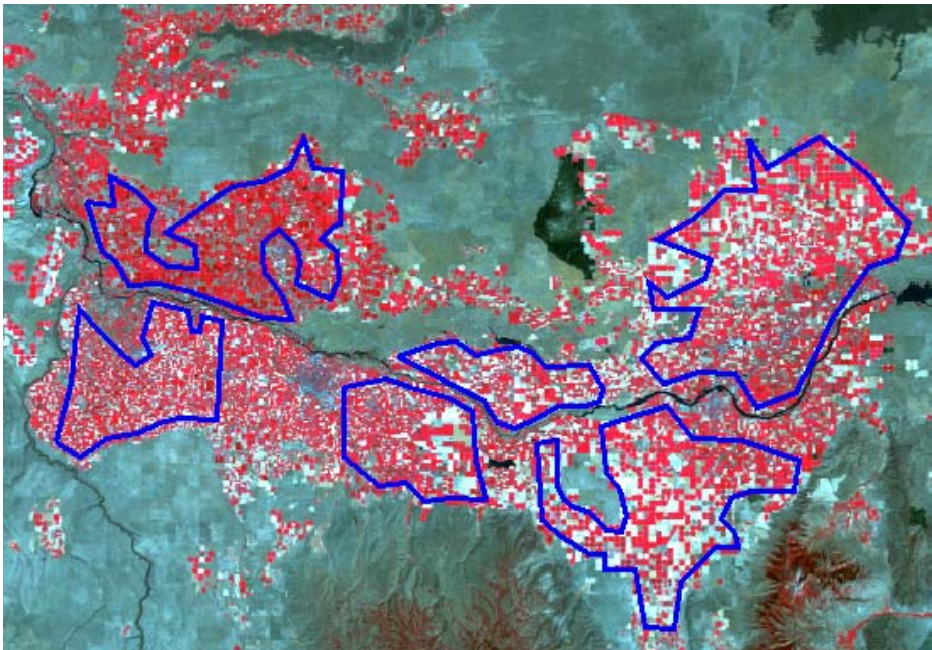


Figure C.1 Carefully delineated agricultural AOI's for the statistical selection of cold and hot anchor pixels for path 40, row 30, year 2000.

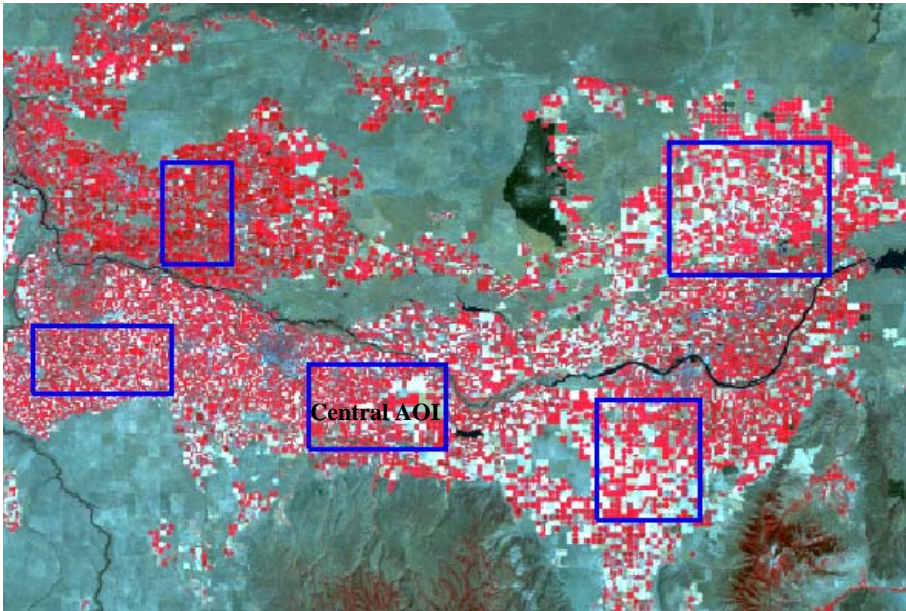


Figure C.2 Rectangular agricultural AOI's for the statistical selection of the cold and hot anchor pixels for path 40, row 30, year 2000.

The sensitivity of AOI selection was then tested by performing the statistical selection process on AOI's selected quickly using simple rectangular delineation (Figure C.2). The resulting temperatures for hot anchor pixels using all 5 areas outlined in blue in figure C.2 are presented in Figure C.3. The average absolute difference in the temperature selected for the hot pixel using the statistical method and the user defined temperature was about 3 K. The statistics were then conducted using only the small central area (shown in Figure C.2) and the average absolute deviation reduced to about 2 K. While the quick selection of agricultural areas from which to perform the statistical methods of obtaining the temperature of the hot anchor pixel provides reasonable results, it was found that as more care was taken to exclude non-agricultural pixels (desert), statistical selection of the hot pixel gave less deviation from experienced user defined hot pixels.

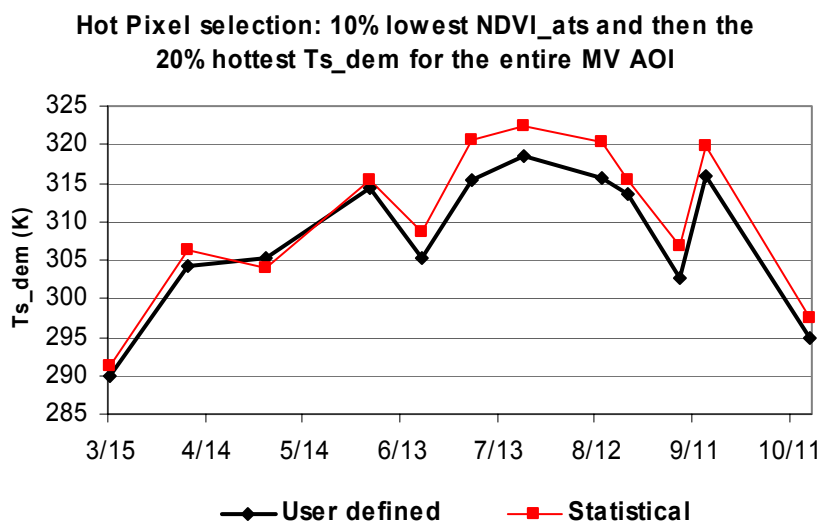


Figure C.3 Comparison of the statistically selected hot pixel for path 40 with the user defined hot anchor pixel using multiple AOI's throughout the Magic Valley.

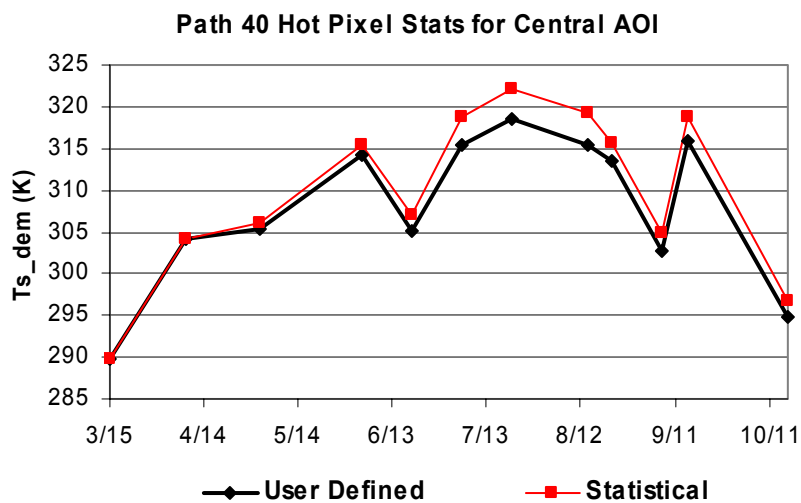


Figure C.4 Comparison of the statistically selected hot pixel for path 40 with the user defined hot anchor pixel using single AOI (central AOI Figure 10.2-2) throughout the Magic Valley.

D. METRIC ANCHOR PIXEL DATA PATH 40, ROW 30, YEAR 2000

Table D.1 Anchor pixel characteristics for pixels selected by experienced METRIC user for path 40, row 30, year 2000.

METRIC with experienced user calibration										
Date	Pixel	X	Y	ETrF assigned	ETrF calculated	Albedo	NDVI_TOA	LAI	Ts (K)	Ts_dem (K)
3/15/2000	Cold	447809	166501	0.75	0.75	0.20	0.79	4.34	283.29	282.67
	Hot	471201	161200	0.336	0.34	0.19	0.12	0.01	289.94	289.89
4/8/2000	Cold	447809	166501	0.8	0.80	0.17	0.81	4.48	293.92	293.30
	Hot	474433	152238	0	0.00	0.23	0.10	0.01	303.93	304.26
5/2/2000	Cold	484115	156941	1.05	1.04	0.16	0.73	3.05	289.92	290.39
	Hot	483205	157801	0.072	0.07	0.23	0.14	0.02	304.75	305.25
6/3/2000	Cold	483681	156897	1.05	1.05	0.19	0.84	5.29	294.66	295.17
	Hot	456272	156755	0	0.00	0.28	0.10	0.01	314.07	314.26
6/19/2000	Cold	483398	154082	1.05	1.04	0.19	0.84	5.33	289.92	290.60
	Hot	455154	164124	0	0.00	0.25	0.10	0.01	305.71	305.23
7/5/2000	Cold	457318	154924	1.05	1.05	0.18	0.79	4.26	294.66	294.91
	Hot	455154	164124	0	0.00	0.24	0.16	0.03	315.86	315.38
7/21/2000	Cold	483940	150561	1.05	1.03	0.18	0.81	4.42	298.22	298.76
	Hot	495543	145725	0	0.00	0.29	0.17	0.05	317.63	318.42
8/14/2000	Cold	484030	150788	1.05	1.04	0.18	0.82	4.77	298.11	298.65
	Hot	454893	162127	0	0.00	0.32	0.19	0.07	315.87	315.53
8/22/2000	Cold	459869	151133	1.05	1.04	0.19	0.73	3.42	294.66	295.46
	Hot	469584	161913	0	0.00	0.27	0.12	0.02	313.62	313.53
9/7/2000	Cold	495408	151650	1.05	1.05	0.24	0.82	5.23	289.92	290.58
	Hot	469584	161913	0.191	0.19	0.26	0.12	0.02	302.81	302.71
9/15/2000	Cold	469871	154828	1.05	1.05	0.21	0.77	4.20	298.11	298.20
	Hot	455154	164124	0	0.00	0.23	0.14	0.03	316.40	315.92
10/17/2000	Cold	453221	176371	1.05	1.05	0.21	0.79	4.27	287.66	286.90
	Hot	467611	163197	0.220	0.22	0.23	0.10	0.01	295.11	294.86

Table D.2 Anchor pixel characteristics for pixels selected using statistical procedures for path 40, row 30, year 2000 METRIC processing.

METRIC with statistical calibration and larger albedo at the cold anchor pixel										
Date	Pixel	X	Y	ETrF assigned	ETrF calculated	Albedo	NDVI_TOA	LAI	Ts (K)	Ts_dem (K)
3/15/2000	Cold	469082	158286	0.75	0.75	0.21	0.74	3.68	284.42	284.38
	Hot	497081	141932	0.336	0.33	0.22	0.11	0.01	288.85	289.86
4/8/2000	Cold	472348	162645	0.8	0.80	0.18	0.72	3.04	294.53	294.36
	Hot	464442	154102	0	0.00	0.25	0.12	0.01	305.06	305.18
5/2/2000	Cold	476561	153116	1.05	1.05	0.23	0.77	4.23	289.38	289.85
	Hot	502133	151014	0.072	0.07	0.25	0.11	0.01	303.78	304.73
6/3/2000	Cold	482592	149942	1.05	1.06	0.25	0.84	5.87	294.66	295.21
	Hot	506159	146644	0	0.00	0.23	0.22	0.09	313.60	314.49
6/19/2000	Cold	479983	150484	1.05	1.05	0.23	0.82	5.32	289.92	290.45
	Hot	495567	153861	0	0.00	0.26	0.15	0.03	304.75	305.49
7/5/2000	Cold	476939	158275	1.05	1.05	0.23	0.85	5.82	295.18	295.51
	Hot	447064	159087	0	0.00	0.25	0.16	0.04	316.75	316.96
7/21/2000	Cold	475809	150783	1.05	1.06	0.22	0.79	4.53	297.22	297.64
	Hot	505855	137737	0	0.00	0.22	0.20	0.06	318.50	319.53
8/14/2000	Cold	469684	154786	1.05	1.06	0.21	0.80	4.74	296.93	297.02
	Hot	479063	149391	0	0.00	0.24	0.14	0.02	316.40	316.88
8/22/2000	Cold	443582	162656	1.05	1.05	0.23	0.79	4.74	295.18	295.07
	Hot	494805	147351	0	0.00	0.26	0.13	0.02	312.26	313.03
9/7/2000	Cold	476886	152344	1.05	1.05	0.25	0.84	5.77	290.99	291.41
	Hot	471168	157174	0.191	0.19	0.25	0.14	0.02	302.80	302.89
9/15/2000	Cold	469782	154838	1.05	1.05	0.21	0.75	3.75	298.11	298.20
	Hot	489081	147736	0	0.00	0.22	0.10	0.01	315.37	315.97
10/17/2000	Cold	472770	159512	1.05	1.08	0.23	0.80	4.78	288.30	288.31
	Hot	466851	151538	0.220	0.22	0.25	0.14	0.02	295.11	295.32

Table D.3 Anchor pixel characteristics for statistical selection using tighter range for albedo values at the cold pixel for path 40, row 30, year 2000.

METRIC with statistical calibration and albedo at the cold anchor pixel similar to METRIC/user calibration										
Date	Pixel	X	Y	ETrF assigned	ETrF calculated	Albedo	NDVI_TOA	LAI	Ts (K)	Ts_dem (K)
3/15/2000	Cold	469082	158286	0.75	0.75	0.21	0.74	3.68	284.42	284.38
	Hot	497081	141932	0.34	0.33	0.22	0.11	0.01	288.85	289.86
4/8/2000	Cold	472348	162645	0.80	0.80	0.18	0.72	3.04	294.53	294.36
	Hot	464442	154102	0.00	0.00	0.25	0.12	0.01	305.06	305.18
5/2/2000	Cold	511008	142571	1.05	1.05	0.18	0.77	3.83	289.38	290.27
	Hot	502133	151014	0.07	0.07	0.25	0.11	0.01	303.78	304.73
6/3/2000	Cold	505474	145947	1.05	1.05	0.18	0.81	4.64	294.14	295.03
	Hot	506159	146644	0.00	0.00	0.23	0.22	0.09	313.60	314.49
6/19/2000	Cold	509915	170968	1.05	1.05	0.18	0.81	4.69	289.92	290.50
	Hot	495567	153861	0.00	0.00	0.26	0.15	0.03	304.75	305.49
7/5/2000	Cold	493932	161827	1.05	1.05	0.18	0.80	4.55	294.66	295.25
	Hot	447064	159087	0.00	0.00	0.25	0.16	0.04	316.75	316.96
7/21/2000	Cold	456515	184672	1.05	1.05	0.19	0.82	4.76	298.22	297.80
	Hot	505855	137737	0.00	0.00	0.22	0.20	0.06	318.50	319.53
8/14/2000	Cold	474757	150770	1.05	1.05	0.18	0.79	4.28	296.93	297.27
	Hot	479063	149391	0.00	0.00	0.24	0.14	0.02	316.40	316.88
8/22/2000	Cold	456519	183242	1.05	1.05	0.19	0.78	4.09	295.69	295.22
	Hot	494805	147351	0.00	0.00	0.26	0.13	0.02	312.26	313.03
9/7/2000	Cold	492882	162975	1.05	1.05	0.18	0.80	4.27	290.99	291.61
	Hot	471168	157174	0.19	0.19	0.25	0.14	0.02	302.80	302.89
9/15/2000	Cold	469782	154838	1.05	1.05	0.21	0.75	3.75	298.11	298.20
	Hot	489081	147736	0.00	0.00	0.22	0.10	0.01	315.37	315.97
10/17/2000	Cold	475173	161758	1.05	1.05	0.22	0.82	4.88	288.30	288.39
	Hot	466851	151538	0.22	0.22	0.25	0.14	0.02	295.11	295.32